MODELING AND CONTROL OF HEAT TRANSFER IN A SINGLE VERTICAL GROUND HEAT EXCHANGER FOR A GEOTHERMAL HEAT PUMP SYSTEM

by

KHALED ASHAREF ASSUDANI SALHEIN

A dissertation submitted in partial fulfillment of the
requirements for the degree of

DOCTOR OF PHILOSOPHY IN ELECTRICAL AND COMPUTER ENGINEERING

2023

Oakland University
Rochester, Michigan

Doctoral Advisory Committee:

Mohamed A. Zohdy, Ph.D., Chair
Christopher J. Kobus, Ph.D.
Daniel N. Aloi, Ph.D.
Richard Olawoyin, Ph.D.
Darrell P. Schmidt, Ph.D.

© Copyright by Khaled Asharef Assudani Salhein, 2023
All rights reserved

To my parents, brothers, and sisters.

ACKNOWLEDGMENTS

First, I would like to thank my advisor, Professor Zohdy, for his unwavering support, guidance, and significant contributions to my Ph.D. research, as well as his wisdom, patience, motivation, and vast knowledge. Many thanks to Dr. Christopher Kobus for his continuous support, counsel, and valuable input throughout my Ph.D. studies. I also express my gratitude to the rest of the dissertation advisory committee members: Dr. Daniel Aloi, Dr. Richard Olawoyin, and Dr. Darrell Schmidt for their valuable comments and encouragement.

Additionally, I would like to thank Dr. Louay Chamra, Dean of the School of Engineering and Computer Science, and Dr. David Stone, Vice President of the Research Office at Oakland University, for their support.

Next, I would like to thank Oakland University, Oklahoma State University, and the University Politècnica de València for providing the Geothermal Heat Pump System datasets for this research.

Furthermore, I would like to express my gratitude to my family, and particularly my parents, who spiritually supported and encouraged me to begin my Ph.D. program and continue to pursue and achieve my goals.

Finally, I would like to thank everyone who supported and motivated me, even if it was just a kind word or smile, during my Ph.D. studies at Oakland University.

Khaled Asharef Assudani Salhein

ABSTRACT

MODELING AND CONTROL OF HEAT TRANSFER IN A SINGLE VERTICAL GROUND HEAT EXCHANGER FOR A GEOTHERMAL HEAT PUMP SYSTEM

by

KHALED ASHAREF ASSUDANI SALHEIN

Adviser: Mohamed A. Zohdy, Ph.D.

The Ground Heat Exchanger (GHE) is regarded as the most critical component of a Geothermal Heat Pump System (GHPS) due to its direct contact with the Earth and ability to benefit from its relatively steady temperature. A GHE can attain the maximum benefit from the Earth's heat when the water temperature reaches the ground, which occurs when the water velocity is moderate, allowing the heat exchanger to balance. Optimally, controlling water velocity is crucial such that the water reaches the desired temperature. Therefore, in this dissertation, I proposed a novel mathematical model of heat transfer behavior between the water inside the underground pipe and the surrounding ground for heating and cooling modes in a GHE. The proposed dynamic model was applied to three case studies of GHPS at Oakland University, the University Politècnica de València, and Oklahoma State University in heating and cooling modes to assess its validity and further enhance the performance of the GHE by determining the optimum velocity range. The results revealed the optimal water velocity ranges for three GHPSs.

Model Predictive Control (MPC) was designed to optimize the GHE's output temperature by controlling the water velocity, which can reduce the power consumption used for the water circulation pump and therefore maximize efficiency.

In this dissertation, I also introduced an Improved Grey Prediction Model (IGM (1,1)). The proposed IGM (1,1) model was based on optimizing the current predicted value by subtracting the error prediction between the previous accumulated time response of the GM (1,1) model and the previous background value throughout the prediction length. The IGM (1,1) model was applied to perform the GHPS's output temperature prediction eight hours in advance at Oklahoma State University, the University Politècnica de València, and Oakland University, respectively. Thus, the IGM (1,1) model outperformed the traditional GM (1,1) model for all used datasets.

TABLE OF CONTENTS

ACKNOWLEDGMENTS iv

ABSTRACT v

LIST OF TABLES xii

LIST OF FIGURES xiii

LIST OF ABBREVIATIONS AND SYMBOLS xv

CHAPTER ONE
INTRODUCTION 1

1.1 Motivation and Challenges 1

1.2 Dissertation Objectives 3

1.3 Problem Statement 4

1.4 Dissertation Outline 4

CHAPTER TWO
GEOTHERMAL SYSTEMS OVERVIEW 6

2.1 Geothermal Power 6

2.1.1 Using GP to Produce Electricity 7

2.1.2 GP Components 8

2.1.3 GP Historical Applications 8

2.2 Geothermal Heat Pump System 9

2.2.1 Definition 9

2.2.2 GHPS Historical Applications 9

2.2.3 Advantages 10

2.2.4 Disadvantages 12

TABLE OF CONTENTS—Continued

2.2.5 Geothermal System Utilizations 14

2.2.6 Geothermal Heat Pump System Functionality 15

2.2.7 GHPS Components 16

2.2.7.1 Heat Pump 16

2.2.7.2 Ground Heat Exchanger 18

2.2.7.3 Distribution System 18

2.2.8 GHPS Types 19

2.2.8.1 Open-Loop Systems 19

2.2.8.2 Closed-Loop Systems 20

2.2.8.2.1 Vertical Configuration 21

2.2.8.2.2 Horizontal Configuration 23

2.2.8.2.3 Pond/Lake Configuration 24

2.3 Comparison of Closed-Loop Ground Heat Exchanger Configurations 25

CHAPTER THREE
VERTICAL GROUND HEAT EXCHANGER PERFORMANCE FACTORS 30

3.1 Introduction 30

3.2 GHE Performance Factors 30

3.2.1 Soil Thermal Properties 32

3.2.2 Backfill Material Thermal Properties 34

3.2.3 Borehole Layout 38

3.2.4 Pipe Thermal Properties 40

TABLE OF CONTENTS—Continued

3.2.5 Working Fluid Properties 43

3.2.5.1 Fluid Type 43

3.2.5.2 Fluid Velocity 45

3.3 Summary 48

CHAPTER FOUR
MODELING HEAT TRANSFER 52

4.1 Heating and Cooling Modes 52

4.2 Heat Transfer Modeling 54

4.2.1 Model Assumptions 54

4.2.2 Governing Equations 55

4.2.3 Thermal Resistance Network 59

CHAPTER FIVE
CONTROLLING HEAT TRANSFER 64

5.1 Bilinear State Space Model 64

5.2 System Linearization and Discretization 66

5.3 Model Predictive Control 68

5.3.1 Prediction 70

5.3.2 Optimization 72

CHAPTER SIX
KEY VARIABLE PREDICTION OF GEOTHERMAL HEAT PUMP SYSTEM 75

6.1 Methodology 76

6.1.1 Traditional GM (1,1) model 78

TABLE OF CONTENTS—Continued

6.1.2 Improved IGM (1,1) model 80

6.2 Data Description 81

6.3 Model Accuracy Evaluations 81

CHAPTER SEVEN
SIMULATION RESULTS AND DISCUSSION 83

7.1 Case Study I: GHPS at Oakland University 83

7.1.1 System Description 83

7.1.2 Physical Setup 85

7.1.3 Heat Transfer Model Implementation 87

7.2 Case Study II: GHPS at the University of the Politècnica de València 91

7.2.1 System Description 91

7.2.2 Physical Setup 92

7.2.3 Heat Transfer Model Implementation 93

7.3 Case Study III: GHPS at Oklahoma State University 96

7.3.1 System Description 96

7.3.2 Physical Setup 97

7.3.3 Heat Transfer Model Implementation 98

7.4 Controlling 106

7.4.1 MPC Implementation 106

7.5 GHPS Output Temperature Prediction 109

TABLE OF CONTENTS—Continued

7.5.1 Case Study I: Oklahoma State University's GHPS Output Temperature Prediction 109

7.5.2 Case Study II: The Politècnica de València University's GHPS Output Temperature Prediction 113

7.5.3 Case Study III: Oakland University's GHPS Output Temperature Prediction 114

CHAPTER EIGHT
CONCLUSION AND CONTRIBUTIONS 118

8.1 Conclusions 118

8.2 Contributions 120

8.3 Future Work 120

REFERENCES 122

LIST OF PUBLICATIONS 136

LIST OF TABLES

Table 3.1	Soil thermals properties	33
Table 6.1	The MAPE criteria	82
Table 7.1	HDPE Pipe Geometric Characteristics	85
Table 7.2	Ground heat exchanger parameters for Oakland University's GHPS	87
Table 7.3	Ground heat exchanger parameters for the University of Politècnica de València's GHPS	93
Table 7.4	Ground heat exchanger parameters for Oklahoma State University's GHPS	97
Table 7.5	Appropriate range of water velocity in varying vertical GHEs	100
Table 7.6	Water circulation pump and heat pump power consumption (kW)	105
Table 7.7	The Hourly Oklahoma State University's GHPS Output Temperature Predictions	111
Table 7.8	The Hourly Politècnica de València University's GHPS Output Temperature Predictions	113
Table 7.9	The Hourly Oakland University's GHPS Output Temperature Predictions	115
Table 7.10	The accuracy assessment metrics to compare the GM (1,1), and IGM (1,1) models for three GHPSs output temperature predictions	116

LIST OF FIGURES

Figure 2.1	Geothermal systems	6
Figure 2.2	Geothermal power system	8
Figure 2.3	Geothermal heat pump system	16
Figure 2.4	Types of GHPS	19
Figure 2.5	Open loop geothermal system	20
Figure 2.6	Vertical closed-loop geothermal system	21
Figure 2.7	Horizontal closed-loop geothermal system	23
Figure 2.8	Pond closed-loop geothermal system	25
Figure 3.1	Thermal performance factors of the vertical GHE	31
Figure 3.2	Illustration of shank-space in a horizontal cross-section through a U-tube pipe of the vertical GHE	42
Figure 4.1	Schematic diagram of heat transfer behavior of the vertical GHE for (a) heating mode and (b) cooling mode	53
Figure 4.2	The rate of heat transfer from the water inside the pipe to the surrounding ground	55
Figure 4.3	Diagram of a vertical single U-tube ground heat exchanger	59
Figure 5.1	MPC basic concept	69
Figure 5.2	Block diagram of a closed loop MPC controlling heat transfer in a GHE for Oakland University's GHPS	73
Figure 7.1	Schematic diagram of the GHPS at Oakland University	84
Figure 7.2	Water temperature behavior in a vertical U-tube pipe for GHPS at Oakland University in heating mode	88
Figure 7.3	Water temperature behavior in a vertical U-tube pipe for GHPS at Oakland University in cooling mode	89

Figure 7.4	Water temperature behavior in a vertical U-tube pipe for GHPS at the University of Politècnica de València in heating mode	94
Figure 7.5	Water temperature behavior in a vertical U-tube pipe for GHPS at the University of Politècnica de València in cooling mode	95
Figure 7.6	Water temperature behavior in a vertical U-tube pipe for GHPS at the Oklahoma State University in heating mode	98
Figure 7.7	Water temperature behavior in a vertical U-tube pipe for GHPS at the Oklahoma State University in cooling mode	99
Figure 7.8	Relationship of the heat transfer rate and thermal resistance	102
Figure 7.9	Relationship of the geothermal pipe length and water velocity	103
Figure 7.10	Relationship of the geothermal heat transfer rate and COP	104
Figure 7.11	Water circulation pump and heat pump power consumption	105
Figure 7.12	The MATLAB-Simulink MPC controller design model for water velocity in the vertical ground heat exchanger	107
Figure 7.13	The MATLAB-Simulink model of the MPC water temperature results tracking the reference temperature trajectory	108
Figure 7.14	MPC Control Signal	108
Figure 7.15	Actual and predicted GHPS's output temperature for Oklahoma State University	112
Figure 7.16	Actual and predicted GHPS's output temperature for Politècnica de València University's GHPS	114
Figure 7.17	Actual and predicted GHPS's output temperature for Oakland University's GHPS	116

LIST OF ABBREVIATIONS AND SYMBOLS

1-AGO	First Order Accumulated Generating Operation
AGO	Accumulated Generating Operation
ANFIS	Adaptive Neuro-Fuzzy Inference System
ANN	Artificial Neural Network
BHE	Borehole Heat Exchanger
BI	Bounded Input
BLS	Bilinear System
BO	Bounded Output
BPNN	Backpropagation Neural Network Algorithm
CHTC	Convective Heat Transfer Coefficient
CO2	Carbon Dioxide
COP	Coefficient of Performance
DBHE	Deep Borehole Heat Exchanger
DE	Pipe Diameter
ELM	Extreme Learning Machine Algorithm
FVM	Finite Volume Method
FWP	Fuzzy Weighted Pre-processing
GCHP	Ground Coupled Heat Pump
GHE	Ground Heat Exchanger
GHG	Greenhouse Gas
GHPS 1	GHPS at Oakland University

GHPS 2	GHPS at Universitat Politècnica de València
GHPS 3	GHPS at Oklahoma State University
GHPS	Geothermal Heat Pump System
GM	Grey Prediction Model
GSHP	Ground Source Heat Pump
GSHX	Ground Source Heat Exchanger
HDPE	High-Density Polyethylene
HHB	Human Health Building
HP	Horsepower
HPS	Heat Pump System
HVAC	Ventilation, and Air Conditioning
IEA	International Energy Agency
IGM	Improved Grey Prediction Model
KW	Kilowatts
KWh	Kilowatt-Hour
LSM	Line Source Method
LTI	Linear-Time Invariant
MAE	Mean Absolute Error
MAPE	Mean Absolute Percentage Error
MLR	Multiple Linear Regression

MPC	Model Predictive Control
MW	Megawatts
NC	Control Horizon
NP	Prediction Horizon
ODE	Ordinary Differential Equation
PSO	Particle Swarm Optimization
QP	Quadratic Problem
RMSE	Root Mean Square Error
SISO	Single Input Single Output
SVM	Support Vector Machine Learning Algorithm
TRT	Thermal Response Testing
VFD	Variable-Frequency Drive
A	Pipe's Cross-Section Area, m^2
A, B, C, and D	State Space Matrixes
c_p	Specific Heat, k. J/kg . ℃
d_i, d_o	Pipe's Inner and Outer Diameters, m
E	System Energy, J
$F, \emptyset$	Matrices Used in the Prediction Equation (5.12)
h_i	Convective Heat Transfer Coefficient, $W/m^2.℃$
k, t	Discrete and Continuous Time, s
k_w	Water Thermal Conductivity, $W/m.℃$

k_p	Pipe Thermal Conductivity, $\mathrm{W/m.℃}$
L	Pipe Length, m
$\dot{m}$	Mass Flow Rate, $\mathrm{Kg/s}$
n	Heating/Cooling Exponent
$N_{U_{d_i}}$	Nusselt Number
P_r	Prandtl Number
P_0	Pipe's an Outside Periphery, m
Q	Rate of Heat Transfer, W
$\dot{Q}_x$	Heat Flow in at Position x, W
$\dot{Q}_{x+\Delta x}$	Heat Flow out at $x + \Delta x$, W
$\dot{Q}_p$	Heat Coming out of the Water to the Ground, W
Q_1, Q_2	Weightings for Errors Output and Input, W
$r(k)$	Reference Signal
R	Weightings of Variable Manipulated Change
R_{conv}	Fluid Thermal Resistance, $\mathrm{m^2.℃/W}$
R_g	Ground Thermal Resistance, $\mathrm{m^2.℃/W}$
R_{wall}	Pipe’s Wall Thermal Resistance, $\mathrm{m^2.℃/W}$
R_{TH}	Total Thermal Resistance, $\mathrm{m^2.℃/W}$
R_v	Soil Thermal Resistance, $\mathrm{m^2.℃/W}$
Re_{d_i}	Reynolds Number

T_s	Sample Time, s
T	Temperature,℃
$T(k)$	Measured Temperature at k,℃
$\hat{T}(k)$	Predicted Temperature at k,℃
$T(x)$	Water Temperature at Position x ,℃
T_{int},	Input Temperatures,℃
T_{out}	Output Temperatures,℃
T_g	Ground Temperature,℃
ΔT	Temperature Difference,℃
U_0	Overall Heat Transfer Coefficient, $\mathrm{W/m^2.℃}$
$u(k)$	Control Signal at Time k
v	Working Fluid Velocity, $\mathrm{m/s}$
v_{min}	Minimum Velocity Constraint, $\mathrm{m/s}$
v_{min}	Maximum Velocity Constraint, $\mathrm{m/s}$
W_s	System Work Done, J
$x(k)$	State Vector at Time k
μ	Dynamic Viscosity, Cp
ρ_p	Pipe Density, $\mathrm{kg/m^3}$
ρ_w	Water Density, $\mathrm{kg/m^3}$
a	Developing Coefficient

b	Grey Action Quantity
$x^{(0)}$	A Non-Negative Original Data Sequence
$x^{(1)}$	Accumulated Time Response of $x^{(0)}$
n	Data Sequence Length
$z^{(0)}$	Background Value Sequence
$z^{(1)}$	Accumulated Time Response of $z^{(0)}$
$\hat{x}^{(0)}(k)$	Predicted Time Response of Grey Prediction Model at Time k
$\hat{x}^{(1)}(k)$	Accumulated Time Response of Grey Prediction Model at Time k
α	Weighting Factor
$\delta^{(1)}(k)$	Predicted Value's Error at Time k

CHAPTER ONE

INTRODUCTION

1.1 Motivation and Challenges

The energy needed to power buildings accounts for an estimated 30% of the total world's energy consumption in most regions; however, this figure could reach 40% in colder regions. For example, the United States experiences an increased demand for space heating during winter months, with 60% of those utility bills dedicated to heating buildings alone [1]-[2]. Overall, the energy demand is rapidly increasing, particularly for heating and cooling in buildings, as the world's population grows, and climate conditions change. These changes continue to increase costs, making these bills too expensive for many households. Furthermore, conventional heating and cooling systems are entirely powered by fossil fuel-produced electricity, adding to air pollution. This has become a major source of concern as the globe faces future challenges of unaffordable fossil fuel energy, and climate conditions change which will influence all aspects of daily living. Thus, an innovative and efficient technology known as the geothermal heat pump system (GHPS) was proposed to address this issue by utilizing the relatively constant temperature of the earth. The GHPS technology was developed over decades to provide high-efficiency heating and cooling for buildings and domestic hot water production that can be used in different applications.

The performance of vertical ground heat exchanger (GHE) systems faces several challenges to maximize the benefits from the Earth's heat including the installation site,

borehole depth, and optimum water velocity inside the U-tube pipe. Moreover, the performance of the GHE is highly site dependent; while it may work correctly in one site, it does not function the same in other sites with higher soil thermal properties, such as thermal conductivity and heat transfer capacity. This indicates that choosing a suitable geological site with better soil conditions, preferably moist soil, is essential to maximizing efficiency. Furthermore, the vertical GHE systems require a lot of depth to function effectively, which is estimated to be around 120 m. If the GHE performance parameters are improved, they might be able to achieve that level of efficiency even if they were installed in a shorter borehole, which would prevent the need for further drilling and thereby decreases initial capital costs. For example, increasing the thermal conductivity of backfill material can shorten the length of the borehole drilling depth.

Additionally, the working fluid (i.e., water or antifreeze solution) velocity inside the U-tube pipe should be optimal—not too low or too high—to ensure that the heat pump system delivers the desired temperature from the ground. For instance, if the water velocity is low, the water temperature will reach the ground even before the loop ends, rendering most of the pipe useless. However, if the water velocity is high, which consumes more energy than is used for the water circulation pump to increase its velocity, the water temperature will not reach the ground temperature. In this case, the heat pump needs to compensate for the heat that is not being delivered from the ground. This indicates that allowing sufficient time for the heat exchanger process between the water inside the pipe and the surrounding ground is critical to reach the equilibrium point and ensure that the exit temperature is the same as the ground temperature and that the entire loop is utilized equally.

1.2 Dissertation Objectives

The main objectives of this research are to address the challenges of the vertical ground heat exchanger performance caused by the water flow rate within the U-tube pipe to obtain the most benefit from the earth's heat without wasting energy. To do so, I proposed a novel mathematical model of heat transfer behavior between the working fluid inside the U-tube pipes and the surrounding ground in a GHE. The proposed dynamic heat transfer model was applied to three case studies of GHPS at Oakland University, the University Politècnica de València, and Oklahoma State University, in both heating and cooling modes, to evaluate its validity and identify the optimal water velocity ranges to maximize the efficiency of their GHE.

Model Predictive Control (MPC) was designed to control the water velocity inside the U-tube pipe to optimize the water temperature and was implemented in MATLAB/Simulink. This research investigated of the effect of water velocity on the performance of the GHE and loop exit temperature by applying four different water velocities in various U-tube pipe diameters as well as the energy consumed by the water circulation pump.

Additionally, this research aimed to improve the Grey Prediction Model (GM (1,1)) that can be used to predict the GHE's output temperature precisely up to eight hours in advance. The Improved Grey Prediction Model IGM (1,1) was applied to all three GHPS datasets. These GHPS temperature datasets were used to validate the IGM (1,1) model accuracy.

1.3 Problem Statement

Circulating water through a U-tube pipe affects the GHE's output temperature, which consumes energy as velocity increases. When the water velocity is too high, more energy is required to circulate the water, but more importantly, the exit temperature from the loop is not different enough from the entrance. However, when the flow velocity is too low, the water temperature reaches the ground temperature well before the exit, rendering most of the loop useless. Optimally, one would control the velocity such that the exit temperature is the same as the ground and that the entire loop is utilized equally.

Furthermore, due to the GM (1,1) model producing an inaccurate prediction, its accuracy prediction needs to be improved. Thus, the IGM (1,1) model was proposed to reduce prediction error and improve the overall GM (1,1) model performance. The IGM (1,1) model can be used to precisely predict the GHE's output temperature up to eight hours in advance.

1.4 Dissertation Outline

This dissertation is arranged as follows: Chapter II describes the overview of the geothermal systems including their definition, history, types of GHPS, application, operation principles, advantages, disadvantages, and dissertation contributions. Chapter III discusses the vertical ground heat exchanger and its performance factors in detail, making suggestions on how to maximize the benefits from the heat of the Earth while exerting the minimum amount of energy used for the water circulation pump. Chapter IV presents the mathematical model of heat transfer behavior between the water flowing inside the U-tube pipes and the surrounding ground for heating and cooling modes in a

GHE. Chapter V describes the linearization system model and MPC control approach design. Chapter VI presents the Grey Prediction model. Chapter VII presents the simulation results and discussion. Finally, Chapter VIII offers the conclusion and future work.

CHAPTER TWO

GEOTHERMAL SYSTEMS OVERVIEW

This chapter will give a general overview of geothermal systems, covering their definition, history, applications, system components, and operations in both heating and cooling modes, as well as their advantages and disadvantages. Open-loop and closed-loop geothermal heat pump systems will be thoroughly detailed. The configuration of a closed-loop ground heat exchanger is comprehensively compared and discussed. Geothermal systems can be classified into geothermal heating/cooling and geothermal power, as shown in Figure 2.1.

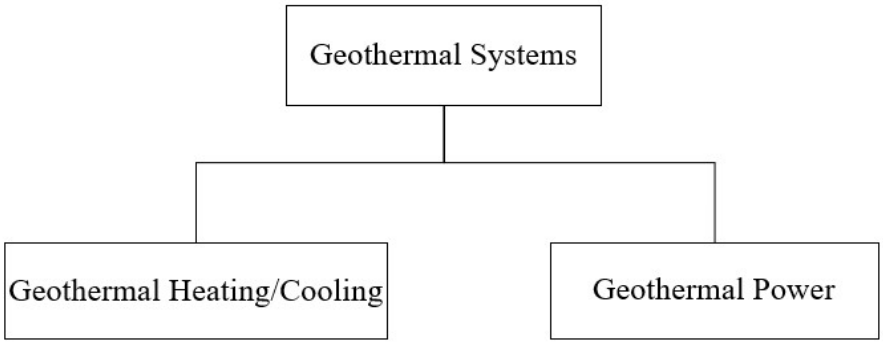

Figure 2.1. Geothermal systems

2.1 Geothermal Power

Geothermal Power (GP) is a renewable energy source that is defined as thermal energy generated and stored within the Earth. Additionally, GPs—are referred to as deep geothermal power as they go hundreds of meters beneath the earth's surface to reach

boiling temperatures of up to 150 °C (i.e., the full heat region) [3, 4]. GPs are the preferred solution to produce electricity owing to their reliance on the Earth's relatively constant heat to drive steam and spin turbines that generate electricity. Therefore, GP is considered a clean, reliable, renewable, and sustainable source of energy that is available all year and is unaffected by weather conditions, which typically stabilizes energy output to meet baseload electricity demand, unlike other renewable energy sources including wind, hydro, and solar energy. Furthermore, geothermal power can be installed anywhere on the Earth's surface, taking up less space than wind, solar, or hydropower installations. For instance, using geothermal power, wind energy, or solar energy, to produce one gigawatts-hour (GWh) of electricity would require roughly 404, 1,335, and 2,340 square miles of the land surface, respectively [5]. However, despite all the advantages, GPs do have some disadvantages. Due to the extensive drilling required to reach the Earth's innate heat and the high costs of facility construction, giving geothermal power a significantly higher initial capital cost than other renewable energy sources. Therefore, the initial cost of constructing geothermal energy ranges between $4,000 and $6,000 per kilowatt-hour (kWh) according to Lazard's Levelized Cost of Energy (LCOE) [6].

2.1.1 Using GP to Produce Electricity

Geothermal Power wells are drilled deep enough to bring hot water or steam to the Earth's surface. Hot water is pumped at high pressure from deep underground to the surface through a well. When the hot water reaches the surface, the pressure drops, causing the water to condense into steam. Then, the steam spins a turbine connected to an electrical generator, resulting in the generation of electricity. The steam condenses back

into the water after cooling in the designated tower. Cooled water from this cycle is then pumped back into the ground, where it circulates in loop pipes to repeat the process.

2.1.2 GP Components

Geothermal Power consists of underground loop pipes specifically designed for high temperatures, a turbine, a generator, and a cooling tower, as shown in Figure 2.2.

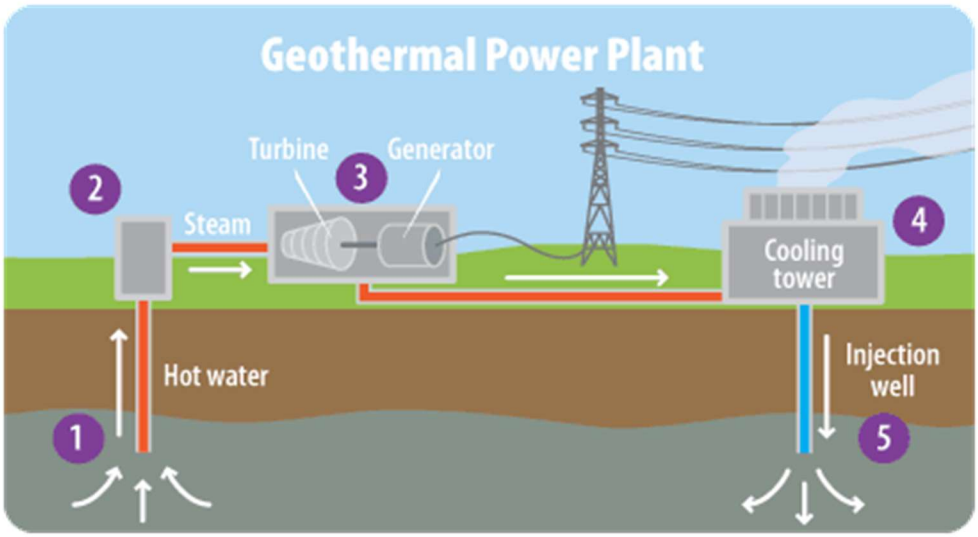

Figure 2.2. Geothermal power system [3].

2.1.3 GP Historical Applications

Geothermal power has been used to generate electricity since 1913 and this output has increased dramatically over the last three decades. Even with the initial capital costs of constructing the geothermal power plant, the installation of new geothermal power units has grown in popularity around the world. Currently, the global geothermal power installation capacity exceeded 15,644 megawatts (MW), according to Statista [7]. This

usage has been identified in over 27 countries. Annually, approximately 865 MW of new installed capacity is added to the existing stock of geothermal power generation systems. Furthermore, the global geothermal power installed capacity is expected to reach 25,436 MW by 2030 [8].

2.2 Geothermal Heat Pump Systems

2.2.1 Definition

The geothermal heat pump harnesses the “heat energy from the earth,” which is denoted in the origin of the name: "Geo" is the Greek word for "earth" and "thermal" translates to heat. Additionally, geothermal heat pumps (GHP)—referred to as ground source heat pumps (GSHP) or ground-coupled heat pumps (GCHPs), as they are commonly known in North America—are a preferred solution for heating and cooling buildings owing to their cost-effectiveness and high efficiency when compared to the conventional heating and cooling systems. The GHPSs—also colloquially referred to as heat pumps—draw heat from the ground and transfer it into the building through a loop of underground, liquid-filled pipes by taking advantage of the relatively constant temperature of the earth. GHPSs do not burn fuel to provide heat; rather, they simply transfer existing heat from one place to another.

2.2.2 GHPS Historical Applications

The heat pump was initially introduced by Lord Kelvin in 1853, and Peter Ritter von Rittinger further developed it a couple of years later in 1855. In 1940, Robert Webber built into the first direct exchange ground source heat pump after experimenting

with it using a freezer [9]. In the late 1940s, Professor Carl Nielsen of Ohio State University constructed the first open loop ground heat exchange configurated for use at his home. This configuration became dominant for use until the invention of polybutylene pipe in 1979, which made closed-loop system configuration achievable [10]. After decades of theoretical and practical research and development, GHPS has been gaining popularity globally. This is especially true in colder regions because of its high efficiency and utility bill cost savings compared to conventional heating and cooling systems. As of 2021, there were 6.46 million ground source heat pump units in operation in approximately 30 countries; of those, 1.7 million—or roughly 26.2%—were in operation in the United States with 60% of those installations being commercial and the remaining 40% being residents, according to the International Energy Agency (IEA) 2020 Geothermal Report [11]. Therefore, GHPS technology is now becoming the most popular heating and cooling system for both commercial and residential buildings.

2.2.3 Advantages

Even though the GHPS uses very little electricity to power its heat pump, it still consumes between 25% and 50% less electricity than conventional heating and cooling systems, which is regarded as its significant advantage. This indicates that a GHPS has a high coefficient of performance (COP) which can move three units of heat from the ground to the heat pump system while using only one unit of electricity [12]. The GHPS can lower heating bills by 30 to 60% and cooling costs by 20 to 50%, in comparison to conventional heating and cooling systems [13, 14]. It would be preferable if the power needs of the GHPS were met by renewable energy sources rather than electric utilities.

Thus, the heat pump supplies heat without generating any carbon emissions while lowering utility costs. Moreover, GHPSs are an incredibly energy-efficient technology than traditional heating and cooling systems, especially during the winter because they do not burn fuel to provide heat. Instead, their main operating principle is to transfer existing heat from one place to another. For instance, the heating efficiency of the GHPS is 30% to 70% higher than conventional heating and 20% to 50% higher than air conditioning systems; it is also effective in controlling humidity [15, 16]. The GHPS does have a longer lifespan than other most conventional heating and cooling systems, with high-density polyethylene (HDPE) pipes that are expected to last up to 50 years and a heat pump unit lasting up to 25 years [12]. Consequently, the GHPS is regarded as a clean, dependable, renewable, and sustainable source of energy that requires exceptionally little maintenance leading to an increase in its popularity when compared to conventional heating and cooling systems.

It is also regarded as the most promising stable renewable energy source because it is continuously available, unaffected by weather conditions, and relies entirely on the relatively constant temperature of the Earth, allowing it to consistently maintain the indoor temperature, regardless of weather conditions, unlike other renewable energy sources such as solar and wind which change according to the weather condition. The GHPS runs very quietly because its piping loops are buried in the ground, with very little noise like that of a typical refrigerator coming from the heat supplier's indoor unit. Even better, using this GHPS technology will bring significant environmental benefits such as reducing greenhouse gas (GHG) emissions, which perpetuate global warming, as well as producing a quieter atmosphere with less noise pollution. For instance, GHPS could

dramatically reduce overall GHG emissions by 66% and carbon dioxide (CO_2) emissions by up to 50% when compared to the conventional heating and cooling system powered by fossil fuels [9]. Better yet, after incurring initial installation costs, the GHPS is expected to return the initial capital investment in as little as four years, depending on system configuration and underground loop size [15-21]. Despite a high initial investment cost for installation, the geothermal heat pump technology is rapidly expanding because it promises cost savings as previously mentioned in section 2.2.2. GHPS is regarded as a fast-growing technology worldwide, evidenced by the increasing number of new geothermal installed units each year. For example, each year, approximately 50,000 units are installed in the United States [22]. Since there are few restrictions, GHPS technology can be installed effectively anywhere, but it should be installed in a suitable site with good soil conditions, preferably moist soil, to maximize the benefits of the Earth's heat [23].

2.2.4 Disadvantages

However, despite all the advantages, GHPSs do have a few disadvantages. First, they require drilling to install the loop pipes, in contrast to other renewable energy equipment like solar and wind, which affects system installation costs. The initial cost of GHPS is relatively high and is typically 30%–50% more expensive than the cost of conventional heating, ventilation, and air conditioning (HVAC) systems [24]. Therefore, residential GHPS installation costs between $10,000 and $30,000, depending on the system configuration, the underground loop size, the amount of drilling required, and the soil conditions. For example, installing GHPS in a typical 2,000 square foot house in the

United States will cost between $10,000 and $20,000 [21]. The vertical ground loop configuration requires heavy drilling, which typically extends from 30 to 130 m below ground. This configuration is costly, and it will become even more expensive if it is done in dense materials like rocks or stone. The horizontal ground loop configuration requires less drilling and is simpler to construct than the vertical configuration, which is typically 1.5 to 4 m below the surface and is thus preferred by many households. However, it requires a large amount of proximate land to bury the looping pipes. Overall, the pipe materials, heat pumps, and construction service are costly.

The process from exploration to heat extraction may take longer than other renewable energy equipment installations, such as solar and wind, which can be stressful for designers and laborers. For example, GHPS system installation is expected to take 6 to 8 weeks, depending on the system capacity, configuration, and soil condition [25]. Furthermore, the installation process can be disruptive to neighbors, especially during the drilling process, and it is even more disruptive if the configuration is vertical. Moreover, the GHPS's output is limited and can only provide buildings with a certain amount of heat if the system functions properly because it depends on the earth's temperature, which remains relatively constant over the year. Because the GHPS cannot fulfill all the building heat demands during the cold months, especially in January and February in the northern hemisphere, the building requires an alternative heating source, which incurs additional costs; this drawback could be sufficient to deter installation. The performance of the GHPS is highly site-dependent; while it might function properly in one site, it may not perform as well in an area with poor soil. Due to these factors, the GHPS is not utilized as widely as it would be if the installation costs were cheaper.

2.2.5 Geothermal System Utilizations

The geothermal system is entirely dependent on the Earth's heat and varies by region due to differences in radioactive decay, volcanic activity, and rock properties. For example, the Oakland University GHPS ground temperature was 11.6 ℃ at 98 m depth, while the University Politècnica de Valencia's was 22.1 ℃ at 50 m depth and the Oklahoma State University was 18.5 ℃ at 20 m depth [26-28]. Therefore, the ground temperature depends not only on depth, but also on geography. The utilization of geothermal energy resources is classified into the following categories according to the ground temperature:

- Low Ground Source Temperature ($T_g < 32$ ℃)

These heat sources are used to provide high-efficiency heating and cooling for commercial, industrial, and residential buildings through the GHPS. Furthermore, these systems are the most widely used and well-known applications of geothermal systems.

- Intermediate-and-Low Ground Source Temperature (32 ℃ $< T_g < 150$ ℃)

This category refers to heat energy sources that can produce hot water and can be used directly for different applications, including industrial processes, agriculture, mineral extraction, snow melting, space heating, greenhouse heating, fish farming, bathing, and swimming. These sources can also be used for GHPS applications if the ground temperature is 32 ℃ or less.

- High Ground Source Temperature ($T_g > 150$ ℃)

Finally, these heat sources can generate hot water or steam, which can be used to produce electricity. Temperatures between 110 ℃ and 150 ℃ are not appropriate for generating electricity.

2.2.6 Geothermal Heat Pump System Functionality

The geothermal heat pump system, unlike other traditional heating systems powered by electricity, fossil fuels, or wood, is an efficient and clean heating system that does not burn fossil fuels to produce heat. Simply, its main operating principle is to transfer existing heat from one place to another. During the winter, the surface air temperature is always cooler than underground. Therefore, the GHPS operates in a heating mode by pumping the cooled fluid through loop pipes to the ground, absorbing heat from the ground, and transferring it to the heat pump. The heat pump compresses the liquid to increase its temperature, which depends on the desired room temperature and the amount of heat absorbed from the ground, which ultimately warms the air. Fans circulate the warm air around the building to exchange it with the cooler air. The cool liquid from this cycle is pumped back into the ground to continue circulating in loop pipes forming a closed loop. By contrast, during the summer, the system operates in reverse; the cooler temperature refrigerant absorbs heat from the building, as it is warmer than the ground. The heated liquid then transfers the heat from the building into the ground and returns the cooled liquid to the building to cool it. Interestingly, the heat pump is not needed for summer because the ground temperature is cooler than the room temperature, thus overall reducing operation costs.

2.2.7 GHPS Components

The GHPS typically consists of a heat pump, Ground Heat Exchanger (GHE), and a distribution unit system, as shown in Figure 2.3.

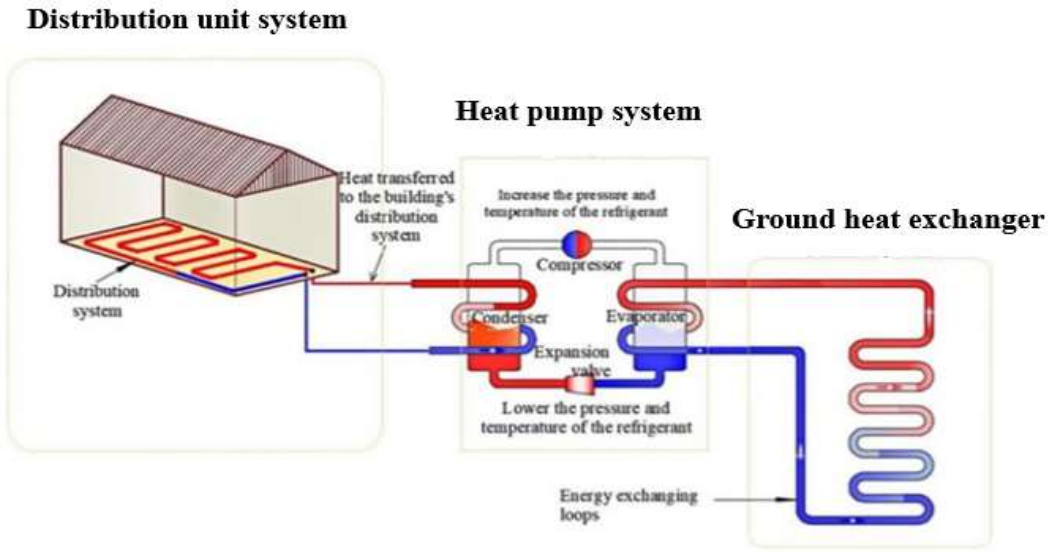

Figure 2.3. Geothermal heat pump system [29].

2.2.7.1 Heat Pump

The heat pump is an electrical device that collects the heat from the ground, water, or air, and concentrates it using an electrically driven compressor so that it is at the proper temperature for heating the building. However, the process is reversed for cooling, where the heat pump collects the heat from the inside of the building and efficiently transfers it to the outside. The heat pump uses less electricity to produce heating and cooling than does heat production powered by oil, gas, and electricity. Additionally, the heat pump reduces carbon dioxide by 50% when compared to the production of heat

utilizing the resources mentioned above [15]. The heat pump is a key component of the GHPS and typically comes in two primary types: the water-to-water heat pump and the water-to-air heat pump, with the latter being the most popular in North America. The three components of the heat pump system are the compressor, condenser, and evaporator.

The heat pump efficiency is measured using the Coefficient of Performance (COP), which typically ranges from 3 to 6. Accordingly, the heat pump uses one unit of electricity to generate between 3 and 6 units of heat. When the COP is high, it leads to better performance, less power consumption, and consequently lower operational expenses. On the other hand, when COP is low, it causes low performance and will ultimately result in more power consumption. The heat pump efficiency is greatly influenced by operating conditions and the absolute and relative temperatures between the ground and the building. These characteristics are crucial to the efficiency of the system. The COP is given by the following equation.

$$COP = \frac{|\dot{Q}|}{\dot{W}} = \frac{\dot{Q}}{\dot{W}} \tag{2.1}$$

where Q is the heat supplied and W > 0 is the system work done which is considered in one cycle.

The COP for cooling is:

$$COP_{cooling} = \frac{|\dot{Q}_C|}{\dot{W}} = \frac{\dot{Q}_C}{\dot{W}} \tag{2.2}$$

The COP for heating is:

$$COP_{heati} = \frac{|\dot{Q}_H|}{\dot{W}} = \frac{\dot{Q}_C + \dot{W}}{\dot{W}} = COP_{cooling} + 1 \tag{2.3}$$

where $Q_C > 0$ is the amount of heat that is supplied into the system and extracted from the low-temperature reservoir, QH is the heat released into the hot reservoir; and $QH < 0$, is negative because it loses by the system mechanism [30].

2.2.7.2 Ground Heat Exchanger

The GHE is regarded as the most critical component of a GHPS due to its direct contact with the earth and ability to benefit from its relatively steady temperature. This system is classified into a few types according to the pipes inserted into the ground which will be detailed in section 2.2.8. The GHE consists of a network of loop pipes that are buried into the ground to exchange heat with the surrounding ground. These pipes are made of High-Density Polyethylene (HDPE) plastic and are specifically designed for use in geothermal applications. Additionally, these GHE pipes are often filled with either pure water or a water-antifreeze mixture and are then continuously circulated by a water circulation pump to promote the heat transfer between the water inside the pipe and the surrounding ground, which ultimately transfers the heat to the heat pump.

2.2.7.3 Distribution System

The distribution system is comprised of a network of ducts specifically designed for air use that are mounted to the underside of the building's roof and wall sides and connected to the heat pump. The distribution network system circulates heated and conditioned air distribution through ductwork to keep the entire building room temperatures consistent.

2.2.8 GHPS Types

The GHPS systems can be classified into open-loop and closed-loop systems according to their GHE, as shown in Figure 2.4.

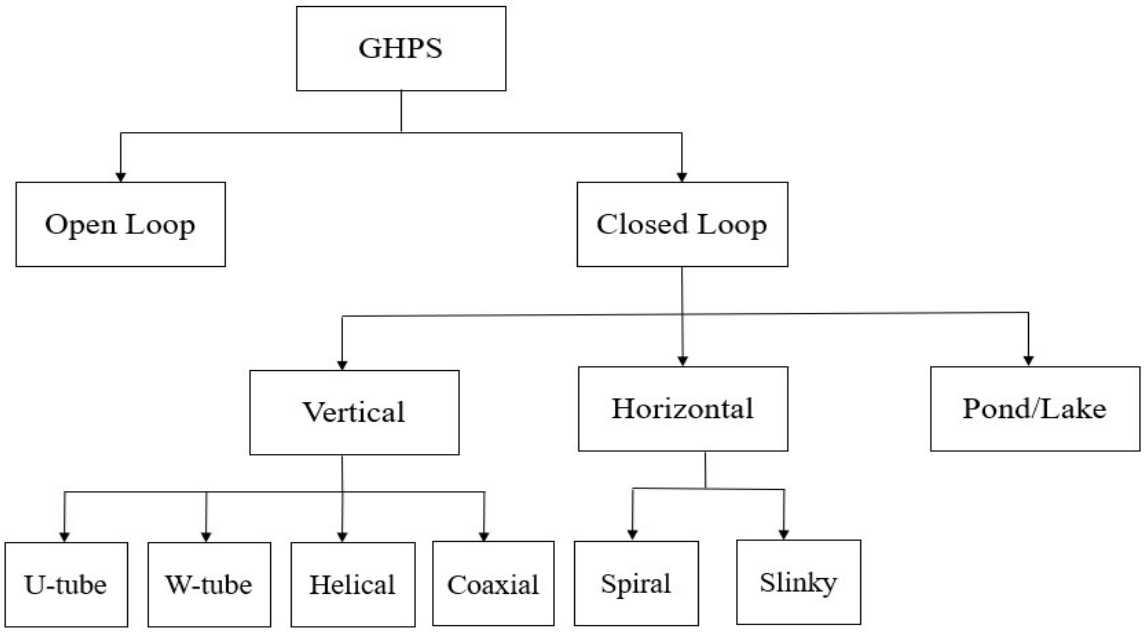

Figure 2.4 Types of GHPS

2.2.8.1 Open-Loop Systems

The open loop system depends entirely on the existing flow of groundwater for the heat exchange process, by pumping the groundwater into an opened pipe. The open loop system also is commonly known as pump-and-dump. Figure 2.5 shows the open loop system. This type of geothermal has better heat performance and requires lower installation costs in comparison to the closed-loop systems [15], but its lifespan is reduced due to the usage of unclean fluid, (i.e., groundwater). This groundwater could

contain contaminants and sediment that cause damage to the heat pump system by clogging pipes and blocking airflow, raising the expense of maintenance for the system. Consequently, its application is limited because it needs an adequate supply of clean water. This disadvantage does not occur with closed-loop systems because the pipes are filled with clean fluid before sealing, circulating it in a closed-loop, without actual contact with groundwater. This system only allows heat to pass through efficiently in both directions from the water inside the pipe to the ground or from the ground to the water.

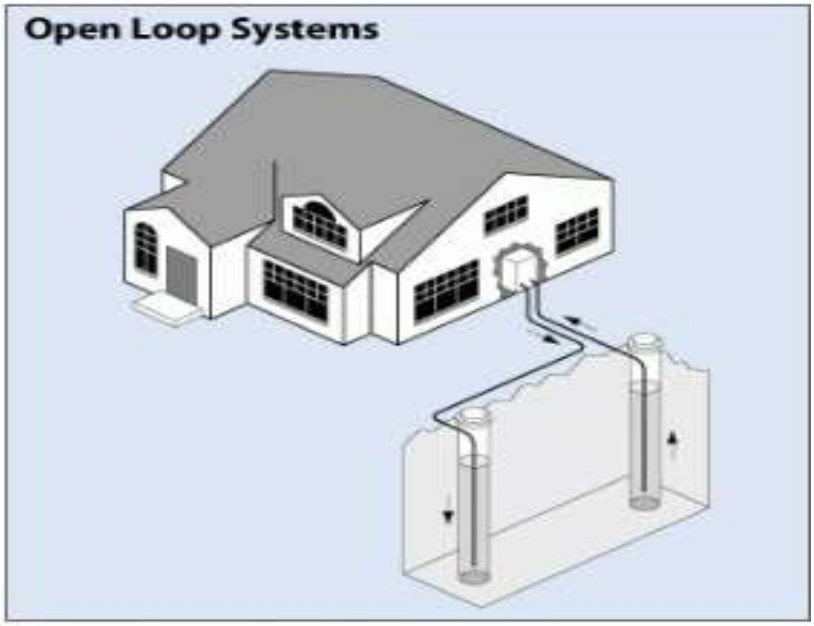

Figure 2.5. Open loop geothermal system [22].

2.2.8.2 Closed-Loop Systems

In a closed-loop system, the working fluid circulates within the loop pipes. A closed-loop system is the most typical type of geothermal heat pump system used, in

which the loop pipes are buried to reach the ground in a variety of configurations, including vertical, horizontal, and pond loop configurations.

2.2.8.2.1 Vertical Configuration

The vertical GHE, also known as a borehole heat exchanger (BHE), is the most common application of GHPS. A schematic diagram of a vertical closed-loop ground heat exchanger is illustrated in Figure 2.6.

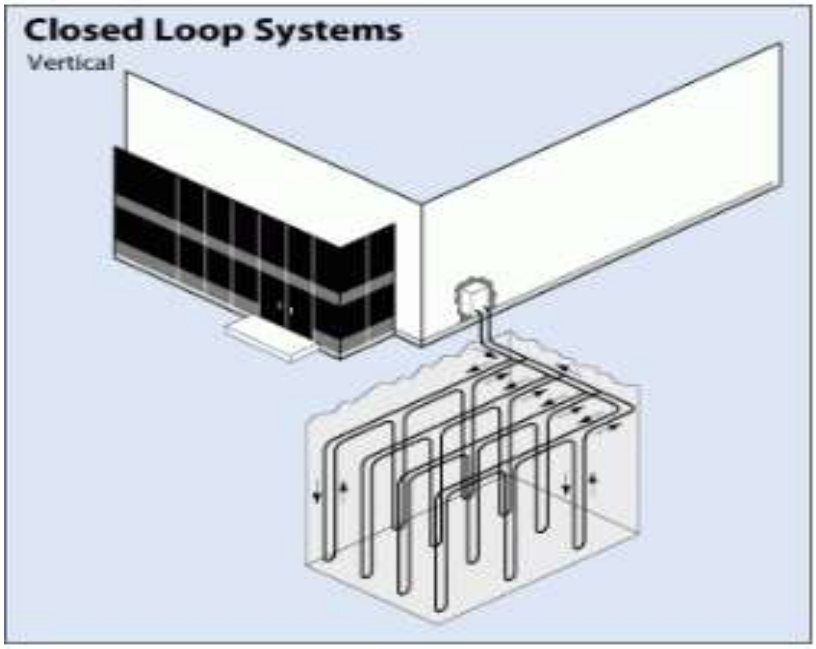

Figure 2.6. A vertical closed-loop geothermal system [22].

The vertical GHE is an alternative option when there is little available space, and the ground surface is rocky. Furthermore, the vertical GHEs have a more stable performance than the horizontal GHEs configuration because the vertical configuration is placed several meters beneath the surface, where the ground temperature is unaffected by

weather changes. The vertical configuration allows the ground to be utilized as a heat source, a heat sink, as well as a thermal heat storage medium. The vertical ground loop installation is significantly more expensive than the horizontal configuration. The loop pipes in this configuration are inserted vertically into geothermal boreholes with a depth range of 30 to 120 m that depends on the soil thermal properties, but remains effective at around 120 m to maximize benefits from the heat in the Earth, with borehole diameters typically ranging from 0.1 to 0.2 m. The drilling depth is based on the specification design of each soil's thermal properties and the building's capacity. The pipes are spaced 5 to 7 m apart to prevent any thermal interference as it affects the performance of the GHE [31]. The space between the loop pipes and the borehole wall is often well-filled with backfill material that has high thermal conductivity to avoid the borehole wall collapsing and groundwater contamination, and extends system life, providing a more efficient transfer of heat between the water inside the pipe and the sounding ground. Preferably, soil moisture. These pipes can be configured in one borehole as a single U-tube, double U-tube, triple U-tube, multi-tube, W-tube, helical, or coaxial loop configuration, connected in either a series or parallel to the heat pump system for heating and cooling applications. The series connection uses fewer pipes, but it performs less efficiently than a parallel connection. Despite its lower performance than other configurations, a single U-tube GHE is the most commonly used vertical ground heat exchanger due to its ease of installation, small space requirement, and low cost. A major advantage of the vertical loop configuration is that it can be installed in small places, but this configuration is costly because considerable drilling is required. The number, depth, and diameter of the boreholes are determined based on the soil properties, temperature

variations, and the building's heating and cooling needs. Interestingly, single U-tube BHE configurations are more common in North America, while double U-tube ground heat exchangers are more common in Europe [32].

2.2.8.2.2 Horizontal Configuration

The horizontal ground heat exchanger is the most economical choice when enough ground space is available and/or if the soil is rock [33]. A schematic diagram of a horizontal closed-loop ground heat exchanger is shown in Figure 2.7.

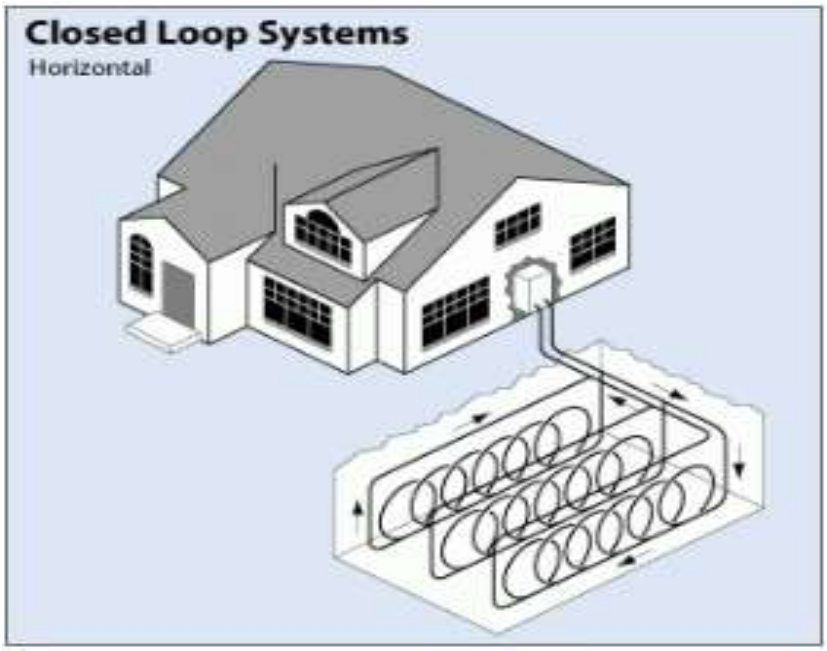

Figure 2.7. Horizontal closed-loop geothermal system [22].

This configuration involves burying the loop pipes horizontally in trenches a minimum of 1.5 meters apart, and typically 2 to 6 meters below the surface, with a length

of 35 to 60 meters for every kilowatt (kW) capacity for both the heating and cooling modes [34]. These systems necessitate a large space to build their ground loop pipes. The pipes can be placed in trenches and are either connected in series or parallel spiral or slinky configurations. The slinky loop occupies the same space as the other trench connections, as well as the series or parallel pipe connections, but additional coils of pipes are used to overlap themselves and can be buried in a shallow trench to conserve space. However, the performance of this configuration is lower than the ground heat exchanger horizontal loop configuration [35]. Nevertheless, the parallel connection is more widely applied because of the advantage that it consumes less power than a series connection. As a result, the spiral and vertical arrangements outperform the horizontal and slinky configurations in terms of heat transfer capacity.

2.2.8.2.3 Pond/Lake Configuration

Finally, the pond loop configuration, also known as the lake loop configuration, consists of loop pipes connected in series that are typically slinky-shaped and expanded in a lake, pond, river, or other available body of water near the building to utilize its heating and cooling outputs. This type of geothermal is regarded as the most efficient among all configurations mentioned because it relies on preexisting natural water sources, whose thermal conductivity is higher than that of soil. These systems are simple to install because drilling is not required, and the pipes can be placed on skids and pushed into the water, which cuts down on installation costs [36]. However, despite all this configuration's advantages, its applications are limited because it requires a body of water to be near the building that is available to use for its heating and cooling output services.

A schematic diagram of a pond closed loop ground heat exchanger is illustrated in Figure 2.8.

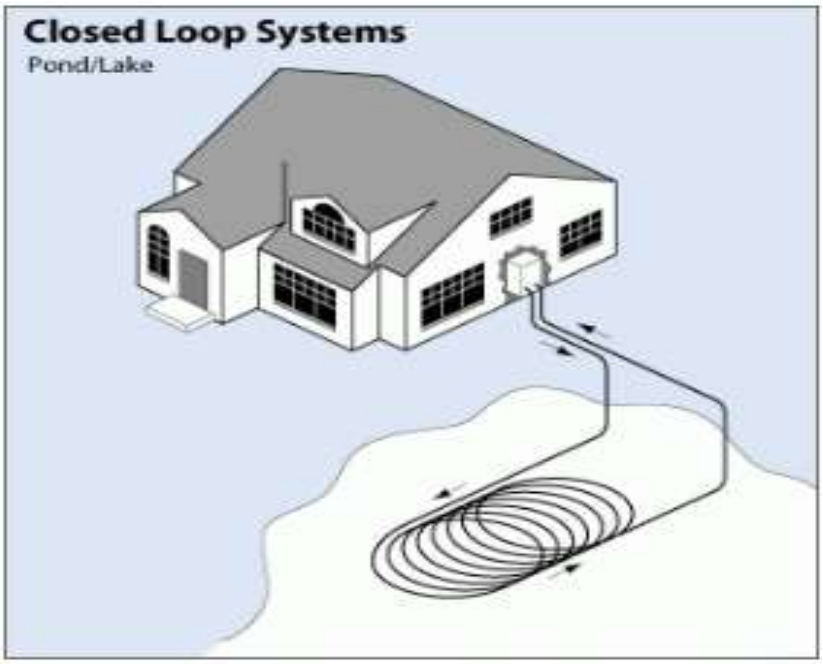

Figure 2.8. Pond closed loop geothermal system [22].

2.3 Comparison of Closed-Loop Ground Heat Exchanger Configurations

Some closed-loop configurations perform better in terms of heat transfer efficiency and have lower installation costs than others. For instance, the authors in [37] pointed out that a vertical GHE often has better energy performance than a horizontal configuration. The spiral GHE configuration requires less drilling depth than the U-tube configuration, resulting in significant savings in initial capital cost, as stated by the authors in [38]. The authors in [39] conducted a comparative analysis of double U-tube GHE and helical-shaped pipe configurations. They found that the helical heat

exchanger has better thermal performance than the double U-tube.

Furthermore, the authors in [40] assessed the performance of heat transfer in various ground heat exchanger arrangements, such as single U-tube, double U-tube, triple U-tube, and W-shaped tube configurations. The findings demonstrated that the W-shaped tube performed better than the mentioned comparison configurations. The authors in [41] compared W-pipe and single-U-pipe vertical ground heat exchanger configurations. They found that the W-shaped heat exchanger in diaphragm walls has a heat transfer rate that is 25–40% higher than the U-pipe configuration. Additionally, the authors in [42, 43] compared the heat transfer performance of three various piles-foundation GHE configurations, including the U-tube, the W-tube, and the spiral-tube configurations, and proved that the spiral configuration was found to be the most efficient, followed by the W-tube, then the U-tube configuration. The findings demonstrated the spiral coil ground heat exchanger configuration performs heat transfer about 10-15% better than the W-tube configuration [44]. Moreover, the authors in [45] investigated the cooling and heating performance of the spiral tube, double W-tube, and double U-tube GHE configurations. The findings demonstrated that the spiral tube and double W-tube configurations have a higher thermal efficiency than the double U-tube configuration by 67-69%. According to their findings, the thermal efficiency of double W-tube and spiral tube configurations is the same. In the spiral tube GHE configuration, increasing the pipe diameter from 25 mm to 32 mm can increase the heat transfer rate by 32% as indicated by the authors in [45].

Another performance factor to consider is the borehole configuration, which could enhance the GHE's thermal performance, as stated by the authors in [46]. The authors in [47] examined the impact of pipe spacing and bending number on a horizontal

GHE and stated that increasing the bending number improved the heat transfer rate of the horizontal GHE. The authors in [48] presented a numerical model to investigate the performance of the single U-tube, spiral, and spiral double GHEs. According to their findings, the spiral-double GHE outperformed the single U-tube and spiral GHE in terms of thermal heat transfer performance. The authors in [49] also examined the heat extraction capabilities of three ground heat exchanger configurations, including a spiral-tube and multiple-tubes with parallel and series connections, and concluded that the spiral-tube configuration was the most efficient.

A comparison of heat transfer performance in series and parallel connections of one U-tube shaped, one W-tube shaped, and W-shaped-all round configurations for vertical loop design was carried out by the authors in [43]. The results revealed that the W-shaped-all loop configuration in a series connection was the most efficient in comparison to the other mentioned configurations. Moreover, the W-tube BHE configuration, which is approximately 14% more efficient than the U-tube ground heat exchanger, was investigated by the authors in [50]. The W-tube GHE configurations have a 10-15% higher average heat exchange rate than the U-tube GHEs configurations, according to the authors in [51], due to the W-GHEs having a larger heat exchange area than the U-tube GHE. Given these advantages, the W-tube GHE configuration is the preferred configuration for ground heat exchanger thermal performance. The authors in [33] compared the heat performance of single and double U-tube GHE configurations connected in series and parallel. They found that the double U-tube configuration, in both series and parallel connections, outperformed the single U-tube BHE configuration. The authors in [49] investigated the performance of multi-tube vertical ground heat

exchangers connected in parallel, serial, as well as spiral tubes. They concluded that the spiral tube GHE configuration demonstrated the best thermal performance among these configurations. Additionally, the spiral tube GHE configuration achieved the highest rate of heat extraction when compared to other vertical ground heat exchanger configurations.

Additionally, the authors in [35] assessed the thermal performance of slinky and spiral GHE configurations and found that the spiral GHE configuration outperforms the slinky GHE configuration. Regardless of soil conditions, the horizontal GHE coil configuration has a 10-11% higher heat exchange rate than the horizontal GHE slinky configuration, as stated by the authors in [35]. The coaxial BHE loop configuration is more effective than the U-tube BHE loop configuration because of its borehole's low thermal resistance, as stated by the authors in [52]. The authors in [53] conducted an analytical evaluation of the thermal performance of a coaxial tube GHE. According to their findings, the coaxial tube GHE can reduce the depth of the borehole by 23% due to a reduction in BHE thermal resistance. The authors in [54] compared the thermal performance of helical and triple U-tube ground heat exchangers and discovered that the thermal performance of a helical ground heat exchanger is significantly better than that of a triple U-tube ground heat exchanger. Therefore, this configuration becomes more attractive than other GHE configurations because it is based on short GHEs, as noted by the authors in [55].

Furthermore, the installation fees and material costs of the spiral heat exchanger capacity are 30% less expensive than the double U-tube heat exchanger configuration [56]. The authors [57] compared the techno-economic performance of spiral, linear, horizontal, and vertical slinky GHE configurations. They discovered that spiral and linear

GHE configurations had the lowest initial installation costs, in both single and parallel connections. The cost-benefits evaluation shows that the triple-U-shaped ground heat exchanger has the highest economic performance, followed by double-U, spiral, and double-W types. The installation cost of the triple U-tube, double U-tube, double W-tube, and spiral tube ground heat exchangers was evaluated by the authors in [45]. According to their findings, the triple U-tube GHE configuration has the best economic performance, followed by the double U-tube, spiral tube, and double W-tube GHE configurations. Furthermore, the authors in [44] compared the installation costs of coil-tube, W-tube, and triple U-tube GHE configurations and found that the coil-tube configuration was 200-250% more expensive than the W-tube and triple U-tube GHE configurations. The authors in [58] conducted a comparative analysis of heat transfer performance in single and double U-tube BHE configurations. The results demonstrated that the double U-tube BHE outperformed the single U-tube ground heat exchanger configuration. The authors in [58] agreed with the authors in [40] that the double U-tube BHE configuration outperformed the single U-tube ground heat exchanger in terms of heat transfer performance. Finally, the authors in [59] examined the heat transfer efficiency of the enhanced coaxial and U-shaped vertical BHE configurations. The findings revealed that the enhanced coaxial BHE configuration can heat transfer by a factor of 1.46, and 1.45 times faster than a U-shaped BHE in winter and summer operations, respectively.

CHAPTER THREE

VERTICAL GROUND HEAT EXHNGER PERFORMANCE FACTORS

3.1 Introduction

The ground heat exchanger (GHE) is an important component of the geothermal heat pump system (GHPS), which can exploit the earth's heat by exchanging energy with it. Most benefits from the earth's heat can be attained when the borehole heat exchanger (BHE) is improved by lowering its thermal resistance. This ensures efficient heat transfer between the water inside the pipe and the surrounding ground, allowing the GHE's output temperature to be delivered to the heat pump. The ground heat exchanger performance is affected by numerous factors, including operational and thermo-physical variables. In particular, the underground thermal properties have the biggest impact on GHE's thermal performance. Hence, understanding these performance factors is crucial for improving the overall GHPS efficiency. This chapter discusses the thermal performance factors for vertical GHE and how they impact the efficiency of heat transfer between the flowing water in the U-tube pipe and the surrounding ground. This concept is further discussed in the following literature review, including examples and suggestions to achieve the optimal thermal parameters for each performance factor.

3.2 GHE Performance Factors

The GHE's principal objective is to efficiently transfer heat between the ground and the heat pump system through an underground loop pipe filled with a heat carrier fluid (i.e., pure water or antifreeze solution). Numerous factors can affect the

performance of the vertical GHE, including the thermal properties of the soil and backfill material, the depth of the borehole, spacing between two boreholes, the thermal properties of the U-tube pipe, the spacing between the legs of the U-tube pipes, the type of working fluid and its velocity. Figure 3.1 illustrates the thermal performance factors of the vertical GHE.

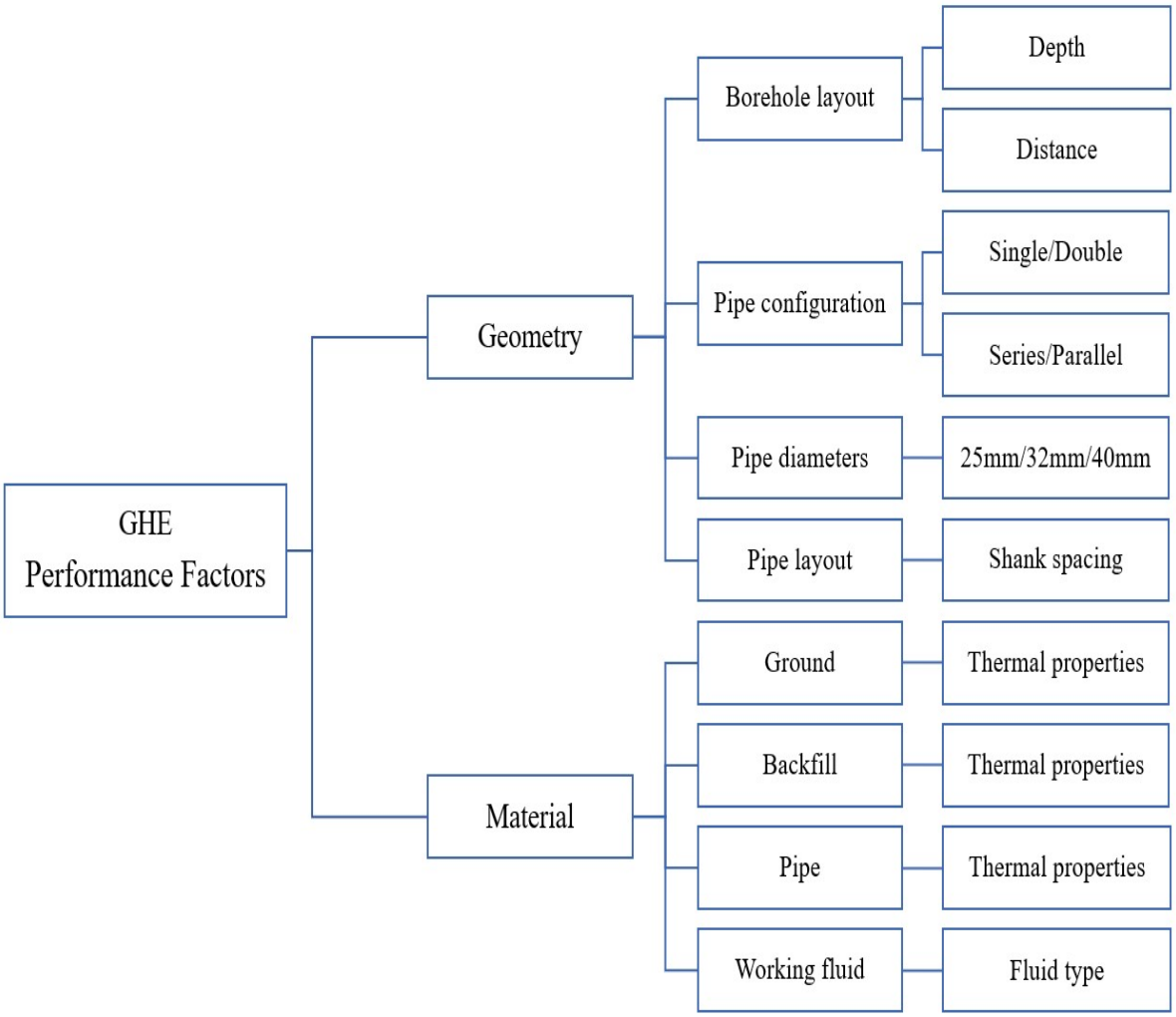

Figure 3.1 Thermal performance factors of the vertical GHE [23].

3.2.1 Soil Thermal Properties

The thermal properties of each type of soil vary depending on its thermal conductivity and heat capacity, which are controlled by the degree of saturation. Saturated soil has a high thermal conductivity which lowers its thermal resistance and enables rapid heat conduction through its layers—even more rapidly than in unsaturated soils. By contrast, dry or unsaturated soil has a low thermal conductivity, increasing its thermal resistance and slowing the flow of heat, making this type of soil less effective for heat transfer. Sand-rich soil typically has a thermal conductivity that is higher than clay, but lower than rock and sandstone. Sandstone has a high quartz content, which increases its thermal conductivity. The proportion of quartz must be accurate because a low quartz percentage will affect the thermal conductivity of the sandstone, while a very high percentage will increase thermal conductivity beyond an adequate level and decrease the efficiency of heat transfer interactions in vertical GHEs [60]. Due to moisture migration, increasing the water content in soil results in higher thermal conductivity and decreases thermal resistance [61]. Hence, three important parameters—sand content, dry density, and degree of saturation—significantly influence the soil's thermo-physical properties and ultimately the heat exchange process between the circulating water inside the U-tube pipe and the surrounding ground. Soil thermal conductivity can be increased by adding additives such as quartz, bentonite, and metal particles as indicated by authors in [61].

The GHPS is site-dependent, meaning it only functions properly and attains maximum use of the earth's heat when the loop pipes are installed in a site with soil that has high thermal conductivity and a high capacity for heat conduction. Consequently, finding a suitable geological site with appropriate soil properties before the GHPS design

process commences is essential. Table 3.1 displays soil thermal properties, such as density, specific heat, and thermal conductivity.

Table 3.1 Soil thermal properties.

Parameters	Thermal Conductivity (W/m.K)	Specific Heat Capacity(J/kg.K)	Density (kg/m^3)
Sand	1.26	1710	1500
Clay	1.2	1800	1700
Sandy-silt	1.3	1200	1847
Sandy-clay	2.1	1200	1960

The authors in [62] evaluated the thermal properties of several soil materials including loam, clay, and sand using a coupled moisture diffusion and heat transfer model on unsaturated soil. The results demonstrated that the thermal migration ability of sand was better than loam and clay, whereas clay and sand had better moisture migration than loam. The authors in [63] developed a numerical model to assess the annual performance of the GHE across various soil types. The results revealed that a ground heat exchanger installed in sand performed 8% better than one installed in clay. The authors in [64] used finite element numerical simulation to examine the influence of unsaturated soil on the intermittent operation of the vertical ground heat exchanger system. The results showed that the saturated soil conditions could increase the mean heat exchange rate between the water inside the pipe and surrounding ground by up to 40% when compared to the unsaturated soil conditions. A good soil's thermal conductivity ranges between 1.5

and 5 W/m.K, which could contribute to a good GHE thermal performance. This concept was validated by the authors in [65].

3.2.2 Backfill Material Thermal Properties

The installation of vertical GHEs on sites with thermal soil is not the only concern; additional steps must also be taken, such as backfilling the borehole with suitable material. Following the insertion of the U-tube pipe into the borehole, the space between the pipe and the borehole wall must be completely grouted to ensure the grout fills the borehole without any air gaps, which can cause thermal discontinuity (i.e., contact resistance) [23]. In addition, preventing the borehole wall from collapsing and groundwater contamination from occurring extends system life and provides an efficient transfer of heat between the water inside the pipe and the surrounding ground. The backfill material's thermal conductivity affects the borehole thermal resistance, and basically the entire performance of the GHE. Highly conductive backfill material can reduce the borehole thermal resistance, whereas low conductivity backfill causes higher thermal resistance.

Many experimental studies on backfill materials have been conducted. For instance, the thermal conductivity of backfill materials ranges between 1.7 to 2.5 W/m. K, as noted by the authors in [66]. The authors in [67] studied the impact of the backfill material on the temperature distribution of the vertical ground heat exchanger. They concluded the importance of using high thermal conductivity backfill material to establish a strong connection between the pipe and the surrounding soil and the necessity of avoiding the use of high shrinkage backfill material because it can result in a reduction

in the heat flux surrounding the pipe. Moreover, the authors in [68] assessed the vertical GHE's borehole thermal resistance components and revealed that the backfill material thermal resistance—which accounts for more than 65% of the total borehole thermal resistance—plays a crucial role in the transfer of heat between the pipe and the surrounding ground. Giving this occurrence, the GHE performs well in terms of thermal performance when the borehole thermal resistance is low. Furthermore, the authors in [69] investigated how the backfill material influences the rate of heat transfer. The findings demonstrated that improving thermal conductivity could enhance heat transfer efficiency between the water inside the U-tube pipe and the surrounding ground, as well as increase the heat capacity of the GHEs. Also, the author in [70] investigated the positive effect of the thermal conductivity of the backfill materials using four different U-tube pipe diameters. The results showed that increasing the thermal conductivity of backfill material can reduce the pipe length, where the biggest reduction occurred in a double U-tube pipe De 32mm (outer diameter), followed by a double U-tube De 25mm, a single U-tube De 32mm, and a single U-tube De 25mm. The authors in [71] noted that the moisture migration in the soil increased the gap between the U-tube pipe and the soil, further increasing the borehole thermal resistance and thus reducing the system performance. To reduce moisture migration and further enhance heat diffusion, the authors in [72] suggested using a sand/kaolin blend as the backfill material for vertical GHEs. Overall, the selection of the appropriate backfill material relies on the thermal properties, GHE’s operational modes, and economic conditions.

Grout diameter is the distance from the pipe to the borehole wall and has a positive effect on the performance of the borehole heat exchanger because of its high capacity for

heat conduction. The grout diameter typically ranges from 0.10 to 0.22 m. The authors in [63] tested grout with various diameters of 0.10, 0.14, 0.18, and 0.22 m. The optimum grout diameter was determined to be 0.14 m.

Some of the pure materials used to backfill the borehole space between the U-tube pipe and the surrounding soil of the vertical GHEs include sand, clay, and gravel. In addition, cement materials are preferred for utilization in dry soil because of their high desiccation and shrinkage properties [73]. The authors in [74, 75] pointed out that sand and cementitious materials outperform the other types of pure materials in terms of geological location and thermal properties, making them more desirable for use. The authors in [76] pointed out that the thermal conductivity of the pure backfill ranges from 0.8 W/m.K to 2.4 W/m.K, but it could be increased when mixed with other materials.

Mixed materials are primarily composed of pure materials that are combined with one or more additional mediums, depending on each material's condition, to enhance the thermal properties thereof. These mixtures contain materials like graphite, acrylic latex, pure silica, and quartz, among others. Bentonite is a form of phyllosilicate clay primarily made of montmorillonite and is regarded as a potential backfill material additive for vertical heat exchanger uses because of its high ability to absorb water, as well as its poor hydraulic conductivity [77-79]. Historically, GHPS installations used bentonite with various additives to enhance its thermal conductivity. In the late 1980s, granular bentonite-water mixtures were being used as backfill materials [80]. However, these mixed materials have a low thermal conductivity, ranging from 0.65 W/m.K to 0.9 W/m.K. Thus, their thermal conductivity could be enhanced. Today, thanks to the prior work of researchers in this area, the most utilized backfill material in vertical GHEs is

bentonite, followed by silica sand and coarse/fine sand, bentonite and water mixtures, and concrete backfill materials. For example, the authors in [81] improved the sand/bentonite blend thermal conductivity by a graphite addition. The addition of quartzite sand to bentonite-based grout can improve its thermal conductivity as demonstrated by the authors in [82]. In addition, the authors in [66] concluded that adding graphite and silica to bentonite grouts can enhance their thermal conductivity. As they added more of each, the viscosity and thermal conductivity increased, indicating the amount of graphite and silica in bentonite and their composition play a key role in the overall thermal properties. Graphite could also be used to enhance cement thermal conductivity as demonstrated by the authors in [83]. The authors in [70] observed that incorporating bentonite into the main soil can improve its thermal conductivity. Furthermore, the authors in [84] demonstrated that mixing cement with silica sand and graphite can increase its thermal conductivity by 2.6 W/m.K when undergoing tested in situ thermal response testing (TRT). Better yet, the authors in [66] concluded that adding graphite or silica sand to backfill material can increase its thermal conductivity to reach 3.5 W/m. K. Even better, the authors in [85] enhanced the thermal conductivity of the backfill by adding graphite flakes to bentonite. According to the results, thermal conductivity could reach 5 W/m. K.

Improving the thermal properties of backfill materials could dramatically enhance the vertical GHEs overall efficiency, as the authors in [86] demonstrated. By increasing the thermal conductivity of the backfill material to 3 W/m. K it improved heat extraction by 10%, decreased the thermal gradient in the borehole, and enhanced the efficiency of the heat exchanger rate per meter. The authors in [87] concluded that the heat transfer rate can be increased by 40% and 48%, respectively, by

increasing the thermal conductivity of both the ground and backfill material from 0.5 to 2 W/m.K. Furthermore, the authors in [88] observed that increasing the thermal conductivity of backfill materials from 0.7 W/m.K to 2.3 W/m.K can reduce borehole thermal resistance from 0.135 m.K/W to 0.054 m.K/W. Additionally, the authors in [89] concluded that using quartz sand instead of bentonite can reduce the borehole thermal resistance by 30%. Furthermore, the authors in [90] concluded that utilizing the enhanced bentonite-based backfill materials could shorten the borehole by 10% of its total length. Backfilling the geothermal borehole with a sand-bentonite mixture can increase the heat exchanger rate by up to 31% when compared to standard sand-clay material, as discovered by the authors in [91]. Consequently, the backfill material should have high thermal conductivity and be at least the same or higher than the surrounding soil to promote the heat transfer process between the water inside the pipe and the surrounding ground.

3.2.3 Borehole Layout

Heat transfer increases with the depth of the borehole until it reaches a point where heat loss exceeds heat gain. At that point, the temperature difference between the input and output fluid increases, and heat transfer efficiency drops, causing higher initial capital costs. It is important to note that the borehole length is the most expensive aspect of the system installation while also being the most important geometric factor influencing the vertical GHE's performance. As a result, it is critical to choose the appropriate length to achieve the desired temperature from the earth's heat while lowering the initial capital cost. Surprisingly, increasing the depth of the borehole does not provide

as many advantages in terms of system efficiency and the economy as other performance factors, such as improving backfill material. This is primarily because the water needs more energy to circulate because it takes longer as the borehole depth increases. Reduced borehole depth can reduce water circulation pump power consumption and vice versa as stated by the authors in [23]. Hence, the borehole depth should not be too deep. To limit heat losses, the authors in [92] suggested that the depth of the single borehole would be approximately 80 m. Furthermore, the authors in [93] proposed that the borehole depth for double U-tube pipe De32 mm (outer diameter) should be between 80 and 100 m, while the depth for double U-tube pipe De 25 mm should be between 80 and 100 m. The influence of thermal interference decreases as borehole depth and borehole diameter increase, as stated by the authors in [94].

Some GHE configurations have a better ability to lower borehole thermal resistance and enhance system performance than others. For example, the authors in [95] examined the thermal resistances of two boreholes with double and single U-tube pipe configurations. They found that the double U-tube borehole outperformed the single U-tube borehole, as demonstrated by the fact that the thermal resistance of the double U-tube borehole was 30 to 90% lower than those in a single configuration. Better yet, more heat transfer performance was achievable when the double U-tube configuration was connected in parallel instead of in series. For instance, the authors in [96] developed a mathematical model to investigate the heating thermal performance of a U-tube GHE in both series and parallel configurations. According to their findings, the parallel configuration outperformed the series configuration in terms of heating performance. Moreover, the authors in [33] compared the heat transfer performance of single and

double U-tube BHE configurations connected in series and parallel. They noticed that the double U-tube BHE configuration outperformed the single U-tube BHE configuration in both series and parallel connections. Even better, the authors in [97] concluded that the performance of the multi-U-tube borehole configuration was superior to that of the double-U-tube and single-U-tube borehole configurations.

Additionally, the separation between two boreholes affects their thermal resistance. Hence, it is important to choose enough space between two boreholes to effectively avoid the negative effects of thermal interference, which improves GHE thermal performance efficiency. Thermal interference occurs when there is a small space between two boreholes. However, thermal interference can be avoided when there is a large distance between two boreholes, but this results in higher initial capital and operating costs because it requires more land to install the GHE pipes and additional pipes to connect. Thus, this distance should neither be too small nor too large. Notably, increased space between two boreholes can dramatically enhance the heat transfer performance of GHEs, as stated by the authors in [98]. The authors in [31] found that there should be 4.5 to 6 m between each borehole. Finally, the authors in [99] pointed out that the optimum space between two boreholes is 5 m, and thermal interferences can be neglected.

3.2.4 Pipe Thermal Properties

The pipe functions as a heat transfer contact between the liquid (i.e., water or antifreeze) within the pipe and the surrounding soil. Heat transfer performance is influenced by the pipe material's thermal conductivity. Hence, the material of the pipe

should have good thermal properties to promote the heat exchanger process in either direction. High-density polyethylene (HDPE) pipe is used in many GHPS engineering applications owing to its durability, flexibility, and longer lifespan of up to 50 years [12]. However, its thermal conductivity ranges between 0.35 W/m.K and 0.49 W/m.K [100] [101], indicating that the pipe material has a lower thermal conductivity than the water and surrounding soil. This decrease causes a reduction in the GHE's performance. Thus, the thermal conductivity of the pipe material should be increased to promote heat transfer performance between the water inside the pipe and the surrounding soil. For example, the authors in [102] mixed both 0.002 m and 0.003 m micro aluminum wire with the original HDPE pipe material. They found that the thermal conductivity of the new composite material increased by 25% and 150%, respectively, when compared to the original HDPE pipe. The authors in [103] added longitudinal fins to the inner surface of the original HDPE pipe, which increased the heat extraction by 7% in comparison to the original. Better yet, the authors in [104] enhanced the thermal conductivity of the HDPE material by incorporating graphite into its original material. The results showed that the new composite graphite/HDPE reduced the borehole length by 12.76%, in comparison to the original HDPE pipe. Even better, the authors in [105] added polymer resin to the original HDPE pipe and mixed other certain additives to the original HDPE pipe's polymer resin. The findings demonstrated that the thermal conductivity of the improved pipe material increased by 75% from 0.4 W/m.K to 0.7 W/m.K, which could reduce the borehole thermal resistance by 24% when compared to the original HDPE pipe. Thus, improving the thermal conductivity of the pipe material provides some benefits, such as reduced borehole thermal resistance, increased heat extraction, and shorter pipe length, thus

lowering initial installation capital and operation costs.

The U-tube pipe's leg-to-leg spacing is referred to as the "shank space," as shown in Figure 3.2. U-tube pipes must have appropriate spacing between their legs to increase the heat flow rate and raise the output fluid temperature. This will prevent the thermal short circuit phenomenon, lowering heat transfer efficiency. This phenomenon occurs when the shank space is extremely small or the pipes come into contact [106]. Therefore, the U-tube pipes must be positioned in the center of the borehole with the appropriate spacing between them to prevent thermal short circuits, enhance the heat transfer rates, and reach the desired output temperature.

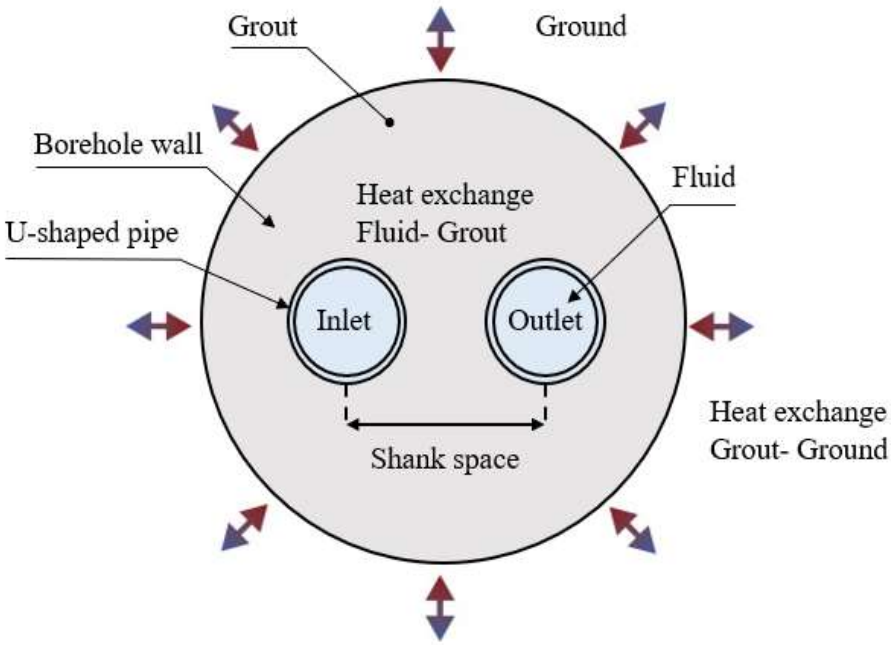

Figure 3.2. Illustration of shank-space in a horizontal cross-section through a U-tube pipe of the vertical GHE.

The authors in [106] investigated the effect of different shank spacings on thermal heat transfer rates, including 0.01 m, 0.02 m, 0.04 m, 0.06 m, 0.08 m, and 0.10 m. The results showed that the heat transfer rate and output temperature increased as the shank space increased. They determined that if the shank space was less than 0.06 m, a thermal short circuit would occur, resulting in heat transfer deterioration [107]. Yet, when the space exceeds 0.06 m a thermal short circuit cannot occur, and the influence of shank spacing becomes insignificant. For instance, the shank spacing between two U-tube legs in this GHPS system was 0.07 m, and no thermal heat short circuit occurred [108]. Furthermore, the Oakland University GHPS shank spacing was 0.085 m and no thermal short circuit transpired [27]. Better yet, the heat transfer rate was stabilized if the shank spacing was larger than 0.09 m [63]. Even better, the optimum spacing was identified as being between 0.1 m and 0.2 m [99].

3.2.5 Working Fluid Properties

3.2.5.1 Fluid Type

The working fluid—usually water, or antifreeze solution—flows continuously in loop pipes to transfer heat between the ground and the heat pump system and vice versa. To avoid convection thermal resistance between the fluid inside the pipe and the surrounding ground, the working fluid should have high thermal conductivity, low viscosity, and high heat capacity. The authors in [109] assessed the thermal properties of three different working fluids, including water, gasoline, and glycol. The results showed that water can absorb, store, and recover more thermal energy than gasoline and glycol. Pure water was used as the heat-carrying fluid in GHPS systems because of its high

capacity to absorb and store, as well as its availability and low cost. However, despite all its benefits, water lacks antifreeze properties. Therefore, in cold regions, water must be treated with antifreeze to keep it from freezing and causing system damage. It is important to note that when mixing antifreeze with the working fluid, the volume concentration must be precise to avoid freezing and achieve good viscosity. This could enhance GHE's thermal performance without significantly increasing operating costs [63, 110]. If the concentration is not in the optimum proportion, it can impact the convective thermal resistance (i.e., between the fluid inside the pipe and the inner pipe wall).

Furthermore, the working fluid affects the thermal performance of the GHE. The authors in [111] pointed out that calcium chloride 20% solution outperforms propylene glycol at 25%, 33%, and 24% volume concentrations, as well as ethanol at 24% volume concentration. In a mild climate, the GHE's fluid temperature with 25% ethylene glycol mixed with water is higher than that of pure water [112]. Nanofluids' viscosity and heat capacity are important in geothermal energy extraction, as indicated by the authors in [113]. The nanofluid's thermal conductivity increases as the particle volume fraction increases and the nanoparticle size decreases [114, 115]. Using AI_2O_3/water nanofluid as a heat transfer carrier instead of pure water can reduce the vertical GHE borehole depth by 1.3%, as stated by the authors in [116]. The authors in [117] assessed four types of hybrid nanofluids, including, Fe_3O_4 multi-wall carbon nanotube/water, Al_2O_3-CuO/water, TiO_2-Cu/water, and Ag-MgO/water. The results showed that the Ag-MgO/water was found to be the most appropriate heat-working fluid compared to other hybrid nanofluids. Furthermore, using an Ag-MgO/water hybrid nanofluid as a working fluid with a 0.1 volume fraction of nanoparticles and a Reynolds number of 3200 could reduce the

borehole thermal resistance of a single U-tube GHE by 1.14% when compared to pure water. Additionally, the addition of hybrid nanofluids within a microchannel can dramatically improve the thermal convective heat transfer coefficient, as stated by authors in [118]. Despite the obvious improvement in the convective heat transfer coefficient using nanofluid technology as a heat-carrying fluid, it is still relatively new for use in geothermal heat pump systems. Therefore, more theoretical, and empirical research on nanofluid technology should be conducted.

3.2.5.2 Fluid Velocity

Many studies have been conducted on the effect of water velocity within the U-tube pipe on the exit temperature and heat transfer performance in the vertical GHE. For example, the authors in [93] examined how increasing the water velocity through vertical ground heat exchanger pipes with varying diameters and configurations affected heat transfer performance. The findings demonstrated that the optimum water velocity ranges for a single U-tube De 32 mm (outer diameter of 32 mm), a double U-tube De 25 mm (outer diameter of 25 mm), and a double U-tube 32 mm are between 0.4 and 0.6 m/s, 0.4 and 0.5 m/s, and 0.3 and 0.4 m/s, respectively. The authors in [119] pointed out that to maximize the benefits of the earth's energy, the optimal water velocity range for a single U-tube should be between 0.4 and 0.7 m/s. Similarly, the authors in [120] also investigated the impact of water velocity on heat transfer performance in the U-tube De 32 mm. They found that the water velocity should be between 0.3 and 0.4 m/s for optimal heat transfer efficiency. The authors in [121] assessed the influence of flowing water velocity on the heat exchanger rate by applying three different water velocities: 0.26 m/s,

0.51 m/s, and 1.02 m/s, where the input water temperature was kept constant at 35 °C during the operational test. The findings revealed that the heat exchanger rates per meter were 84 W/m, 116 W/m, and 94 W/m when the water velocities were 0.26 m/s, 0.51 m/s, and 1.02 m/s, respectively. The heat exchange rate of 116 W/m was higher when the water velocity was 0.51 m/s compared to 0.26 m/s and 1.02 m/s. The heat exchange rate per meter was insufficient due to the high-water velocity. As a result, the appropriate circulating water velocity range is between 0.5 and 0.6 m/s. In addition, controlling water velocity can lower the borehole thermal resistance and thereby enhance the heat transfer efficiency, as findings from [122] pointed out. The authors in [96] concluded that decreasing the fluid flow rate can improve the vertical GHE heating performance. The authors [123] examined the thermal heat performance of a U-tube GHE in a warm climate at four inlet water temperatures: 30, 35, 40, and 45 °C. They concluded that the heat transfer coefficient and heat exchanger rate are improved by increasing the GHE's inlet water temperature.

Furthermore, the authors in [124] developed a numerical model to investigate the influence of water velocity on the heat transfer efficiency of deep borehole heat exchangers (DBHE). They concluded that the water velocity should be between 0.3 and 0.7 m/s for better performance. Moreover, the authors in [125] presented a heat transfer model to analyze the heat exchanger performance and temperature distribution of a vertical double U-tube BHE with a variety of flow velocities ranging from 0.1 to 0.5 m/s. According to their simulation results, when the flow velocity was between 0.1 to 0.3 m/s, the heat exchanger rate was higher than when the flow velocity exceeded 0.3 to 0.5 m/s. Meanwhile, the optimum flow velocity result was recorded at 0.3 m/s. The authors in

[106] developed a 3D transient heat transfer model based on the finite volume method (FVM) to investigate the effect of fluid flow rate on the output fluid temperature and heat transfer rate. They applied different flow rates ranging from 0.1 m^3/h to 1.2 m^3/h in the U-tube De 32 mm. According to their simulation results, the output fluid temperature increased when the liquid flow rate increased from 0.1 m^3/h to 0.7 m^3/h but decreased as the flowing rate moved beyond 0.7 m^3/h to 1.2 m^3/h. Notably, this simulation did not use the same unit of measure (i.e., m/s vs. m^3/h); however, these results equate to 0.57 to 0.76 m^3/h. Therefore, after converting, we found that 0.57 to 0.76 m^3/h equates to 0.3 and 0.4 m/s. Additionally, the authors in [106] and [120] agreed that the optimal water velocity range in the U-tube De 32 mm is between 0.3 and 0.4 m/s. Furthermore, the authors in [23] presented a mathematical model of heat transfer behavior between the water inside vertical underground pipes and the surrounding ground to examine the influence of water velocity on the output water temperature. The simulation results indicated that the output water temperature reaches the ground when the water velocity is reduced sufficiently enough to allow complete heat exchange between two heat mediums (i.e., the water and surrounding ground). To maximize the benefit of the earth's temperature, the authors in [23] determined that the optimum water velocity ranges in vertical single U-tube pipes with outer diameters of De 25 mm (outer diameter of 25 mm), De 32 mm (outer diameter of 32 mm), and De 40 mm (outer diameter of 40 mm) at a depth of 98 m should be between 0.33 and 0.43 m/s, 0.35 to 0.45 m/s, and 0.38 to 0.48 m/s, respectively. These studies demonstrated that the water velocity should be neither too high nor too low to promote better heat transfer and maximize the output temperature without wasting any additional power, which is needed to increase the water velocity. When the flow velocity

is low, the water temperature reaches the desired temperature (i.e., ground temperature) well before the exit, making the remainder of the pipe useless. However, when the water velocity is high, more power is required to increase its velocity. Ultimately, the output water temperature will not reach the ground due to the insufficient time for the heat exchange between the water and the ground to reach equilibrium. Therefore, controlling water velocity is crucial to achieving the desired output temperature [23].

3.3 Summary

This chapter provided a comprehensive discussion of the vertical GHE performance factors, or essentially, the heat transfer efficiency between the flowing liquid inside the pipe and the surrounding ground. Additionally, this chapter highlighted data on the effect of each performance aspect on the initial capital costs.

The first performance factor is related to the thermal properties of the soil. The installation of the GHPS at a site with poor soil thermal properties may correctly function, but it will not get maximum benefits from the heat of the Earth because of the soil's low thermal conductivity, which causes heat to flow slowly between its layer and the liquid inside the pipe. However, installing GHPS on a site with good thermal properties will allow for efficient heat transfer between the ground and the liquid inside the pipe, maximizing the benefits of the earth's heat. Therefore, it is essential to choose a suitable geological site with better soil—preferably moist soil, sand, or sandstone.

The second performance factor focuses on using a material with low thermal conductivity to backfill the space between the U-tube pipe and borehole wall increases the thermal resistance of the borehole and, ultimately, results in an inefficient heat

transfer. The space between the U-tube pipe and surrounding soil must be completely grouted to ensure that the grout fills the borehole without any air gaps, which can cause thermal discontinuity (i.e., contact resistance), to prevent the borehole wall from collapsing and groundwater contamination, which extends system life. This enables a strong connection between the pipe and the surrounding ground, which provides an efficient transfer of heat in either direction. Some suggestions include adding components like graphite flakes, silica, or enhanced bentonite-based backfill material to bentonite or other minerals like quartz sand to obtain adequate backfill materials with good properties. There are significant benefits to using high thermal conductivity backfill materials, such as a 30% reduction in borehole thermal resistance, a 31% increase in heat exchanger rate, a 10% increase in heat extraction, a 10 % reduction in thermal gradient, and a 10% reduction in borehole depth, all of which lead to a lower initial capital cost [89] [91] [86] [90].

Next, the borehole depth is a critical factor to consider regarding the performance. Heat transfer increases with the borehole depth up until a point where heat loss is more than it gains. Therefore, some suggestions include the depth and configuration of the geothermal borehole to limit heat losses and maximize the benefits of the earth's heat. The borehole depth would be approximately between 80 m and 100 m for single and double U-tube De 0.032 m pipes, respectively [92, 93]. Additionally, the multi-U-tube borehole configuration performs better than the single-U-tube and double-U-tube configurations [97]. The optimum distance between the two boreholes is 5 m to prevent thermal interference, which reduces GHE efficiency [99].

Another important performance factor to consider is that the pipe material should have high thermal conductivity to promote efficient heat transfer between the liquid within the pipe and the surrounding earth. The HDPE pipe is most used in GHPS engineering applications due to its durability, flexibility, and long lifespan, but its material thermal conductivity is relatively low compared to soil and liquid. The pipe's low thermal conductivity can increase the borehole's thermal resistance, ultimately reducing the flow of heat in either direction. Consequently, increasing the thermal conductivity of pipe material is important. Some suggestions have been made to increase the pipe material's thermal conductivity, including adding micro-aluminum wires, polymer resin, or longitudinal fins to the inner surface of the original HDPE piping. Enhancing the pipe material's thermal conductivity could bring some benefits, such as a 7% increase in heat extraction, a 12.76% reduction in borehole length, and a 24% decrease in thermal resistance [103-105].

The fifth performance factor focuses on leaving enough shank space to prevent the thermal short circuit phenomenon, which makes heat transfer ineffective. A thermal short circuit and deterioration in heat transfer will happen if the shank space is less than 0.06 m [107]. Yet, the optimum shank spacing is between 0.1 and 0.2 m [99].

Finally, the last performance factor is the working fluid, thus it should have high thermal conductivity, low viscosity, and high heat capacity to prevent convection thermal resistance between the fluid inside the pipe and the surrounding soil. Water mixed with antifreeze is the most used heat carrier in ground heat exchanger systems. Enhancing the thermal properties of the working fluid could consequence in some advantages, such as a 1.3% reduction in borehole depth and a 1.14% reduction in U-tube GHE borehole

thermal resistance [112] [116] [117]. The water velocity should be within the ideal range, which is neither too high nor too low,(e.g., 0.33 to 0.43 m/s for a single U-tube De 0.025 m, 0.35 to 0.45 m/s for a single U-tube De 0.032 m, and 0.38 to 0.48 m/s for a single U-tube De 0.04 m) to maximize output temperature and promote better heat transfer without wasting any additional power that would be needed to increase the water velocity [23]. Therefore, controlling water velocity, among other performance factors, is crucial to achieving the desired GHE output temperature and can reduce power consumption for the water circulation pump and heat pump, thereby improving system performance [23]. These GHE performance factor discussions can be used as a helpful guide for the design of vertical ground heat exchangers.

CHAPTER FOUR

MODELING HEAT TRANSFER

4.1 Heating and Cooling Modes

The following are the mechanisms by which heat is transferred between the flowing water in the underground pipe and the surroundings: through convection, the heat transfers from the flowing water to the inner pipe wall, and by conduction from the inner pipe wall to the outer pipe wall and from the outer to the surrounding soil. The underground medium, which includes pipe material, backfill material, and soil, has a direct influence on the heat transfer performance of the vertical Ground Heat Exchanger (GHE) because each medium has its thermo-physical properties, including thermal conductivity, density, and specific heat capacity [126, 127]. Figure 4.1a depicts the behavior of heat transfer between the water inside the vertical U-tube pipe and the surrounding ground for the heating mode. $T(x)$ is the water temperature, T_g is the ground temperature, L is the pipe length, and ΔT is the temperature difference, which was calculated $\Delta T = T_g - T(x)$. When the room temperature is cooler than the ground, the Geothermal Heat Pump System (GHPS) operates in its heating mode, in which the cooled water is pumped into the ground through the loop pipes. At the pipe's beginning ($x = 0$), the heat transfers quickly from the ground to the water due to the large temperature difference ΔT and continue to transfer until the temperature difference is around zero ($\Delta T \approx 0$) if the water velocity is low enough. The water temperature $T(x)$ reaches the ground temperature T_g when the water velocity is low enough to allow sufficient time for heat to exchange and reach equilibrium. The heat transfer mechanisms can be classified

as high heat transfer, low heat transfer, or no heat transfer based on the ΔT value, as shown in Figure 4.1.

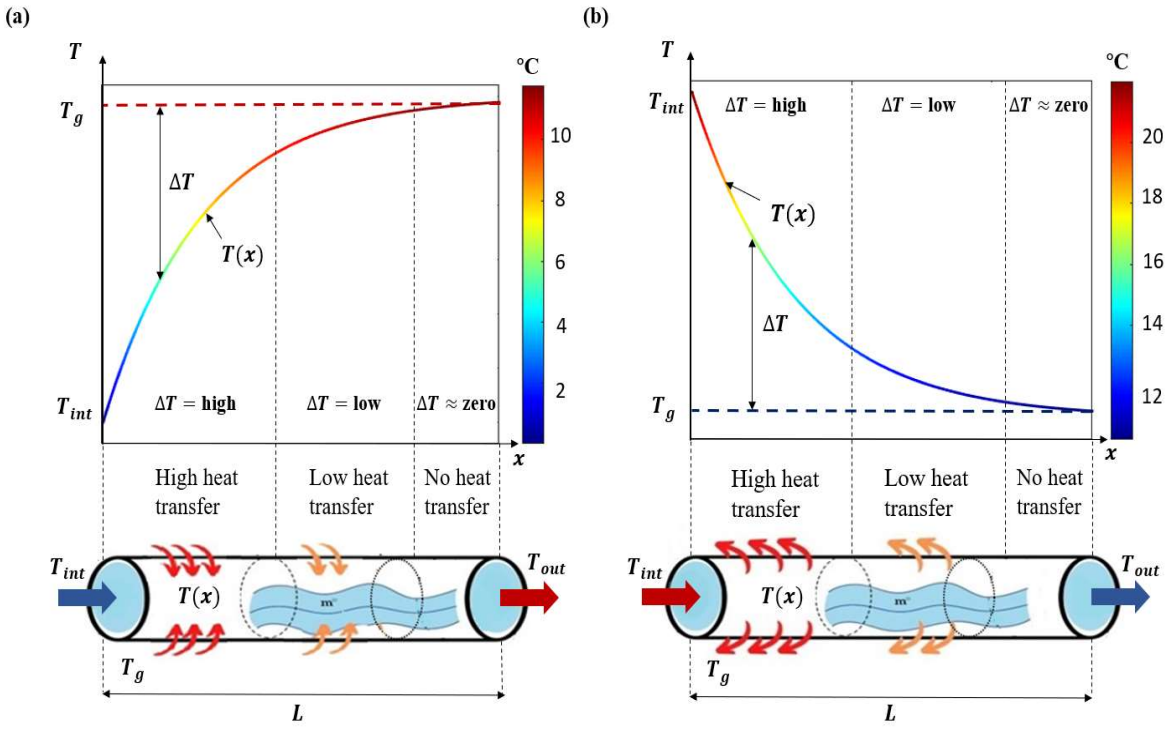

Figure 4.1. Schematic diagram of heat transfer behavior of the vertical GHE for (a) heating mode and (b) cooling mode [23].

High heat transfer occurs when the temperature difference is large ($\Delta T = large$), low heat transfer occurs when the heat transfer is small ($\Delta T = small$), and no heat transfer occurs when there is no temperature difference ($\Delta T \approx 0$), which typically occurs before the pipe's exit. The GHPS switches to a cooling mode in the summer when the room temperature is warmer than the ground. Consequently, the warmed water is pumped into the ground through the loop pipes. In this case, heat transfers from the water inside the

pipe to the surrounding ground, and the water temperature will continue to decrease as it flows until it reaches the ground temperature. The behavior of heat transfer between the water inside the vertical loop pipes and the surrounding ground for the cooling mode is depicted in Figure 4.1b. The temperature difference ΔT is determined as $\Delta T = T(x) - T_g$. The maximum benefits of the earth's heat can be obtained when the warmer water temperature is transferred to the ground. Further explanations, including numerical examples of a case study evaluating the heat transfer behavior of the vertical ground heat exchanger for both the heating and cooling modes, as well as the effect of water velocity on exit temperature, are presented in Chapter 7.

4.2 HEAT TRANSFER MODELING

4.2.1 Model Assumptions

The following assumptions are made to study the heat transfer behavior in a vertical, single-tube GHE configuration:

- One-dimensional, x-only modeling governs the heat transfer process
- Steady-state
- Heat transfers from the liquid inside the pipe and the pipe's inner pipe wall by convection and by conduction between the pipe's outer wall to the surrounding soil (in cylindrical coordinates)
- The soil and backfill material that surrounds the outside pipe wall is treated as a single medium with a single thermal resistance, R_v
- Groundwater flow has no impact on heat transfer
- During both heating and cooling modes, the ground temperature is assumed to

be constant (the water circulating loop is below the frost line)

- Water was chosen as a heat carrier in the GHE
- The following three thermal resistances are considered:
  - R_{conv}: liquid thermal resistance
  - R_{wall}: pipe thermal resistance
  - R_g: ground thermal resistance

4.2.2 Governing Equations

Figure 4.2 depicts the mass flow rate of water flowing uniformly in one direction through an underground pipe, which can be calculated using the formula $\dot{m} = \rho v A$. The $\dot{Q}_x$ is a heat flow in at the position x, the $\dot{Q}_{x+\Delta x}$ is heat flow out at $x + \Delta x$, and $\dot{Q}_p$ is the heat coming out of the water to the ground. This is a cooling mode in which the water temperature is warmer than the ground, and the heat is going out into the surrounding ground.

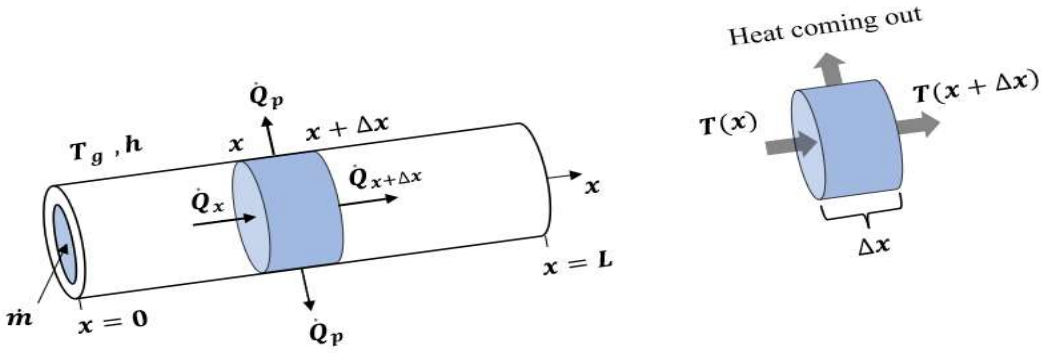

Figure 4.2. The rate of heat transfer from the water inside the pipe to the surrounding ground [23].

The heat transfer that can occur through the pipe from x to $x + \Delta x$ was modeled using the conservation of energy equation expressed:

$$\frac{dEs}{dt} = \dot{Q} + \dot{W}_s + \Sigma \dot{m} \left(h + \frac{1}{2} v + yz \right)_i - \Sigma \dot{m} \left(h + \frac{1}{2} v + yz \right)_o \quad (4.1)$$

where E is the system energy, s is the pipe surface, t is the time, $\dot{Q}$ is the heat transfer rate, $\dot{W}_s$ is the system work done (all types of work other than flow work), $\dot{m}$ is the water's mass flow rate, which equals $\dot{m} = \rho v A$, h is the convection heat transfer coefficient, ρ is the water density, A is the pipe's Cross-Section Area, and v is the water velocity. The total heat transfer rate is written as:

$$\dot{Q} = \dot{Q}_x - \dot{Q}_{x+\Delta x} - \dot{Q}_p \quad (4.2)$$

where $\dot{Q}_x$ is heat flow in at x, $\dot{Q}_{x+\Delta x}$ is heat flow out at $x + \Delta x$, and $\dot{Q}_p$ is the heat coming out of the water to the ground.

Substituting equation (4.2) into equation (4.1), implementing the model assumptions in section 4.1, and rechanging i (inner) and o (outer) with x and $x + \Delta x$, respectively, renders:

$$0 = \dot{Q}_x - \dot{Q}_{x+\Delta x} - \dot{Q}_p + \dot{m}(h_x - h_{x+\Delta x}) \quad (4.3)$$

Using Fourier's Model, express heat conduction in equation (4.3), in terms of temperatures, is shown as:

$$\dot{Q}_x = \left(-k\frac{dT}{dx}\right)_x,\ \dot{Q}_{x+\Delta x} = \left(-k\frac{dT}{dx}\right)_{x+\Delta x} \tag{4.4}$$

where k is the thermal conductivity of the liquid.

The rate of convective heat transfer from the water to the inner pipe wall is calculated using Newton's Law of Cooling equation [128]. The following equation (4.5) is used to determine the heat exchanger rate $\dot{Q}_p$ between the water and the ground temperature:

$$\dot{Q}_p = U_0 A_0[T(x)\ - T_g] \tag{4.5}$$

where U_0 is the overall heat transfer coefficient, A_0 is the surface area of the pipe, which equals $A_0 = P_0\Delta x$, P_0 is the outside periphery of the pipe, $T(x)$ is the water temperature at the position x, and T_g is the ground temperature. Substituting $\dot{Q}_x$, $\dot{Q}_{x+\Delta x}$, $\dot{Q}_p$, and P_0 into the equation (4.3) yields:

$$0 = \dot{Q}_x - \dot{Q}_{x+\Delta x} - U_0 P_0[T(x)\ - T_g]dx + \dot{m}(h_x - h_{x+\Delta x}) \tag{4.6}$$

Next, integrate equation (4.6) with the integration limits x to $x + \Delta x$:

$$0 = \int_x^{x+\Delta x} f q_x dA - \int_x^{x+\Delta x} f q_{x+\Delta x} dA - \int_x^{x+\Delta x} U_0 P_0[T(x)\ - T_g]dx + \dot{m}(h_x - h_{x+\Delta x}) \tag{4.7}$$

where:

$fq(x) = \left(-k\frac{\mathrm{dT}}{\mathrm{dx}}\right)_x$, $fq(x+\Delta x) = \left(-k\frac{\mathrm{dT}}{\mathrm{dx}}\right)_{x+\Delta x}$, and $(h_x - h_{x+\Delta x}) \approx C_{\mathrm{p}}(T_x - T_{x+\Delta x})$

By replacing the integration limits for these fq_x , and $fq_{x+\Delta x}$, we then get $fq_{x+\Delta x} - fq_x$ as follows:

$$0 = \left\{\left(kA\frac{dT}{dx}\right)_{x+\Delta x} - \left(kA\frac{dT}{dx}\right)_x\right\} - \int_x^{x+\Delta x} U_0 P_0\left(T(x) - T_g\right)dx - \dot{m}C_p(T_x - T_{x+\Delta x}) \qquad (4.8)$$

Multiplying equation (4.8) by $1/\Delta x$, then substituting the water's mass flow rate, which equals $\dot{m} = \rho v A$, and setting the limit as zero $\Delta x \to 0$, yields:

$$0 = kA\frac{d^2T}{dx^2} - U_0 P_0\left(T - T_g\right) - \rho v A c_p \frac{dT}{dx} \qquad (4.9)$$

The equation (4.9) represents the heat transfer equation in a second-order differential equation form. Dividing the equation (4.9) by A gives:

$$-k\frac{d^2T}{dx^2} = -\frac{U_0 P_0}{A}\left(T - T_g\right) - \rho v C_p \frac{dT}{dx} \qquad (4.10)$$

Substituting these $P_o = \pi d_o L$ and $A = \frac{\pi}{4} d_i^2$ into the equation (4.10), renders:

$$-k\frac{d^2T}{dx^2} = -\,4\,U_0 L\left(\frac{d_0}{d_i^2}\right)\left(T - T_g\right) - \rho v C_p \frac{dT}{dx} \qquad (4.11)$$

where L is the pipe length, d_i is the pipe's inner diameter, and d_o is the pipe's outer diameter.

4.2.3 Thermal Resistance Network

The heat transfer between the water inside the pipe and the surrounding ground is characterized by the borehole thermal resistance, which is reliant on the thermal properties of the U-pipe and its arrangement, backfill material, and soil. When transferring heat from the water inside the pipe to the surrounding ground, three thermal series resistances are considered: internal convection resistance, exterior convection resistance, and conduction thermal resistance, as depicted in Figure 4.3.

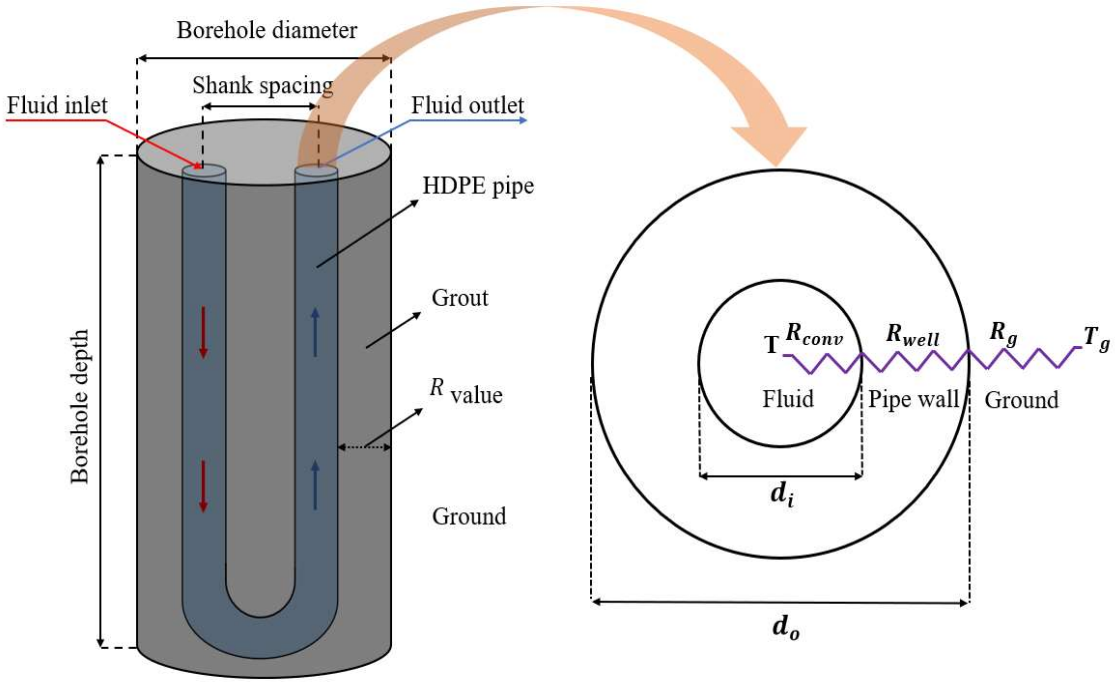

Figure 4.3 Diagram of a vertical single U-tube Ground Heat Exchanger (GHE) [23].

The total thermal resistances are calculated, which equals the sum of the three thermal resistances. These calculations are shown below in equation (4.12):

$$R_{th} = \frac{1}{h_i A_i} + \frac{ln\,(d_0/d_i)}{2\pi k} + R_g \tag{4.12}$$

Multiplying equation (4.12) by $\left(\frac{A_0}{A_0}\right)$ yields:

$$R_{th} = \left[\frac{1}{h_i}\left(\frac{A_0}{A_i}\right)\frac{1}{A_0} + \frac{A_0 ln\,(d_0/d_i)}{2\pi k L A_0} + R_g \frac{A_0}{A_0}\right] \tag{4.13}$$

Pulling out A_0 from the total thermal resistance equation (4.13) to obtain the R-value yields:

$$R_{th}A_0 = \frac{1}{h_i}\left(\frac{A_0}{A_i}\right) + \frac{A_0 ln\,(d_0/d_i)}{2\pi k L} + R_g A_0 \tag{4.14}$$

Simplifying the equation (4.14) in terms of diameter renders:

$$R_{th}A_0 = \frac{1}{h_i}\left(\frac{d_0}{d_i}\right) + \frac{d_0\ ln(d_0/d_i)}{k} + R_g 2\pi d_0 L \tag{4.15}$$

As aforementioned, when heat is transferred through the movement of a liquid or gas rather than a solid object, this is referred to as convection. The convective heat transfer coefficient (CHTC) is denoted by h_i and is measured in $\mathrm{W/m^2.℃}$. The CHTC, which is the most important factor in the heat transfer process between the water and inner pipe wall, is influenced by the water velocity and natural motion, as well as the temperature

difference. Using the Dittus-Boelter Equation (4.16) [129] to calculate the convective heat transfer coefficient produces the following equation:

$$N_{U_{d_i}} = 0.023\ P_r^{\,n} {Re_{d_i}}^{0.8} \tag{4.16}$$

where $N_{U_{d_i}}$ is a Nusselt Number that equals $\left(\frac{h_i di}{k_w}\right)$, P_r is a Prandtl Number that equals $\left(\frac{\mu\, Cp}{k_w}\right)$, Re_{d_i} is the flowing liquid's Reynolds Number which equals $\left(\frac{\rho\, v\, di}{\mu}\right)$, k_w is the water thermal conductivity (calculated at the film temperature), μ is the dynamic viscosity and c_p is the specific heat. Given this, n represents the heating/cooling exponent, which varies depending on the weather conditions. In the winter, when the GHPS is in heating mode and the water temperature inside the underground loop pipes is cooler than the surrounding ground temperature ($T_g > T(x)$), the exponent of heating equals 0.4. However, in the summer, GHPS operates in reverse in cooling mode, and the water temperature inside the pipe is warmer than the surrounding ground temperature ($T(x) > T_g$); in this case, the exponent of cooling equals 0.3.

By substituting these values $N_{U_{d_i}}$, P_r, and Re_{d_i} into the equation (4.16), we obtain the convective heat transfer coefficient h_i as provided below:

$$h_i = \left(\frac{k_w}{di}\right)(0.023)\left(\frac{\mu\, Cp}{k_w}\right)^n \left(\frac{\rho\, v\, di}{\mu}\right)^{0.8} \tag{4.17}$$

The overall heat transfer coefficient is denoted by U_0 and measured by how much heat transfers through these three series resistances, and its units $\mathrm{W/m^2.}$ ℃. The overall heat transfer coefficient U_0 is calculated using the following equation:

$$U_0 = \left\{ \frac{1}{h_i}\left(\frac{do}{di}\right) + \frac{do\ ln\left(\frac{do}{di}\right)}{k_p} + R_v \right\}^{-1} \tag{4.18}$$

where k_p is the pipe material's thermal conductivity, and R_v is the ground resistance. As seen in equation (4.18), there are three components, each of which represents thermal resistance (R-value), which $\frac{1}{h_i}\left(\frac{do}{di}\right)$ represents the water convection R-value, $\frac{do\ ln\left(\frac{do}{di}\right)}{k_p}$ represents the R-value of pipe wall conduction, and R_v represents the R-value of ground resistance. According to equation (4.18), the overall heat transfer coefficient U_0 is inversely proportional to the sum of three R-values. This indicates that when the R-values are high, heat transfers from the hot to the cold region at a lower rate, and vice versa. For example, if the pipe wall's thermal resistance is high, it acts as a physical barrier, thereby reducing heat transfer between the ground and the water inside the pipe. Lowering borehole thermal resistance (i.e., three thermal resistances) is therefore critical for maximizing the benefits of the earth's heat, which is dependent on liquid thermal properties, pipe material thermal conductivity and thickness, backfill material thermal conductivity, and soil thermal conductivity, as discussed in Chapter 3. Further numerical examples of real-world case study explanations of the relationship between the overall heat transfer coefficient and thermal resistance are presented in Chapter 7.

Thus, I obtained the steady-state heat transfer equation in its final form, which describes the behavior of heat transfer between the water inside the vertical underground pipe and the surrounding ground for the heating mode (4.19a) and cooling mode (4.19b).

For heating mode:

$$-k\frac{d^2T}{dx^2} = -\rho v c_p \frac{dT}{dx} - 4\left(\frac{do}{di}\right)U_0(T_g - T) \tag{4.19a}$$

For cooling mode:

$$-k\frac{d^2T}{dx^2} = -\rho v c_p \frac{dT}{dx} - 4\left(\frac{do}{di}\right)U_0(T - T_g) \tag{4.19b}$$

CHAPTER FIVE

CONTROLLING HEAT TRANSFER

This chapter presents the design of model predictive control (MPC) for heat transfer between the water inside the pipe and the surrounding ground of the ground heat exchanger. The chapter starts with an illustration of converting the heat transfer model's ordinary differential equation (4.19), to a state space model representation. It is followed by the linearization process, which ensures the system is controllable and observable at the assumed operating point. The second part of the chapter presents the MPC technique design, which controls the water velocity inside the loop pipes to optimize the GHE's water temperature to achieve the desired temperature. Finally, a real-world case study of Oakland University’s GHPS is used to demonstrate the principle of energy conservation regarding the water circulation pump.

5.1 Bilinear State Space Model

The heat transfer mechanism in the borehole between the working fluid (i.e., water) inside the pipe and the surrounding soil balances the water velocity with the output temperature, controlling water flow to reach the desired output temperature. For this system's physics parameters, the water velocity is an input control variable, the output temperature is the system output, and the ground temperature is a disturbance to the system. Due to the varying water flow rates through the pipe and the dynamic heat transfer in the borehole, the typical system is nonlinear. This subclass of nonlinearity is also referred to as a bilinear system (BLS) and occurs when the dynamic behavior of the

system is influenced by a varying input or other external disturbance to the system. A BLS can behave in a variety of contexts, including chemical reactions, physics, and thermal energy. For example, in this study, water velocity influences the heat transfer process between the water inside the pipe and the surrounding ground, which is basically an inherited bilinear phenomenon. The BLS can be represented as an input-output system (i.e., transfer function) or a state-space model system. The continuous BLS is written in the following equation (5.1).

$$\begin{cases} \dot{x}(t) = A(t)x(t) + B(t)x(t)u(t) \\ y(t) = Cx(t) + Du(t) \end{cases} \tag{5.1}$$

where the $x(t)$ is a state vector, $u(t)$ is an input control vector and $y(t)$ is a control output vector. The A represents a state matrix, B represents an input matrix, C represents an output matrix, and D represents a direct transmission matrix for input (which directly connects the input and output). We converted the mathematical model of the heat transfer equation (4.19) into a state-space model representation, which is written as follows:

$$\begin{cases} \begin{bmatrix} x_1'(t) \\ x_2'(t) \end{bmatrix} = \begin{bmatrix} 0 & 1 \\ \frac{4}{k}\left(\frac{do}{di}\right)U_0 & 0 \end{bmatrix} \begin{bmatrix} x_1(t) \\ x_2(t) \end{bmatrix} + \begin{bmatrix} 0 \\ \frac{\rho c_p}{k} x_2 \end{bmatrix} u(t) \\ y(t) = [1 \quad 0] \begin{bmatrix} x_1(t) \\ x_2(t) \end{bmatrix} \end{cases} \tag{5.2}$$

5.2 System Linearization and Discretization

The heat transfer model in equation (4.19) is a nonlinear system, so designing a nonlinear control to attain optimal performance is a difficult challenge that could result in lower performance than the linear control. Therefore, by linearizing the system around a particular operating point based on the assumed initial condition value, thus, designing a Model Predictive Control (MPC) is suitable to achieve optimal performance. In this study, we utilized MATLAB's function "linmode" to linearize the system model (4.19), which returns the nonlinear ordinary differential equation built-in Simulink block into Command-Window as linear state-space matrices A, B, C, and D. The system state-space model is linearized at one operating point and expressed in the following equation (5.3).

$$\begin{cases} \begin{bmatrix} x_1'(t) \\ x_2'(t) \end{bmatrix} = \begin{bmatrix} 0 & 1 \\ -1.6 & 0 \end{bmatrix} \begin{bmatrix} x_1(t) \\ x_2(t) \end{bmatrix} + \begin{bmatrix} 0 \\ -2.53 \end{bmatrix} u(t) \\ y(t) = [1 \quad 0] \begin{bmatrix} x_1(t) \\ x_2(t) \end{bmatrix} \end{cases} \tag{5.3}$$

Before applying the control technique to the system model, it must be controllable and observable at the operating points. Here, I tested the controllability and observability of the linearized state space system model (5.3) using the Kalman test. The following are controllability and observability matrices, respectively.

$$Q_{\mathrm{C}} = [B \vdots AB \vdots A^2B \vdots \cdots\cdots \vdots A^{n-1}B]_{n*n}$$

$$Q_{\mathrm{P}} = [C^T \vdots (A^T)^2\, C^T \vdots CA^2B \vdots \cdots\cdots \vdots CA^{n-1}B]_{p*nm}$$

where Q_{C} is the controllability matric, Q_{P} is the observability matrix, and n is the system order. The system is controllable and observable if the $Q_{\mathrm{C}}, Q_{\mathrm{P}}$ have the full rank of the system order, i.e., rank $Q_{\mathrm{C}} = Q_{\mathrm{P}} = n$. In the meantime, the determinants of Q_{C} and $Q_{\mathrm{P}} \neq 0$. Since the $|Q_{\mathrm{C}}| = 1.6 \neq 0$ and $|Q_{\mathrm{P}}| = 1 \neq 0,$ and the ranks of $Q_{\mathrm{C}} = Q_{\mathrm{P}} = 2 = n$. Thus, the system is controllable and observable at the operating point. The system must be discretized to design a discrete control approach. The linearized continuous-time state-space model in equation (5.3) was then discretized using the following equation (5.4) over a specific sample time ($Ts = 0.1$ sec).

$$A_d = e^{A_c T_s} \quad B_d = {A_c}^{-1}(e^{A_c T_s} - I)B_c \quad C_d = C_c \quad \text{and } D_d = D_c \tag{5.4}$$

I verified the discretization results using MATLAB's function "c2dm." In general, the linear discrete-time state-space equation can be written concisely as follows:

$$\begin{cases} x_d(k+1) = A_d x(k) + B_d u(k) \\ y_d(k) = C_d x(k) + D_d u(k) \end{cases} \tag{5.5}$$

Therefore, the discrete-time system model matrixes A_d, B_d, C_d, and D_d are shown below:

$$A_{d1} = \begin{pmatrix} 0.99 & 0.0196 \\ -0.026 & 0.0058 \end{pmatrix}, B_{d1} = \begin{pmatrix} -0.402 \\ -4.96 \end{pmatrix}, C_{d1} = (1 \quad 0), \text{ and } D_{d1} = 0 \tag{5.6}$$

where A_d, B_d, C_d, and D_d are the discrete state-space matrixes.

5.3 Model Predictive Control

A robust control system maintains stability and achieves specific predetermined performance objectives. The goal of a robust design is to identify a controller for a particular system, such as the closed-loop control system is robust because it includes feedback. Model Predictive Control (MPC), which was initially developed throughout the 1970s [130], and is currently an active area of research, is a reliable and effective design approach for linear-time invariant (LTI) control systems and nonlinear systems.

MPC is a modern technique that can determine the next optimal control action based on optimization, which forces the system output to track and stabilize the predefined reference signal trajectory along the prediction horizon (NP) while satisfying the system operating constraints in the states $x(k)$ and inputs $u(k)$. Furthermore, MPC is known as a power optimization approach for feedback control systems. It can impose constraints on the states and inputs such that optimization does not hit the maximum and minimum values, enabling the output single trajectory to track the desired trajectory. It also works for nonlinear control systems that can linearize the system model at a particular state, then apply linear optimization and proceed to the next step. Finally, MPC is a flexible control technique because the control behavior can be modified if the system starts to deviate from the expected trajectory. For these advantages, the MPC controller is superior to other traditional controllers and is therefore regarded as the most effective method of controlling such systems.

The MPC algorithm's main principle is to access the dynamic system model to predict the future evolution of the system, which includes the states (x) and input control singles (u) of the plant over a prediction horizon, by optimizing the control signal to

predict future output behavior (y) to track the predefined reference trajectory (r). Typically, only the initial control action is implemented; it then proceeds with a new control prediction value with a short time horizon. The optimization procedure will be repeated to determine the best control value along the prediction horizon. At every new time step, MPC reassesses the optimal optimization control input. Figure 5.1 illustrates the main concept of MPC [131].

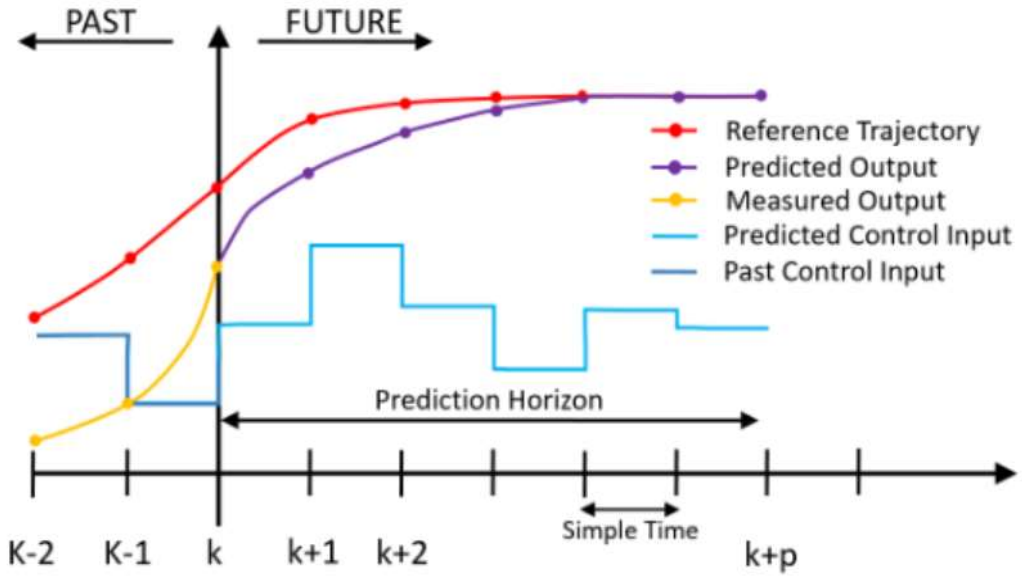

Figure 5.1 MPC basic concept.

Designing the MPC depends on the discrete state space matrices of the proposed system model (A_d, B_d, and C_d) and important parameters, such as the control horizon (NC) and prediction horizon (NP). NP is the number of sample predictions and NC is the samples used to control the system's output, and their values are determined using this formula: $1 \leq \text{NC} \leq \text{NP}$.

Previous studies have demonstrated the MPC outperformed other controllers such as Linear–Quadratic Regulator (LQR) and Proportional-Integral-Derivative (PID) controllers. For example, the authors in [132, 133] compared the performance of PID and MPC controllers and found that the MPC performed better than the PID in terms of system parameters such as settling, rise time, time delay, overshoot, and steady-state error. Furthermore, they found that applying an MPC controller could reduce the effect of disturbances by 77% when compared to a PID controller, as indicated by the authors in [134]. The advantage of using MPC over PID is its ability to deal with complex dynamic systems, even in the presence of constraints, as stated by the authors in [135]. Moreover, the authors in [136] compared the path-tracking performance of MPC, LQR, and Stanley controllers. The results revealed that the MPC was better suited for path-tracking applications than others. Additionally, the authors in [137] presented a comparative study of LQR and MPC and concluded that MPC was a more accurate trajectory tracker than LQR. Performance evaluation of the MPC, LQR, and PID controllers for a DC motor speed control system was carried out by the authors in [138]. The findings demonstrated that the MPC outperformed other controllers in terms of reference tracking and constraint handling. According to these findings, it became clear that applying the MPC controller would produce the most accurate performance in this study.

5.3.1 Prediction

MPC performance depends on the state and input prediction, and it becomes more optimal when its vectors are accurately predicted. The future control signal equation is:

$$u(k),\ u(k+1), u(k+2),\ \ldots, u(k+N_C-1) \tag{5.7}$$

where $u(k)$ is control value at time k and N_C is the control horizon.

The state variable prediction equation is:

$$x(k+1|k), x(k+2|k), \dots, x(k+N_P|k) \tag{5.8}$$

where $x(k)$ is state vector value at time k and N_P is the prediction horizon.

The future state variables are calculated using the future control values based on the system model's discrete state space matrices (A_d, B_d, and C_d) [131].

$$\begin{aligned}
x(k+1|k) &= A_d x(k) + B_d u(k) \\
x(k+2|k) &= A_d x(k+1|k) + B_d u(k+1) \\
x(k+3|k) &= A_d^2 x(k) + A_d B_d u(k) + B_d u(k+1) \\
&\vdots \\
x(k+N_P|k) &= A_d^{N_P} x(k) + A_d^{N_P-1} B_d u(k) + A_d^{N_P-2} B_d u(k+1) + \cdots + \\
&A_d^{N_P-N_C} B_d u(k+N_C-1)
\end{aligned} \tag{5.9}$$

Substituting the predicted state variables and future control values renders the predicted output variables.

$$y(k+1|k) = C_d A_d x(k) + C_d B_d u(k) \tag{5.10}$$

$$\begin{aligned}
y(k+2|k) &= C_d A_d^2 x(k) + C_d A_d B_d u(k) + C_d B_d u(k+1) \\
y(k+3|k) &= C_d A_d^3 x(k) + C_d A_d^2 B_d u(k) + C_d A_d B_d u(k+1) + C_d B_d u(k+2) \\
&\vdots \\
y(k+N_P|k) &= C_d A_d^{N_P} x(k) + C_d A_d^{N_P-1} B_d u(k) + C_d A_d^{N_P-2} B_d u(k+1) + \cdots + \\
&C_d A_d^{N_P-N_C} B_d u(k+N_C-1)
\end{aligned} \tag{5.11}$$

Define the Y and U vectors as follows:

$$Y = [y(k+1|k) \quad y(k+2|k) \quad y(k+3|k) \quad \dots \quad y(k+N_P|k)]^T,$$

$$U = [u(k) \quad u(k+1) \quad u(k+2) \quad u(k+3) \dots \quad u(k+N_C-1)]^T$$

Combining equations (5.10) and (5.11) into a compact matrix form is shown below:

$$Y = Fx(k_i) + \emptyset\, U \tag{5.12}$$

where

$$F = \begin{bmatrix} CA \\ CA^2 \\ \vdots \\ CA^{N_P} \end{bmatrix}; \quad \emptyset = \begin{bmatrix} CB & 0 & & 0 \\ CAB & CB & & 0 \\ CA^2B & CAB & \cdots & 0 \\ \vdots & \vdots & & \vdots \\ CA^{N_P-1}B & CA^{N_P-2}B & & CA^{N_P-N_C}B \end{bmatrix}.$$

5.3.2 Optimization

The MPC's objective is to optimize the GHE's output temperature $\hat{T}(k)$ such that it can track and stabilize the reference temperature trajectory $r(k_i)$ (i.e., ground temperature) by determining the optimal control action $u(k)$ over the prediction horizon, while the error prediction is reduced. The following defines the pre-defined reference signal.

$$r(k) = [r(k+1) \quad r(k+2) \quad r(k+3) \quad \dots \quad r(k+N_P)]^T \tag{5.13}$$

The future output temperature trajectory $\hat{T}(k+1)$ can be anticipated by controlling the water velocity $v(k)$ while minimizing the cost function. The cost function equation $J(k)$:

$$J(k) = \sum_{i=1}^{N_p} Q.[(\hat{T}(k+i|k) - r(k+i|k)]^2 + \sum_{i=1}^{N_C-1} R.[\Delta v(k+i|k)]^2 + \sum_{i=1}^{N_P} Q_1.[v(k+i|k)]^2 \quad (5.14)$$

Subject to

$$\begin{cases} T_{min} \le \hat{T}(k+i|k) \le T_{max} \\ v_{min} \le v(k+i|k) \le v_{max} \\ \Delta v_{min} \le \Delta v(k+i|k) \le \Delta v_{max} \end{cases} \quad (5.15)$$

where $r(k+i|k)$ and $\hat{T}(k+i|k)$ are reference signals and the predicted output temperature at the time $(k+i)$, respectively, and $v(k+i|k)$ and $\Delta v(k+i|k)$ are predicted control and predicted rate control changes at the time and predicted rate control $(k+i)$, respectively. The MPC block diagram of heat transfer in a vertical ground heat exchanger for Oakland University's GHPS is depicted in Figure 5.2.

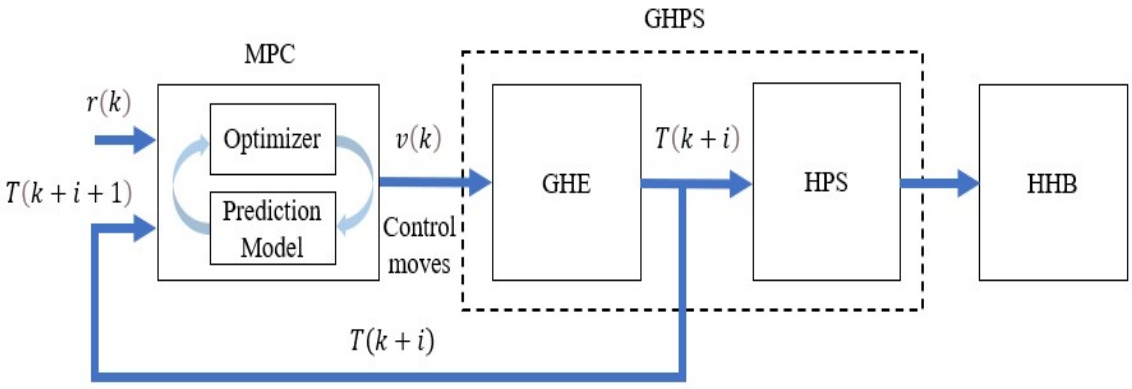

Figure 5.2 Block diagram of a closed loop MPC controlling heat transfer in a GHE for Oakland University's GHPS [23].

This dissertation proposes the MPC control design to optimize its formulation and address the quadratic programming problem (QP) and imposition of constraints on states and inputs.

CHAPTER SIX

KEY VARIABLE PREDICTION OF GEOTHERMAL HEAT PUMP SYSTEM

Predicting the output temperature of the GHPS is important as it can provide information in advance that can be used to evaluate the system's performance, optimization, and fault detection, as well as provide temperature readings to personnel in the building hours in advance. Numerous prediction approaches have been proposed for use in geothermal heat pump systems and applications. For example, the authors in [139] introduced an algorithm based on the infinite line source method (LSM) to forecast the GHE's output fluid temperature. An artificial neural network (ANN) model was proposed to predict the GHE's output temperature [140]. Furthermore, in [141], the researchers developed the adaptive neural-fuzzy inference system (ANFIS) with a fuzzy weighted pre-processing (FWP) technique to predict the daily performance (COP) of a ground-source heat pump (GSHP) system. The results demonstrated that the FWP-based ANFIS algorithm outperformed the standard ANFIS algorithm. The authors in [142] applied a multiple linear regression (MLR) and an ANN to perform hourly predictions of the GHPS system. The developers in [143] created an ANN model to predict the layered thermal conductivity, with an absolute error of less than 0.1 W/(m. K). The authors in [144] applied the extreme learning machine algorithm (ELM), support vector machine algorithm (SVM), and the backpropagation neural network algorithm (BPNN) to predict the COP of the ground-source heat pump. They concluded that the ELM model was more accurate than the SVM and BPNN models. The authors in [145] predicted the GHPS output temperature eight hours in advance using the grey prediction model (GM (1,1)).

6.1 Methodology

The Grey Prediction Model (GM) is a mathematical model that predicts the behavior of an unknown aspect of the system using insufficient or incomplete information. This information must contain at least four data points [146]. The author of [147] proposed the grey prediction model in 1982, which has continued to be applied to uncertain systems with limited data sets for short-time series forecasting. The GM (m, n) model has m denoting the order of the differential equation and n denotes the number of the prediction variables. For clarity, the GM (1,1) model predicts one variable that uses a first-order differential equation. There are several types of GM models in grey system theory, but the GM (1,1) model is the most widely used for short-term prediction due to its considerable advantages, such as simple calculation, high efficiency, and the ability to predict an unknown part of the system with incomplete information [148, 149]. The authors in [150] pointed out that the GM models could be effective in time series prediction with a small dataset. The GM (1,1) model has been used in many disciplines and has proven to perform accurate prediction results when improved [8, 151, 152]. The GM (1,1) model depends on the system dataset, which must be devoid of negatives, randoms, and anomalies, and preferably consistent for the model to forecast accurately. The authors in [145] observed that a more consistent dataset could produce more accurate predictions. The Accumulated Generating Operation (AGO) smooths the system dataset and reduces the randomness in the raw data, which is the most important characteristic of grey system theory. Furthermore, the essential tools of the grey system theory are the whitening equation and time response functions.

Even the traditional GM (1,1) model is an accepted prediction tool in different fields; however, its predictive accuracy is limited. Thus, the traditional GM (1,1) model's prediction accuracy should be improved. Many improvements are implemented to enhance its prediction accuracy. For example, the authors in [153] used the Markov chain model and Fourier residual model to enhance the GM (1,1) model's prediction accuracy. The proposed model was more accurate than the traditional model. The authors in [154] increased the prediction accuracy of the GM (1,1) model by optimizing the initial condition values. Additionally, the authors in [155] adopted the Simpson formula to reconstruct the GM (1,1) model's background value, which improved its accuracy. Similarly, the authors in [156] enhanced the GM (1,1) model prediction accuracy by restructuring its background values. The authors in [157] combined residual modification with genetic programming sign estimation to improve the GM (1,1) model prediction accuracy. Optimizing the initial condition value can enhance the performance of the GM (1,1) model, as findings from [158] pointed out. The authors in [159] applied the particle swarm optimization (PSO) algorithm to increase the GM (1,1) model's prediction accuracy. The authors in [160] combined the GM (1, 1) and genetic algorithms to enhance the grey forecasting accuracy. The authors in [161] increased the GM (1,1) model prediction accuracy by combining artificial neural network (ANN) sign estimation with residual modification. The authors in [162] enhanced the GM (1,1) model by optimizing its background value and transforming the original data sequence. The authors in [145] increase the GM (1,1) model prediction accuracy by optimizing the current predicted value by subtracting the error between the previous accumulated time response of the GM (1,1) model and the previous background value. Optimizing the initial and

background values can increase the prediction accuracy of the GM (1,1) model, as pointed out by the authors in [163]. The authors in [164] enhanced the GM (1,1) model prediction accuracy by optimizing its background value. Yet, these enhancements still result in prediction inaccuracies, indicating that further enhancements are required.

6.1.1 Traditional GM (1,1) model

This section describes the GM (1,1) model's analysis and modeling approach. Assume that the sequence $X^{(0)}$

$$X^{(0)} = \left(x^{(0)}(1), x^{(0)}(2), x^{(0)}(3), \dots, x^{(0)}(n)\right) \tag{6.1}$$

where $X^{(0)}$ is the original non-negative data sequence, n is the data sequence length and it must contain at least four data points, which is defined as $n \geq 4$.

Applying the First Order Accumulated Generating Operation (1-AGO) to equation (6.1) yields the following accumulative sequence:

$$X^{(1)} = \left(x^{(1)}(1), x^{(1)}(2), x^{(1)}(3), \dots, x^{(1)}(n)\right) \tag{6.2}$$

where is the $x^{(1)}(k) = \sum_{i=1}^{k} x^{(0)}(i) \qquad k = 1, 2, \dots, n$

The background value array sequence $z^{(0)}$ is written as follows:

$$z^{(1)} = \left(z^{(1)}(1), z^{(1)}(2), z^{(1)}(3), \dots, z^{(1)}(n)\right) \tag{6.3}$$

where $z^{(1)}(k) = 0.5x^{(1)}(k) + 0.5x^{(1)}(k-1)$, and $k = 2, 3, \dots, n$.

The first-order differential equation of the GM (1,1) model is shown below:

$$x^{(0)}(k) + az^{(1)}(k) = b \tag{6.4}$$

where a and b are the critical parameters of the GM model, which are the donating developing coefficient and gray action quantity, respectively.

Then, use the least square method to estimate the model parameters.

$$\hat{a}=[\mathrm{a}, b]^T = (B^{\mathbf{T}}B)^{-\mathbf{1}}B^{\mathbf{T}}Y \tag{6.5}$$

where

$$B = \begin{bmatrix} -Z^{(1)}(2) & 1 \\ -Z^{(1)}(3) & 1 \\ \vdots & \vdots \\ -Z^{(1)}(n) & 1 \end{bmatrix},\ Y = \begin{bmatrix} x^{(0)}(2) \\ x^{(0)}(3) \\ \vdots \\ x^{(0)}(n) \end{bmatrix}, \text{ and } x^{(1)}(1) = x^{(0)}(1)$$

The first-order differential equation of the GM (1,1) model, also known as the whitening equation (shadow equation) is expressed as:

$$\frac{dx^{(1)}}{dt} + ax^{(1)} = b \tag{6.6}$$

Using 1-AGO to solve differential equation (6.4), we get the GM (1,1) model predicted sequence $\hat{x}^{(0)}(k)$, as shown in equation (6.7).

$$\begin{cases} \hat{x}^{(0)}(1) = \hat{x}^{(0)}(1) \\ \hat{x}^{(0)}(k) = (1 - e^{-a})\left(x^{(0)}(1) - \frac{b}{a}\right)e^{-a(k-1)} + \frac{b}{a} \quad k = 2, 3, \dots, n \end{cases} \tag{6.7}$$

Restore the $\hat{x}^{(0)}$ value sequence:

$$\hat{x}^{(0)}(k) = \hat{x}^{(1)}(k) - \hat{x}^{(1)}(k-1) \tag{6.8}$$

where $\hat{x}^{(0)}(k)$ is the predicted time response of the GM (1,1) model at time k, $\hat{x}^{(1)}(k)$ accumulated time response of the GM (1,1) model, and $\hat{x}^{(1)}(k)$ is a simulative value of $\hat{x}^{(0)}(k)$.

6.1.2 The Improved IGM (1,1) model

Due to the GM (1,1) model producing an inaccurate prediction, its prediction accuracy needs to be enhanced. To address the weaknesses of the GM (1,1) model prediction accuracy, I proposed Improved Grey Prediction Model (IGM (1,1)) to minimize the GM (1,1) model's error prediction and enhance its overall performance. The IGM (1,1) model was based on optimizing the current predicted value by subtracting the error between the previously accumulated sequence $\hat{x}^{(1)}(k)$ and the previous background value $z^{(1)}(k)$ [145]. Therefore, the following describes the modeling technique for the improved IGM (1,1) model.

Equation (6.9) defines the predicted value's error equation:

$$\delta^{(1)}(2) = \hat{x}^{(1)}(1) - z^{(1)}(1)$$

$$\delta^{(1)}(3) = \hat{x}^{(1)}(2) - z^{(1)}(2)$$

$$\vdots$$

$$\delta^{(1)}(k) = \hat{x}^{(1)}(k-1) - z^{(1)}(k-1), \qquad k = 2, 3, \dots, n \tag{6.9}$$

Substituting equations (6.3) and (6.7) with equation (6.9) renders the following:

$$\delta^{(1)}(k) = \left[(1 - e^{-a})\left(x^{(0)}(1) - \frac{b}{a}\right)e^{-a(k-1)} + \frac{b}{a}\right] - 0.5\left[x^{(1)}(k) + x^{(1)}(k-1)\right] \tag{6.10}$$

Finally, by substituting the predicted value's error equation (6.10) for equation (6.7), we obtain the improved IGM (1,1) model prediction sequence $\hat{x}^{(0)}(k)$ as follows:

$$\begin{cases} \hat{x}^{(0)}(1) = x^{(0)}(1) \\ \hat{x}^{(0)}(k) = \left[(1 - e^{-a})\left(x^{(0)}(1) - \frac{b}{a}\right)e^{-a(k-1)} + \frac{b}{a}\right] - \delta^{(1)}(k) \end{cases} \tag{6.11}$$

where $k = 2, 3, \dots, n$.

6.2 Data Description

In this study, three GHPS output temperature datasets were utilized to assess and validate the improved IGM (1,1) model. The data sets were collected from various places and during various times of operation and were examined for anomalies, negatives, and randomness. The first dataset was obtained from Oklahoma State University and the reading was from January 1 to January 2, 2015 [28]. The second dataset was obtained from the University of Politècnic de Valitècnic and the reading was from May 8 to May 9, 2002 [108]. The third one was obtained from Oakland University and the reading was from July 1 to July 2, 2019 [27]. The 24 data points (i.e., 24 hours) were divided into two periods: an in-sample dataset (i.e., training) from 1 to 24 and an out-of-sample dataset (i.e., prediction) from 25 to 32. In addition, an in-sample component was divided into two parts, with 75% of the data utilized to train the model from 1 to 18 to precisely forecast the GHPS's output temperature for the next eight hours, and the remaining 25% of data from 19 to 24 selected to evaluate the model accuracy. The IGM (1,1) model was applied to predict the GHPS output temperature for each of the data sets described above separately, and it was implemented in MATLAB.

6.3 Model Accuracy Evaluations

In this study, I used the three matrices Mean Absolute Error (MAE), Root Mean Square Error (RMSE), and Mean Absolute Percentage Error (MAPE) to evaluate the prediction accuracy of the IGM (1,1) and GM (1,1) models. Thus, the MAE, RMSE, and MAPE are defined according to equations (6.12) – (6.14), respectively.

$$\text{MAE} = \frac{1}{n}\sum_{i=1}^{n}\left|\hat{x}^{(0)}(k) - x^{(0)}(k)\right| \tag{6.12}$$

$$\text{RMSE} = \sqrt{\frac{1}{n}\sum_{i=1}^{n}\left(x^{(0)}(k) - \hat{x}^{(0)}(k)\right)^2} \tag{6.13}$$

$$\text{MAPE} = \frac{1}{n}\sum_{i=1}^{n}\left|\frac{\hat{x}^{(0)}(k) - x^{(0)}(k)}{\hat{x}^{(0)}(k)}\right| \times 100\% \tag{6.14}$$

where $x^{(0)}(k)$ is the actual value and $\hat{x}^{(0)}(k)$ is the predicted value, and n is the number of observations. Lower MAE, RMSE, and MAPE (%) values indicate that the model is working optimally. Table 6.1 shows the MAPE criteria.

Table 6.1 The MAPE criteria.

MAPE (100%)	**Accuracy**
0 – 10	High
10 – 20	Good
20 – 50	Reasonable
> 50	Inaccurate

CHAPTER SEVEN

SIMULATION RESULTS AND DISCUSSION

7.1 Case Study I: GHPS at Oakland University

7.1.1 System Description

A 400-ton capacity Geothermal Heat Pump System (GHPS) was installed at Oakland University in the summer of 2012. The GHPS provides cooling and heating for the Human Health Building (HHB), which has five floors, a total area of 159,793 m^2 and uses a lot of energy. Thus, a GHPS with a large capacity was appropriate. The GHPS is composed of a vertical GHE, a heat pump, and a distribution system as depicted in Figure 7.1. The GHE consists of 256 geothermal boreholes that are each 98 m deep and spaced 7.62 m apart from one another. Thus, there was no interference between the legs of the two U-tube GHE pipes. A single High-Density Polyethylene (HDPE) pipe was inserted into each borehole as a U-shaped. The HDPE pipe's geometrical properties are shown in Table 7.1. Thermally enhanced bentonite grout with high conductivity was used to fill the space between the HDPE pipe and the borehole wall, creating a strong thermal connection between the pipe and the surrounding ground. Additionally, preventing the borehole wall from collapsing and groundwater contamination from occurring extends system life. Then, these U-tube pipes were connected in parallel with the heat pumps and are filled with water and an anti-freeze solution to promote heat transfer between the ground and the heat pump system. Two 60-horsepower (HP) water pumps with variable-frequency drives (VFDs) were connected in parallel with forty-four heat pumps. The HP-VFDs (i.e., water circulation pumps) flow the water through loop pipes at different rates

as needed. When the first pump is running, the second is in standby mode. After the heat pump delivers the desired temperature in the building, fans in the distribution unit system circulate the warm or cold air there to exchange it with the cooler or warmer air, keeping a consistent temperature throughout the entire building.

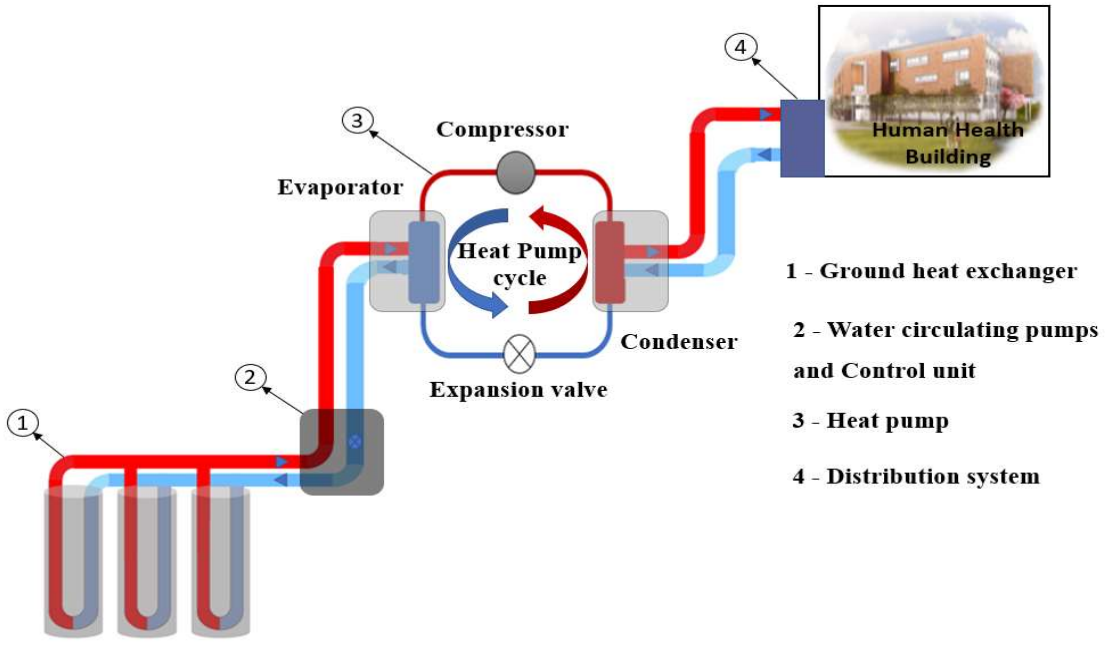

Figure 7.1. Schematic diagram of the GHPS at Oakland University.

The GHPS has been providing the HHB with effective heating and cooling since it began operating in August 2012. The author in [27] evaluated Oakland University's GHPS performance from 2013 to 2015 using its input and output temperature datasets. The author found that the temperature fluctuations were minimal, indicating that the underground loop pipes were an appropriate length to supply the entire building with heating and cooling energy, with the additional ability to supply more.

To keep the GHPS system operating at its maximum efficiency and continuing to provide adequate temperatures to the HHB, water velocity must be optimally controlled so that the water reaches the desired temperature without wasting any additional power used by the water circulation pump. Model Predictive Control (MPC) functions as a power management system, reducing power consumption by controlling water velocity and ensuring that it flows within the optimal range.

Table 7.1. HDPE Pipe Geometric Characteristics.

Symbol	Value	Unit	Description
$\boldsymbol{k_p}$	0.5	$\mathrm{W/m\,.\,℃}$	Thermal conductivity
$\boldsymbol{d_i}$	0.026	m	Inner diameter
$\boldsymbol{d_o}$	0.032	m	Outer diameter
$\boldsymbol{\rho_p}$	959.98	$\mathrm{kg/m^3}$	Density
$\boldsymbol{L}$	98	m	Length

7.1.2 Physical Setup

I assumed the water velocity to be $v = 0.2\ \mathrm{m/s}$, since it is not constant, to determine the heat transfer convective coefficient h_i. Equation (4.17) was used to determine the convective heat transfer coefficients for both heating and cooling modes:

For heating:

$$h_i = \left(\frac{0.5}{0.026}\right)(0.023)\left(\frac{1.726*4.22}{0.5}\right)^{0.4}\left(\frac{999.94*0.2*360*0.026}{1.726}\right)^{0.8} = 2184.08\ \mathrm{W/m^2.℃}$$

For cooling:

$$h_i = \left(\frac{0.5}{0.026}\right)(0.023)\left(\frac{0.974*4.15}{0.5}\right)^{0.3}\left(\frac{997.96*0.2*360*0.026}{0.974}\right)^{0.8} = 2209.55\ \mathrm{W/m^2.℃}$$

The overall heat transfer coefficient U_0 for heating and cooling modes was obtained by substituting the convective heat transfer coefficient into the equation (4.18) as shown below:

For heating:

$$U_0 = \left\{\frac{1}{2184.08}\left(\frac{0.032}{0.026}\right) + \frac{0.032\ ln\left(\frac{0.032}{0.026}\right)}{0.5} + 0.0385\right\}^{-1} = 19.10\ \mathrm{W/m^2.℃}$$

For cooling:

$$U_0 = \left\{\frac{1}{2209.55}\left(\frac{0.032}{0.026}\right) + \frac{0.032\ ln\left(\frac{0.032}{0.026}\right)}{0.5} + 0.0385\right\}^{-1} = 19.10\ \mathrm{W/m^2.℃}$$

The Oakland university's GHE parameter values used in this study are presented in Table 7.2.

Table 7.2 Ground heat exchanger parameters for Oakland University's GHPS.

Symbol	Value		Unit	Description
	Winter	Summer		
$\boldsymbol{\mu}$	1.726	0.974	Cp	Dynamic viscosity
$\boldsymbol{\rho}$	999.94	997.96	kg/m^3	Water density
$\boldsymbol{C_p}$	4.22	4.15	kJ/kg . ℃	Specific heat
$\boldsymbol{k_w}$	0.5	0.5	W/m . ℃	Water Thermal conductivity
$\boldsymbol{v}$	0.35 - 0.45	0.35 - 0.45	m/s	Water velocity
$\boldsymbol{n}$	0.4	0.3	–	Heating/cooling exponent
$\boldsymbol{h_i}$	2105.70	2182.17	$W/m^2.℃$	Convective heat transfer coefficients
$\boldsymbol{U_0}$	19.10	19.10	$W/m^2.℃$	Overall heat transfer coefficient
$\boldsymbol{R_v}$	0.0385	0.0385	$m^2.℃/W$	Soil thermal resistance
$\boldsymbol{T_{in}}$	2	22	℃	Input temperature
$\boldsymbol{T_g}$	11.6	11.6	℃	Ground temperature

7.1.3 Heat Transfer Model Implementation

The heat transfer behaviors between the flowing liquid (i.e., water) temperature inside a single vertical U-tube pipe and its surrounding earth for both heating and cooling modes are demonstrated through the simulations, as well as the effect of water velocity on the GHE's output temperature. The vertical GHE at Oakland University was utilized to validate the proposed heat transfer model in both modes. The heat transfer model equation (4.19) was written in MATLAB script and implemented using an Ordinary Differential Equation (ODE) solver. The parameters of the heat transfer model were presented in Table 7.1 and Table 7.2 and were utilized in equation (4.19a) for heating

mode and equation (4.19b) for cooling mode. The initial temperature values were assumed to be $T(0) = 2$ ℃ for heating mode and 22 ℃ for cooling mode, referring to the temperature at the beginning of the pipe $x = 0$ and decrease or increase according to the surface air temperature as it flowed through the length of pipe L. The ground temperature is constant, which is assumed to be 11.6 ℃ for both modes. The heat carrier (i.e., water) flows at different velocities through the loop pipes and these velocities influence the loop temperature. To demonstrate that, four different water velocities were used for heating and cooling modes: 0.35, 0.45, 0.9, and 1.2 $\mathrm{m/s}$. Subsequently, the proposed model (4.19), was implemented, and the water temperature behavior within the pipe for both modes was observed, as shown in Figures 7.2 and 7.3.

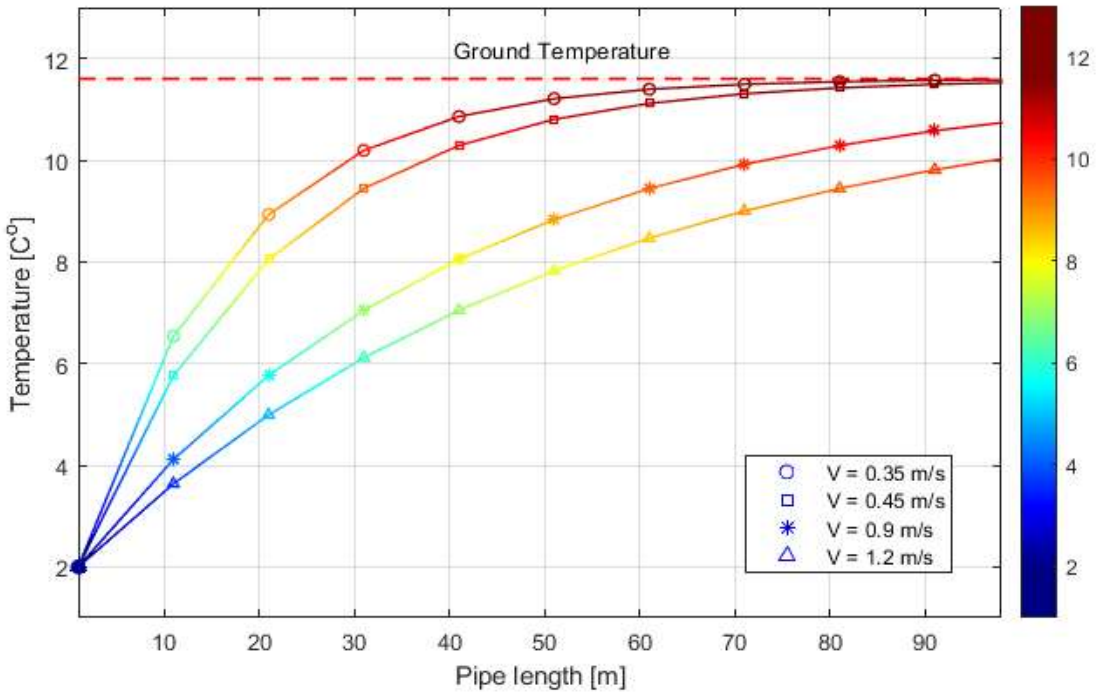

Figure 7.2. Water temperature behavior in a vertical U-tube pipe for GHPS at Oakland University in heating mode.

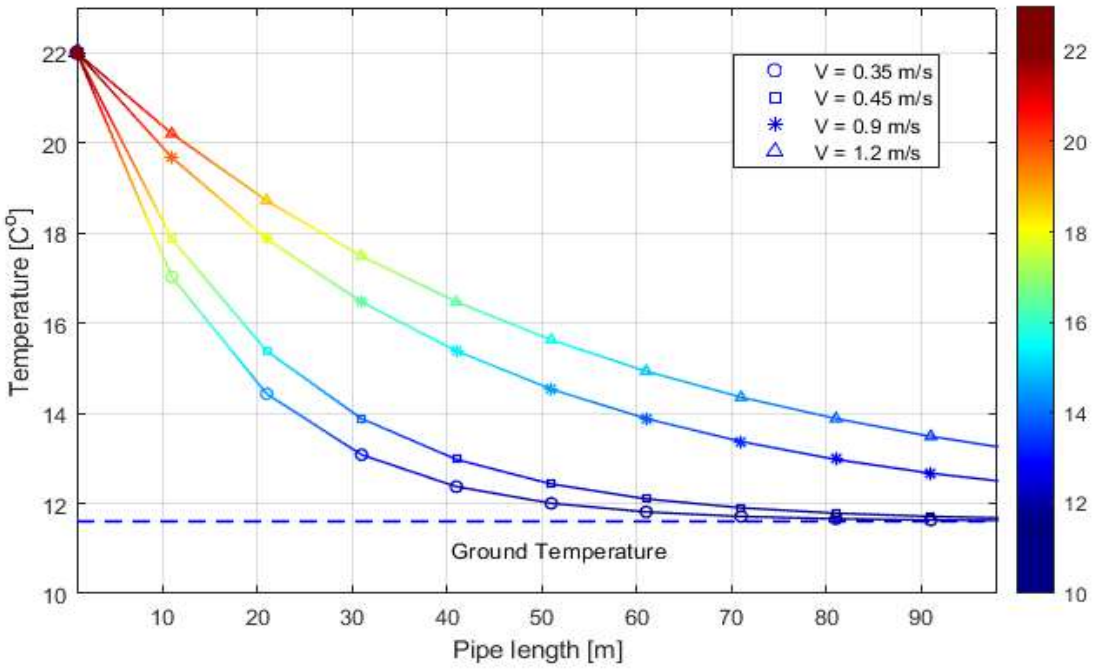

Figure 7.3. Water temperature behavior in a vertical U-tube pipe for GHPS at Oakland University in cooling mode.

Figure 7.2 depicts the water temperature behavior in a single vertical U-tube pipe for heating mode. The water temperature exponentially increased from the beginning of the pipe and continued rising throughout the pipe until it reached the desired temperature (i.e., ground temperature) at 91 m and 96 m at applied velocities of 0.35 and 0.45 m/s, respectively. The heated water temperature gradually stabilized throughout the pipe's exit and can then be transferred to the heat pump system. In this instance, the earth's heat was transferred to the water within the pipe. According to Figure 7.2, it can be observed that the water temperature $T(x)$ reached the ground temperature or the heat exchanger between the water inside the pipe and the surrounding ground was balanced when the

water velocity was between 0.35 m/s and 0.45 m/s. Nevertheless, when the water velocity was raised to 0.9 and 1.2 m/s, the water temperature did not reach the ground temperature despite reaching the exit of the loop pipe. At these high velocities, considerably more power was consumed, which was used for heat and water circulation pumps.

Water temperature behavior in a vertical U-tube pipe for cooling mode is depicted in Figure 7.3. Since the water temperature is warmer than that of the surrounding ground, heat is transferred to the earth. The water temperature decreased exponentially as the water flowed through the pipe until it reached the ground temperature of 11.6 ℃ at 92 m and 96 m when the water velocity was 0.35 m/s and 0.45 m/s, respectively. However, when the water velocity was insufficient to allow enough time for heat exchange, which was between 0.9 to 1.2 m/s, the water temperature did not approach the ground.

According to the simulation results (Figures 7.2 and 7.3), the water velocity was affected by the water temperature, which in turn affected the thermal performance of the GHE. By increasing water velocity, the water had less time to reach ground temperature, resulting in large temperature differences between the water and ground temperatures. Hence, the water temperature only approached the ground temperature when the water velocity was reduced sufficiently to enable it to heat or cool. Allowing enough time for the heat exchanger between the water inside the pipe and the surrounding earth to reach ground temperature is therefore crucial. High-velocity water pushing provided no benefit because it neither delivered an appropriate temperature nor saved power used by the water circulation pump. However, when the water velocity is too low, the water temperature reaches the ground before the exit of the pipe and remains relatively constant

throughout the pipe loop, rendering most of the loop useless. Optimally, controlling water velocity is crucial such that the water temperature reaches the ground temperature without consuming any additional power resources; for instance, the circulation water pump requires more power to increase water velocity. Furthermore, the heat pump must compensate for heat that is not delivered from the ground.

To further validate the proposed dynamic heat transfer model's performance, the proposed model (4.19) was used to simulate the water temperature behavior inside the U-tube pipe in the vertical ground heat exchanger of the geothermal heat pump system at the University of the Politècnica de València and Oklahoma State University.

7.2 Case Study II: GHPS at the University of the Politècnica de València

7.2.1 System Description

The ground source heat pump system was installed at the University Politècnica de València in 2004 to provide efficient heating and cooling for the building's total area of 250 m^2. The ground source heat pump system consists of the ground source heat exchanger (GSHX) and heat pump system, and a hydraulic group. The GSHX is made up of six vertical geothermal boreholes that were drilled to a depth of 50 m, with a diameter of 0.15 m, and spaced 3 m apart from one another. The GSHX was instilled in soil with a thermal conductivity of $1.43\ W/m.K$ and a volumetric heat capacity of 2.25 MJ/m^3. K. A high-density polyethylene (HDPE) pipe was installed into each vertical borehole as a single U-tube borehole configuration, with inner and outer diameters of 0.0254 m and 0.0314 m, respectively. A 0.07 m shank spacing between two U-tube legs ensured that no thermal short circuit occurred. The sand was used to fill the space between the outer pipe

wall and the borehole wall, creating a strong thermal connection between the pipe and the surrounding ground. The exterior surface was finished with a bentonite layer to prevent pollutants from entering the aquifers. The vertical ground loop pipes were then connected to the heat pump in a balanced parallel configuration. Furthermore, these pipes were filled with water to act as heat transfer carriers between the ground and the heat pump system by continually circulating the water. Grundfos pump with a three-phase electrical supply, model CH4-30 (i.e., water circulation pump) flows the water through loop pipes at varying velocities as needed. Furthermore, the system consists of a water-to-water heat pump (IZE-70 model) with nominal cooling and heating capacities of 15.9 KW and 19.3 KW, respectively. The ground temperature tested was 18.5 ℃ [26, 165, 166].

7.2.2 Physical Setup

Although the water velocity was not constant, it was assumed to be 0.2 m/s to calculate the heat transfer convective coefficients h_i for the heating and cooling modes. The convective heat transfer coefficients for both modes were calculated using equation (4.17), and they were 2184.08 and 2209.55 $\mathrm{W/m^2.℃}$ for the heating and cooling modes, respectively. These values were substituted into equation (4.18) to calculate the overall heat transfer coefficients U_0 for the heating and cooling modes. The result was 28.94 $\mathrm{W/m^2.℃}$ for both modes. The various heat transfer model parameters are depicted in Table 7.3 and were used in equation (4.19a) for heating mode and equation (4.19b) for cooling mode.

Table 7.3 Ground heat exchanger parameters for the University of Politècnica de València's GHPS.

Symbol	Value		Unit	Description
	Winter	Summer		
μ	1.3873	0.8693	Cp	Dynamic viscosity
ρ	999.8	996.79	kg/m^3	Water density
C_p	4.22	4.15	$kJ/kg\,.℃$	Specific heat
k_w	0.5	0.5	$W/m\,.℃$	Water Thermal conductivity
v	0.28 - 0.38	0.28 - 0.38	m/s	Water velocity
n	0.4	0.3	–	Heating/cooling exponent
h_i	2184.08	2209.55	$W/m^2.℃$	Convective heat transfer coefficients
U_0	28.94	28.94	$W/m^2.℃$	Overall heat transfer coefficients
R_v	0.0207	0.0207	$m^2.℃/W$	Soil thermal resistance
T_{in}	8	26	℃	Input temperature
T_g	18.5	18.5	℃	Ground temperature
k_p	0.5	0.5	$\mathbf{W/m}\,.℃$	Pipe thermal conductivity
d_i	0.0254	0.0254	m	Inner pipe diameter
d_o	0.0314	0.0314	m	Outer pipe diameter
ρ_p	959.98	959.98	kg/m^3	Pipe density
L	50	50	m	Pipe length

7.2.3 Heat Transfer Model Implementation

Furthermore, the proposed heat transfer model was validated using the vertical GHE at the University of Politècnica de València for both heating and cooling modes. The proposed dynamic model equation (4.19) was written in MATLAB script and

implemented using an ODE solver. The heat transfer model parameters were presented in Table 7.3 and were used in equation (4.19a) for heating mode and equation (4.19b) for cooling mode. The initial temperature values $T(0) = 8℃$ for heating mode and $26℃$ for cooling mode. The ground temperature remained constant at $18.5℃$ for both modes. Four different water velocities of 0.28, 0.38, 0.7, and 1 m/s were used to demonstrate how the water velocity affects the exit loop temperature. Consequently, the proposed model was implemented, and the water temperature behavior within the U-tube pipe was observed for both modes, as shown in Figures 7.4 and 7.5.

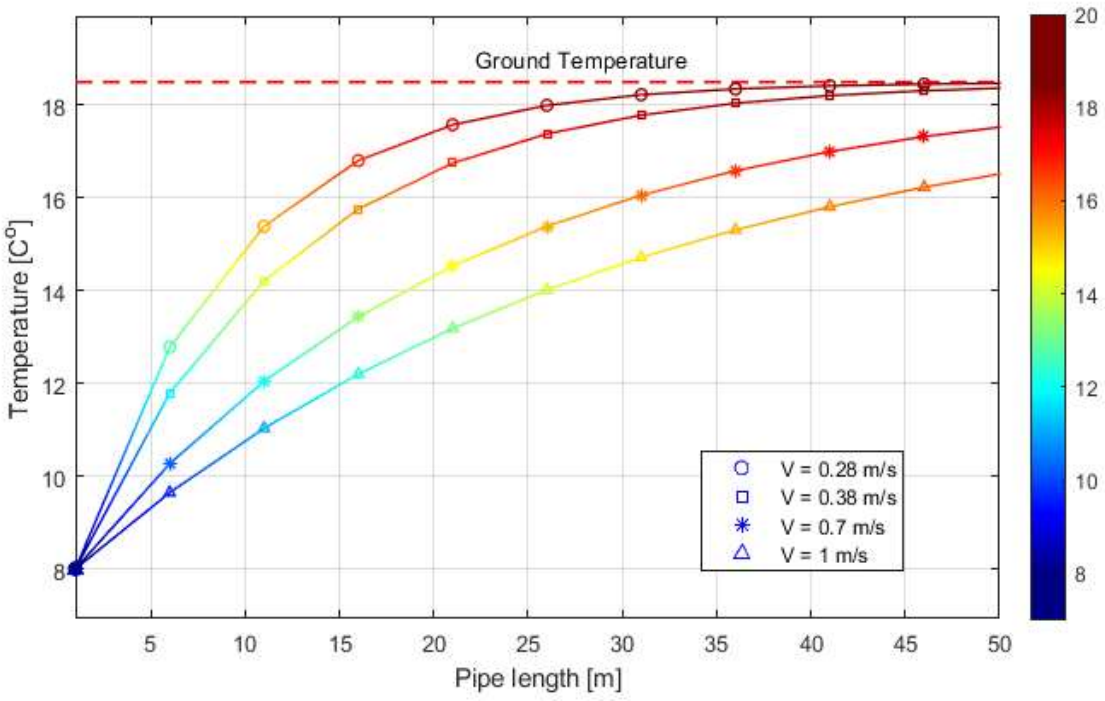

Figure 7.4. Water temperature behavior in a vertical U-tube pipe for GHPS at the University of Politècnica de València in heating mode.

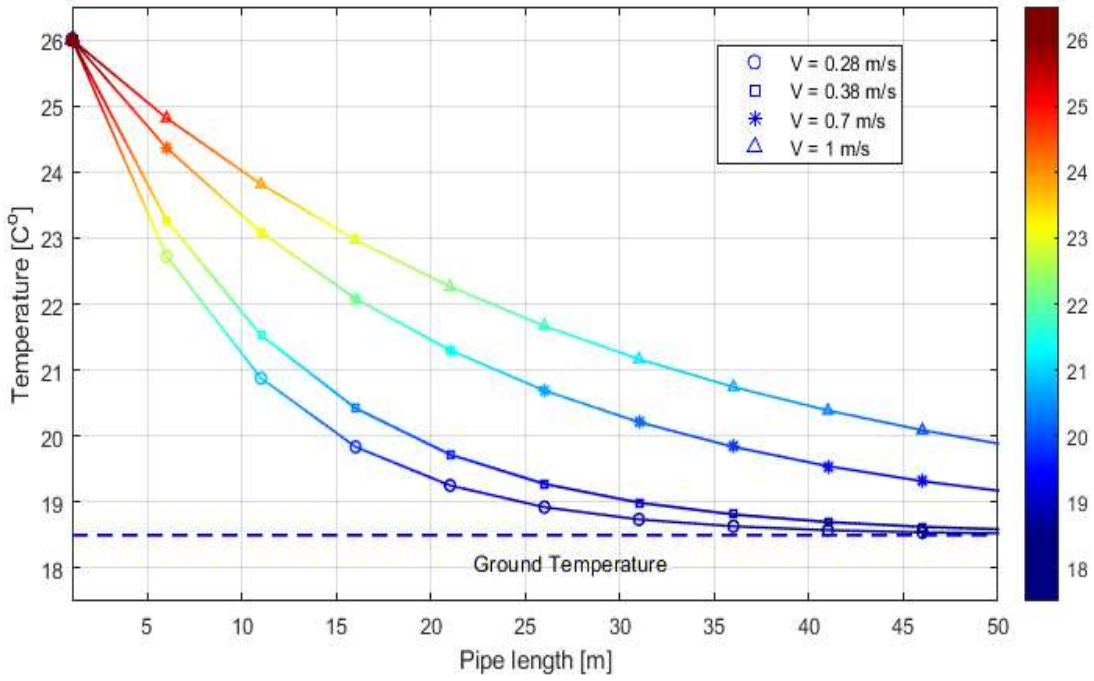

Figure 7.5. Water temperature behavior in a vertical U-tube pipe for GHPS at the University of Politècnica de València in cooling mode.

Figure 7.4 demonstrates the water temperature behavior inside a U-tube pipe for heating in a vertical ground heat exchanger for a geothermal heat pump system at the University of Politècnica de València. According to the figure, the water temperature increased exponentially during water flow inside the pipe from 8 ℃ until it reached the desired temperature (i.e., ground) temperature of 18.5 ℃ at the pipe's exit when the water velocity was 0.28 and 0.38 m/s. However, the water temperature did not reach the ground when the water velocity was 0.7 and 1 m/s. This was due to insufficient time for the heat exchanger between the water inside the pipe and the surrounding ground to balance.

The water temperature behavior inside a U-tube pipe in a vertical ground heat exchanger for cooling mode is depicted in Figure 7.5. The water temperature decreased exponentially along the pipe from 26 ℃ until it reached the ground temperature of 18.5 ℃ at the loop pipe's exit when the water velocity was 0.28 and 0.38 m/s. However, when the water velocity was increased to 0.7 and 1 m/s, the water temperature did not reach the ground temperature.

7.3 Case Study III: GHPS at Oklahoma State University

7.3.1 System Description

The geothermal heat pump system was installed at Oklahoma State University to provide heating and cooling for the building. The datasets for vertical ground heat exchangers are from a large laboratory "sandbox" that includes a borehole with a vertical single U-tube. The GHE is made up of a vertical borehole drilled to a depth of 20 m. A single U-tube HDPE pipe with inner and outer diameters of 0.0273 m and 0.0334 m, respectively, was installed into the vertical borehole. A shank spacing of 0.053 m between two U-tube legs prevented a thermal short circuit. The space between the outer pipe wall and the borehole wall was backfilled with bentonite grout. This enabled a strong connection between the pipe and the surrounding ground, which provides an efficient transfer of heat in either direction. The thermal conductivity of the soil is 2.82 W/ m.K, the volumetric heat capacity is 3.2*106 J/ (m^3 K). In this experiment, water was used as the working fluid with an average volumetric flow rate of 0.197 L/s [28].

7.3.2 Physical Setup

Equation (4.17) was used to calculate the convective heat transfer coefficients h_i for both modes, and they were 2411.22 and 2517.91 $\mathrm{W/m^2.\,℃}$ for the heating and cooling modes, respectively. The overall heat transfer coefficients U_0 for both modes were 41.869 $\mathrm{W/m^2.\,℃}$. The heat transfer model parameters for the vertical ground heat exchanger are depicted in Table 7.4.

Table 7.4 Ground heat exchanger parameters for Oklahoma State University's GHPS.

Symbol	Value		Unit	Description
	Winter	Summer		
$\boldsymbol{\mu}$	1.3076	0.7342	Cp	Dynamic viscosity
$\boldsymbol{\rho}$	994.4	999.65	$\mathrm{kg/m^3}$	Water density
$\boldsymbol{C_p}$	4.20	4.18	$\mathrm{kJ/kg\,.\,℃}$	Specific heat
$\boldsymbol{k_w}$	0.5	0.5	$\mathrm{W/m\,.\,℃}$	Water Thermal conductivity
$\boldsymbol{v}$	0.17 - 0.22	0.17 - 0.22	m/s	Water velocity
$\boldsymbol{n}$	0.4	0.3	–	Heating/cooling exponent
$\boldsymbol{h_i}$	2411.22	2517.91	$\mathrm{W/m^2.\,℃}$	Convective heat transfer coefficients
$\boldsymbol{U_0}$	41.87	41.87	$\mathrm{W/m^2.\,℃}$	Overall heat transfer coefficient
$\boldsymbol{R_v}$	0.01	0.01	$\mathrm{m^2.\,℃/\,W}$	Soil thermal resistance
$\boldsymbol{T_{in}}$	10	34	℃	Input temperature
$\boldsymbol{T_g}$	22.1	22.1	℃	Ground temperature
$\boldsymbol{k_p}$	0.5	0.5	$\mathbf{W/m}\,.\,℃$	Pipe thermal conductivity
$\boldsymbol{d_i}$	0.0273	0.0273	m	Inner pipe diameter
$\boldsymbol{d_o}$	0.0334	0.0334	m	Outer pipe diameter
$\boldsymbol{\rho_p}$	959.98	959.98	$\mathrm{kg/m^3}$	Pipe density
$\boldsymbol{L}$	20	20	m	Pipe length

7.3.3 Heat Transfer Model Implementation

Finally, the vertical GHE at Oklahoma State University was used to validate the proposed heat transfer model. The heat transfer model equation (4.19) was implemented in MATLAB using an ODE solver. The heat transfer model parameters are presented in Table 7.4. The initial temperature values for heating and cooling modes are 10℃ and 34℃, respectively. For both modes, the ground temperature remained constant at 22.1°C. To demonstrate how water velocity affects exit loop temperature, I applied four different water velocities of 0.17, 0.22, 0.4, and 0.6 m/s. Subsequently, the proposed dynamic model was implemented, and the water temperature behavior inside the vertical U-tube pipe was observed for heating and cooling modes (depicted in Figures 7.6 and 7.7).

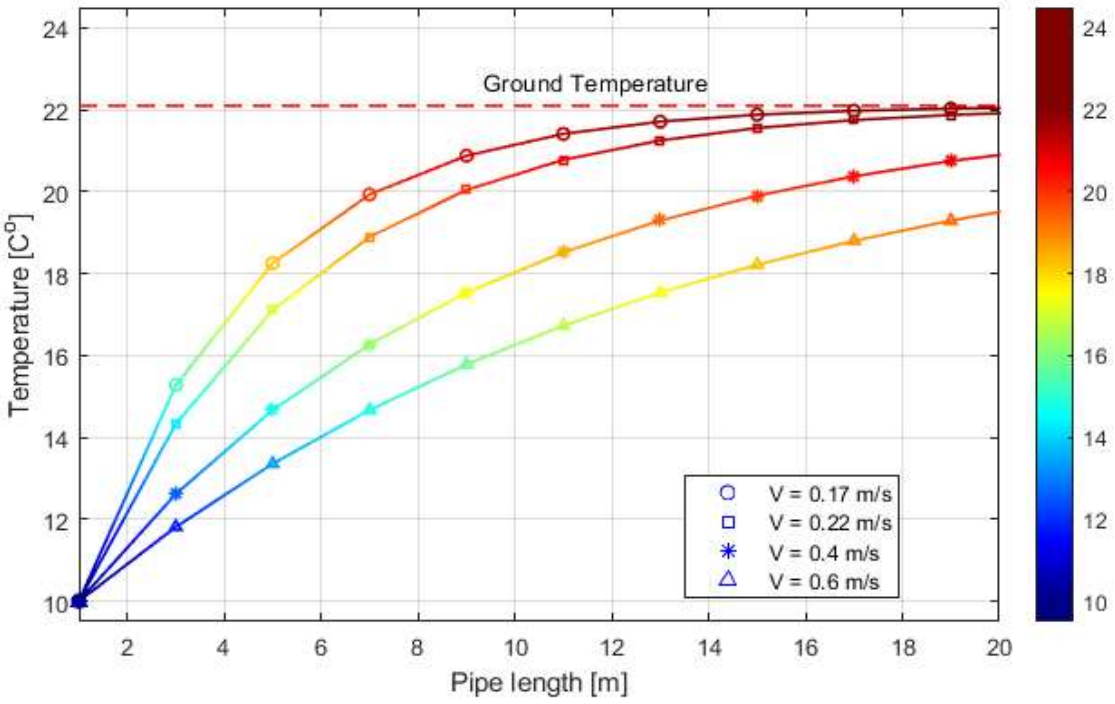

Figure 7.6. Water temperature behavior in a vertical U-tube pipe for GHPS at the Oklahoma State University in heating mode.

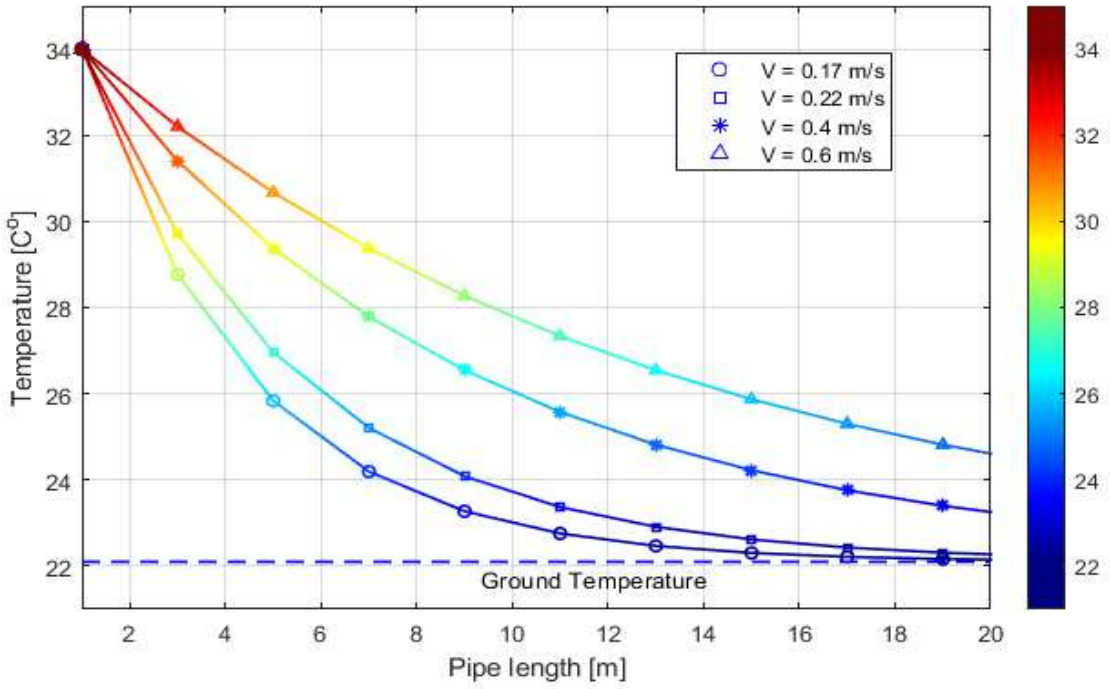

Figure 7.7. Water temperature behavior in a vertical U-tube pipe for GHPS at the Oklahoma State University in cooling mode.

Figure 7.6 depicts the water temperature behavior within a vertical U-tube pipe for the heating mode of the GHPS at Oklahoma State University. The water temperature increased exponentially at the beginning of the pipe and continued to rise as it flowed through the pipe until it reached the ground temperature at 18.5 m and 20 m when the applied velocities were 0.17 and 0.22 m/s, respectively. The heated water temperature can then be transferred to the heat pump system. In this instance, because the ground temperature is higher than the water temperature, thus the earth's heat was transferred to the water inside the pipe. According to the figure, the water temperature reached the desired temperature (i.e., ground temperature) when the water velocity was between 0.17

m/s and 0.22 m/s. However, the water temperature did not reach the ground when the water velocity was raised to 0.4 and 0.6 m/s.

Water temperature behavior in a vertical U-tube pipe for cooling mode is depicted in Figure 7.7. in this case, heat is transferred to the earth because the water temperature is higher than that of the surrounding ground. The water temperature decreased exponentially as it flowed through the pipe until it reached the ground temperature of 22.1 ℃ at 18.5 m and 20 m, respectively when the water velocity was 0.17 m/s and 0.22 m/s. Yet, the water temperature did not approach the ground when the water velocity was increased to 0.4 and 0.6 m/s.

In summary, the proposed model was validated using three real-world case studies of GHPSs at Oakland University, the University Politècnica de València, and Oklahoma State University. The optimal water velocity ranges in the vertical U-tube pipe of the mentioned GHPSs are depicted in Table 7.5. The acceptable range of water velocity in

Table 7.5 Appropriate range of water velocity in varying vertical GHEs.

GHE Location	**Water Velocity Range**
Oakland University	0.35 – 0.45 m/s
University Politècnica de València	0.28 – 0.38 m/s
Oklahoma State University	0.17 – 0.22 m/s

a vertical single U-tube GHE pipe at Oakland University was between 0.35 and 0.45 m/s to ensure that the heat pump delivers the appropriate temperature to provide HHB with comfortable temperatures, regardless of the season. The acceptable water velocity range

for the University Politècnica de València's GHPS was between 0.28 and 0.38 m/s, and from Oklahoma State University, it was between 0.17 and 0.22 m/s.

As previously discussed in Chapter 3, the GHPS is site-dependent, meaning it only functions properly and attains maximum use of the Earth's heat when the GHEs are installed in a site with soil that has strong thermal properties (i.e., high temperature). Furthermore, GHPSs' output temperatures are limited and completely dependent on ground temperature and, they cannot provide heat to the heat pump system at temperatures higher than the ground temperature. Therefore, Oklahoma State University's GHPS was the most beneficial as it provided the highest temperature to the heat pump system, followed by GHPS at the University Politècnica de València, and then Oakland University. This likely occurred because the ground temperature in Oklahoma is higher than those in Valencia and Michigan. One significant advantage of installing GHPSs on sites with strong thermal properties is that it reduces operating costs. For instance, the GHPS at Oklahoma State University consumed less power for the water circulation pump and heat pump than other GHPSs, as shown in Figure 7.11 and Table 7.6.

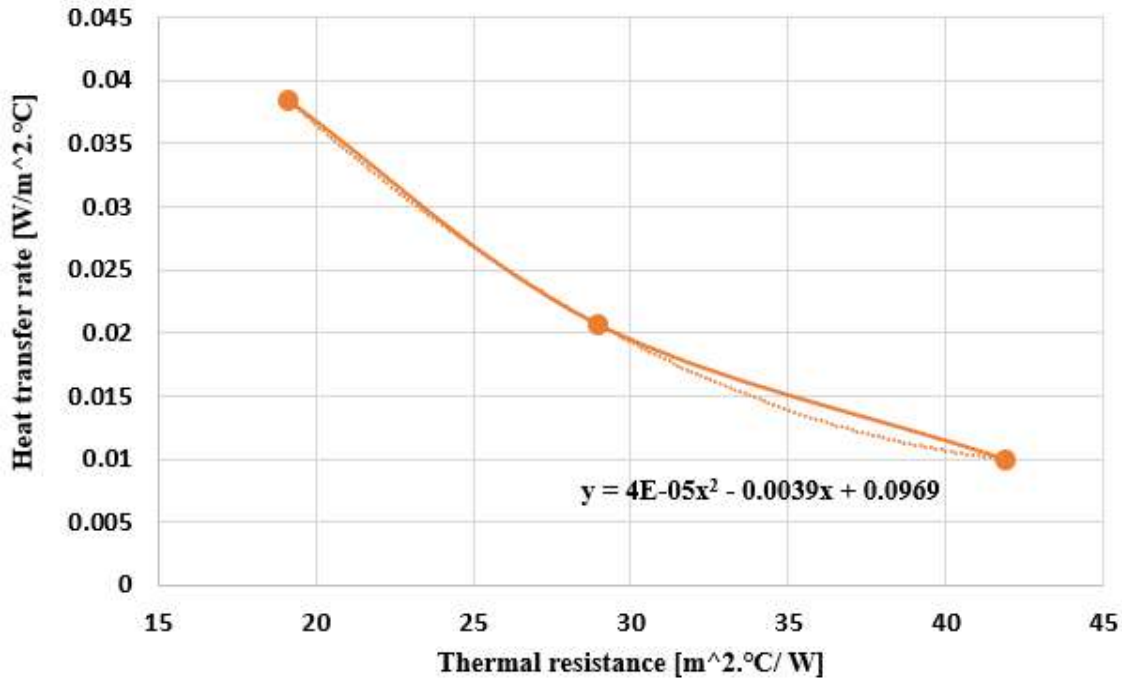

Figure 7.8. Relationship of the geothermal heat transfer rate and thermal resistance.

Figure 7.8. Illustrates the results of the geothermal heat transfer rate, according to the thermal resistance. The heat transfer rate increases as thermal resistance decreases. The maximum heat transfer rate was observed (41.869 $\mathrm{W/m^2.°C}$) when the thermal resistance was 0.01 $\mathrm{m^2.°C/\ W}$. Thermal resistance influences the heat transfer rate between the water inside the pipe and the surrounding ground; therefore, lowering thermal resistance allows more heat to flow quickly in either direction. The correlation equation is defined by $y = 4\,E - \ 05x^2\ - 0.0039x - 0.0969$.

where x represents thermal resistance ($\mathrm{m^2.°C/\ W}$) and y represents the heat transfer rate ($\mathrm{W/m^2.°C}$).

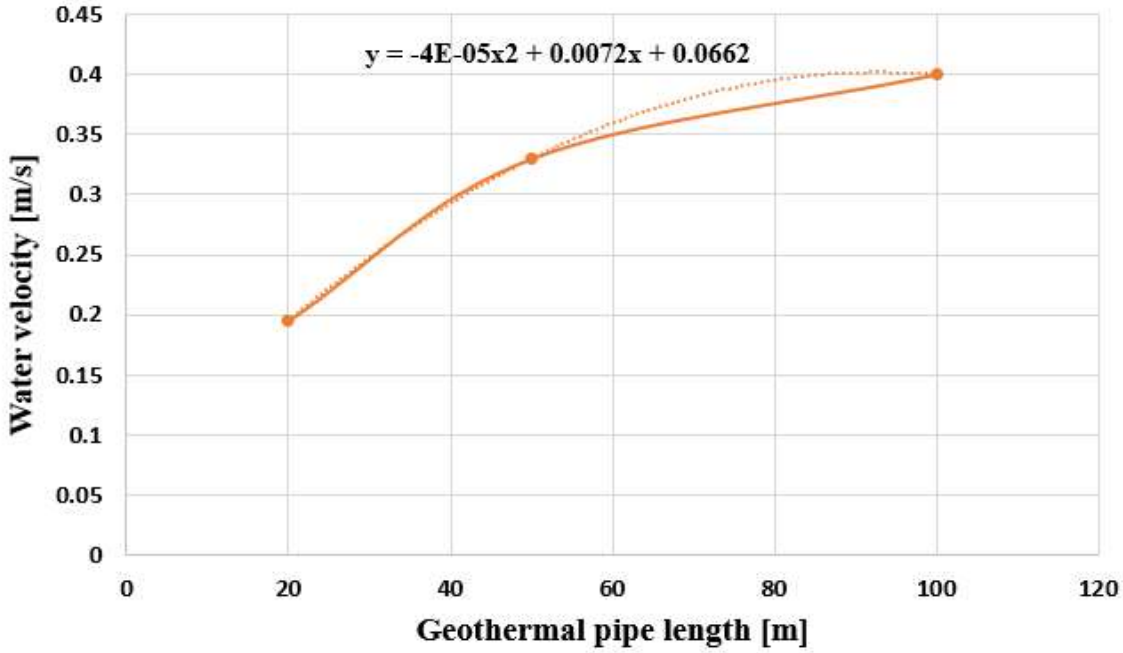

Figure 7.9. Relationship of the geothermal pipe length and water velocity.

The results of the water velocity according to the pipe length are depicted in Figure 7.9. According to the figure, the water velocity increases as the pip length increases. This indicates that controlling the water velocity inside the GHE's U-tube can reduce power consumption for the water circulation pump and heat pump, thereby enhancing GHPS performance. Here, the correlation equation describes the relationship between water velocity and pipe length, which is defined as $y = -4\,E-\ 05x^2 + 0.0072x - 0.0662$. where x represents the pipe length (m) and y represents the water velocity (m/s).

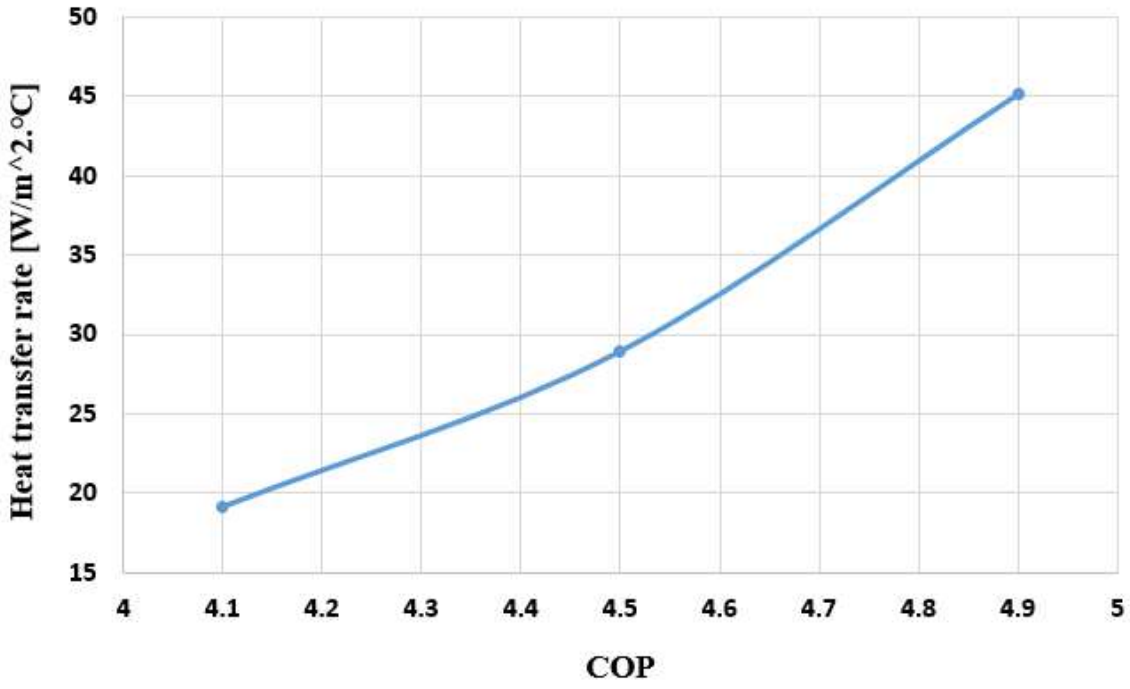

Figure 7.10. Relationship of the geothermal heat transfer rate and Coefficient of Performance (COP).

Figure 7.10. depicts the results of COP according to the geothermal heat transfer rate. The COP of geothermal heat pump systems at Oakland University, the University Politècnica de València, and Oklahoma State University was 4.1, 4.5, and 4.9, respectively. The highest COP 4.9 was observed when the geothermal heat transfer rate was 45.2 $W/m^2.℃$. As the heat transfer rate decreases, the COP decreases. Therefore, any increase in the heat transfer rate between the water inside the pipe and the surrounding ground will result in enhanced overall system performance.

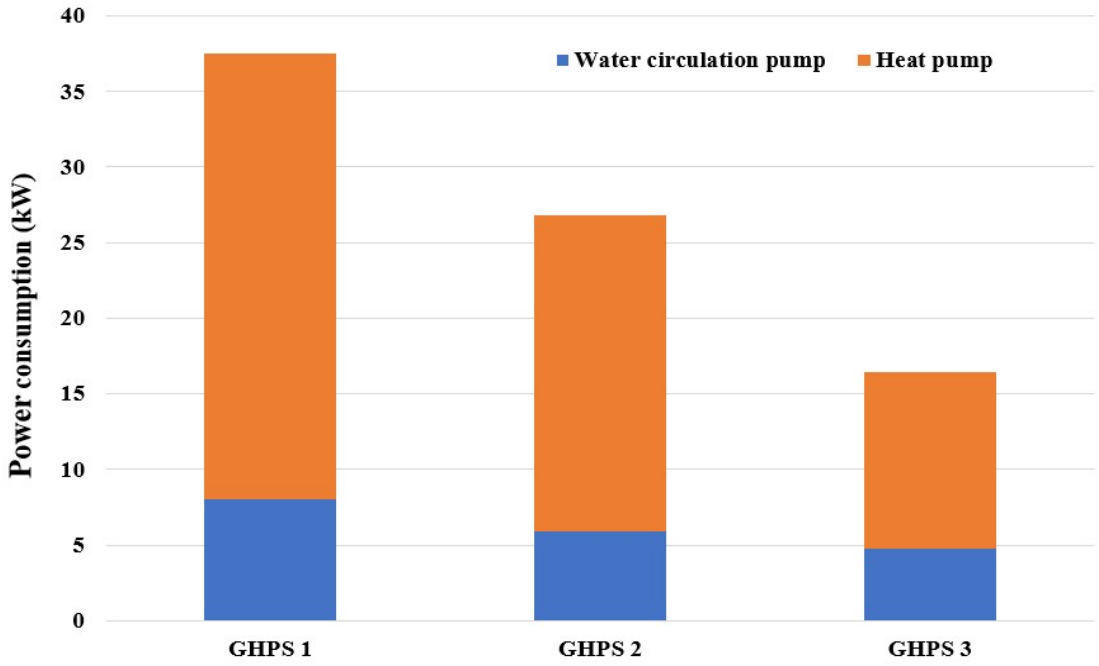

Figure 7.11. Water circulation pump and heat pump power consumption, where GHPS 1 is at Oakland University, GHPS 2 is at the University Politècnica de València, and GHPS 3 is at Oklahoma State University.

Table 7.6. Water circulation pump and heat pump power consumption (kW).

GHPS Location	Water Circulation Pump	Heat Pump	Total
Oakland University	7.99	29.506	37.496
University Politècnica de València	5.93	20.855	26.785
Oklahoma State University	4.77	11.693	16.463

Figure 7.11 depicts the water circulation pump and heat pump power consumption for each GHPS. The total power consumption for GHPS 1, GHPS 2, and GHPS 3 was

37.496 kW, 26.785 kW, and 16.463 kW, respectively, as shown in Table 7.6. According to the table, the power consumption of GHPS 1's water circulation pump and heat pump was the lowest, followed by GHPS 2, and then GHPS 3. As a result, Oklahoma State University's GHPS was the most advantageous because it obtained the greatest amount of earth's heat while consuming less power for the water circulation pump and heat pump, and its COP was higher than the GHPS at those universities.

7.4 Controlling

MPC was designed to control the water velocity inside the vertical underground loop pipe, which can optimize the GHE's water temperature such that it reaches ground temperature near the pipe exit. This ensures that the heat pump will deliver the desired temperature (i.e., ground temperature). The proposed nonlinear heat transfer model is a single input single output (SISO) control system that was previously mathematically modeled in Chapter 4.

7.4.1 MPC Implementation

The working fluid (i.e., water) velocity in the vertical U-tube pipe affects the water temperature in the GHE and consumes power which will increase with higher velocities. To optimize the water temperature, the MPC was designed to control the water velocity by determining the next optimal value $v(k+1+i)$ based on optimization. This forces the water temperature to follow the reference temperature trajectory along the prediction horizon (NP) while satisfying the constraints in control input values v_{min} and v_{max} accomplishing two major goals. First, it keeps the water flowing at an optimal rate and

reduces the power consumption of the water circulation pump because there is no need to increase the water velocity. Second, it allows the water temperature to track the reference temperature signal, as demonstrated in Figure 7.12. The system model's parameter values were defined in Tables 7.1 and 7.2, and the prediction model was calculated using the discrete state space model (5.3). In addition, the MPC parameters were $N_P = 12$, $N_C = 2$, and $T_s = 0.01\ sec$, which were precisely tuned to achieve robust performance. The quadratic problem (QP) was solved subject to input constraints $-10 \leq u(k) \leq 10$ along with the length prediction. Figure 7.12 depicts the MPC controller design of the water velocity in the vertical ground heat exchanger.

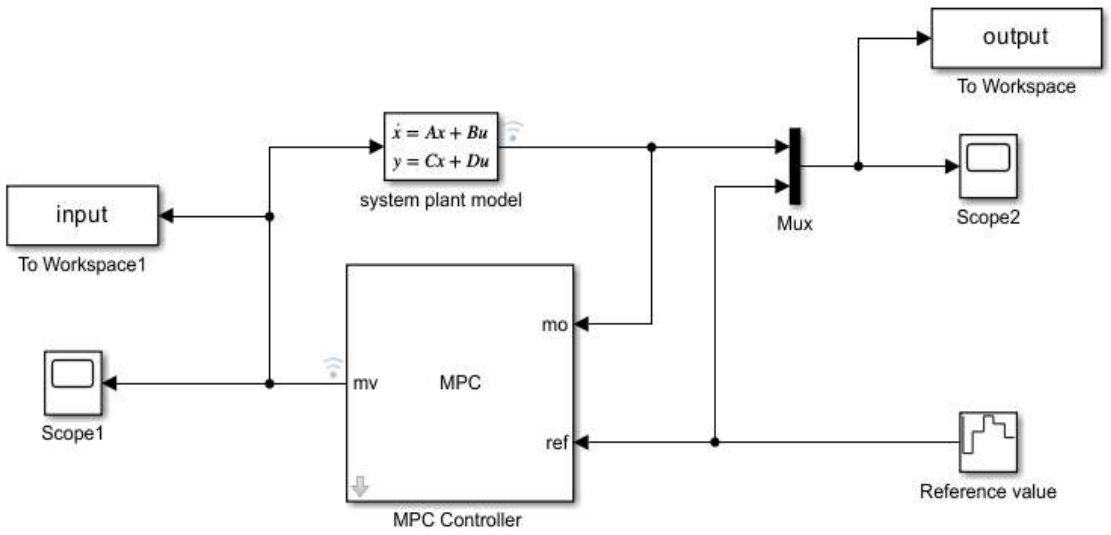

Figure 7.12. The MATLAB-Simulink MPC controller design model for water velocity in the vertical ground heat exchanger.

Subsequently, the MPC simulation results were implemented using a MATLAB script and the Simulink platform, as shown in Figures 7.13 and 7.14.

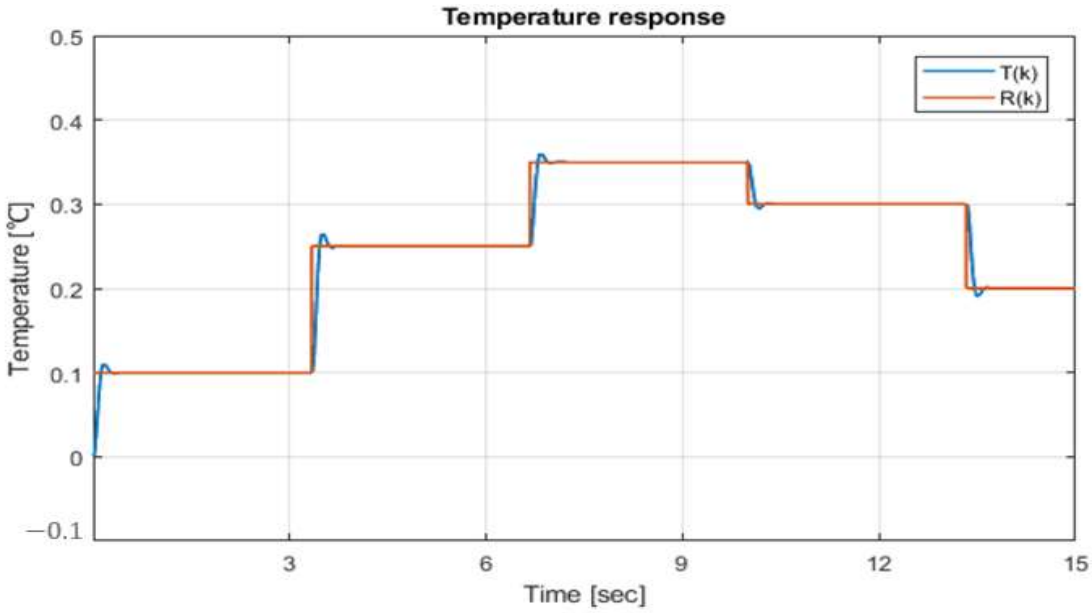

Figure 7.13. The MATLAB-Simulink model of the MPC water temperature results tracking the reference temperature trajectory.

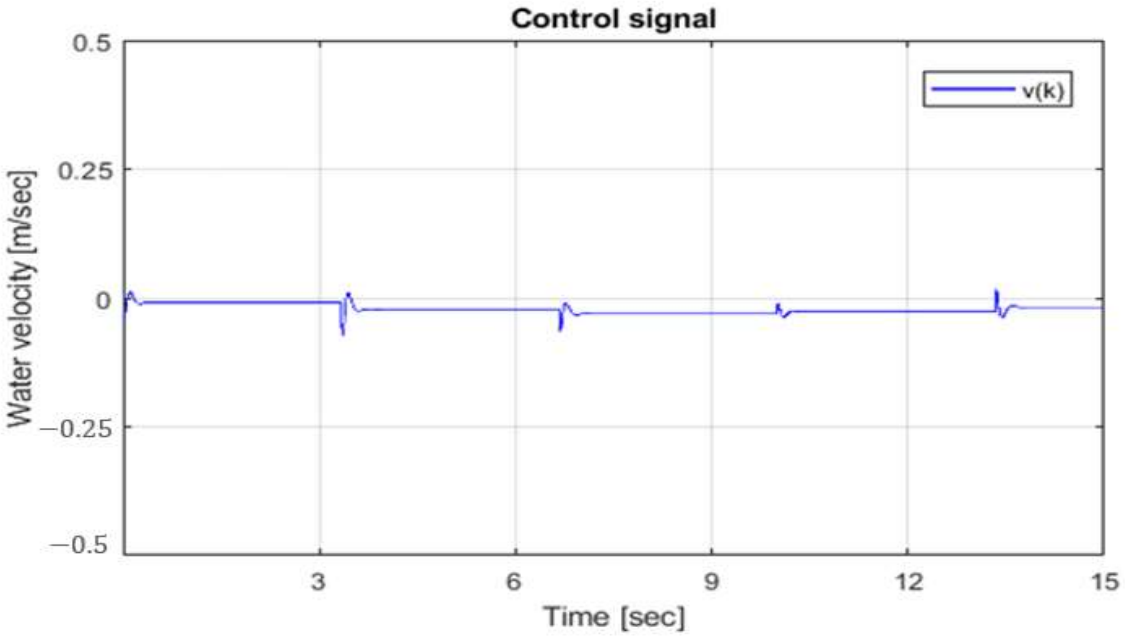

Figure 7.14. MPC control signal.

Figure 7.13 depicts the GHE's water temperature response behavior under the proposed MPC approach. According to this figure, the water temperature precisely tracked the reference temperature trajectory, with a slight over/undershoot. The result reflects the performance of the robust control design, which was influenced by fluctuations in water velocity and occurred when the water velocity exceeded the assumed constraints. The result revealed that the MPC can reduce the energy used by the water circulation pump while also stabilizing the water temperature to achieve the desired temperature. The MPC control signal is stable within the assumed range and fluctuates slightly, especially occurring at each beginning movement step (i.e., at $\sim 3.2, 6.5, 10,$ and 12.5 sec) according to the reference trajectory. The simulation result validated the MPC control design by matching water temperature results to a predefined reference trajectory.

7.5 GHPS Output Temperature Prediction

This section forecasts the GHPS output temperature for the next eight hours at three different locations, including Oklahoma State University, the University of Politècnic de Valitècnic, and Oakland University, using the IGM (1.1) model described in Chapter 6. Furthermore, three datasets are utilized to validate the IGM (1,1) model's accuracy.

7.5.1 Case Study I: Oklahoma State University's GHPS Output Temperature Prediction

Oklahoma State University's GHPS output temperature data set of 24 data points (i.e., 24 hours) from January 1 to January 2, 2015, was used to train the model on its behavior, which was generated in the following sequence.

$x^{(0)}(k) = (x^{(0)}(1), x^{(0)}(2),..., x^{(0)}(24)) = (21.9778, 30.1667, \ldots, 37.6889)$

The IGM (1,1) model's parameters (a, b) were determined using equation (6.5), as follows:

$[a, b]^{\mathbf{T}} = (\mathrm{B}^{\mathbf{T}}\mathrm{B})^{-\mathbf{1}}\mathrm{B}^{\mathbf{T}}\mathrm{Y}$,

where

$$[\mathrm{a}, b]^T = [-0.0065, 33.2012]^T,\ B = \begin{bmatrix} -21.9778 & 1 \\ -37.0611 & 1 \\ -68.3361 & 1 \\ \vdots & \vdots \\ -792.9056 & 1 \\ -830.5667 & 1 \end{bmatrix} \text{and} = \begin{bmatrix} 30.1667 \\ 32.3833 \\ 33.5167 \\ \vdots \\ 37.6333 \\ 37.6889 \end{bmatrix}$$

The predicted sequence $\hat{x}^{(0)}(k)$ of the IGM (1,1) model is computed using equation (6.11), which is as follows:

$$\begin{cases} \hat{x}^{(0)}(1) = x^{(0)}(1) = 21.9778\ ℃ \\ \hat{x}^{(0)}(k) = -33.45e^{0.0065(k-1)} - 5107.88 - (\hat{x}^{(1)}(k-1) - z^{(1)}(k-1)) \end{cases} \quad (7.1)$$

I obtained the model simulation (in-sample) and prediction (out-of-sample) results by substituting the values of $k = 2, 3, \ldots, 32$ into the equation (7.1). Consequently, the prediction results are shown in Table 7.7 and Figure 7.15. According to the prediction results (Figure 7.15), the improved IGM (1,1) model is well-trained on the dataset (in-sample), indicating its robustness to fit the dataset values much closer and thus accurately predicted Oklahoma State University's GHPS output temperature in Celsius (℃) for the next eight hours from 1:00 a.m. to 8:00 a.m., 2 January 2015, as follows: 37.6640, 37.6669, 376698, 37.6727, 37.6756, 37.6785, 37.6814, and 37.6843 (see Table 7.7). The

prediction accuracies of the applied models were evaluated using MAE, MAPE (%), and RMSE and then compared as shown in Table 7.7. According to Table 7.7, it can be observed that the IGM (1,1) model has lower MAE, RMSE, and MAPE (%) values of 0.027, 0.23, and 0.56 (%) than the GM (1,1) model, which has values 0.24, 1.96, and 4.98 (%). Thus, the IGM (1,1) model reduced the error prediction, which enhanced the prediction accuracy of the GM (1,1) model.

Table 7.7. The Hourly Oklahoma State University's GHPS Output Temperature Predictions from 1:00 a.m. to 8:00 a.m. on January 2, 2015.

Time (Hour)	**Actual Temperature Values ℃**	**IGM (1,1) Values ℃**	**GM (1,1) Values ℃**
25	37.7277	37.6640	38.8703
26	37.7666	37.6669	39.1248
27	37.8222	37.6698	39.3809
28	37.8777	37.6727	39.6387
29	37.9055	37.6756	39.8982
30	37.9444	37.6785	40.1594
31	38	37.6814	40.4223
32	38.0444	37.6843	40.6869

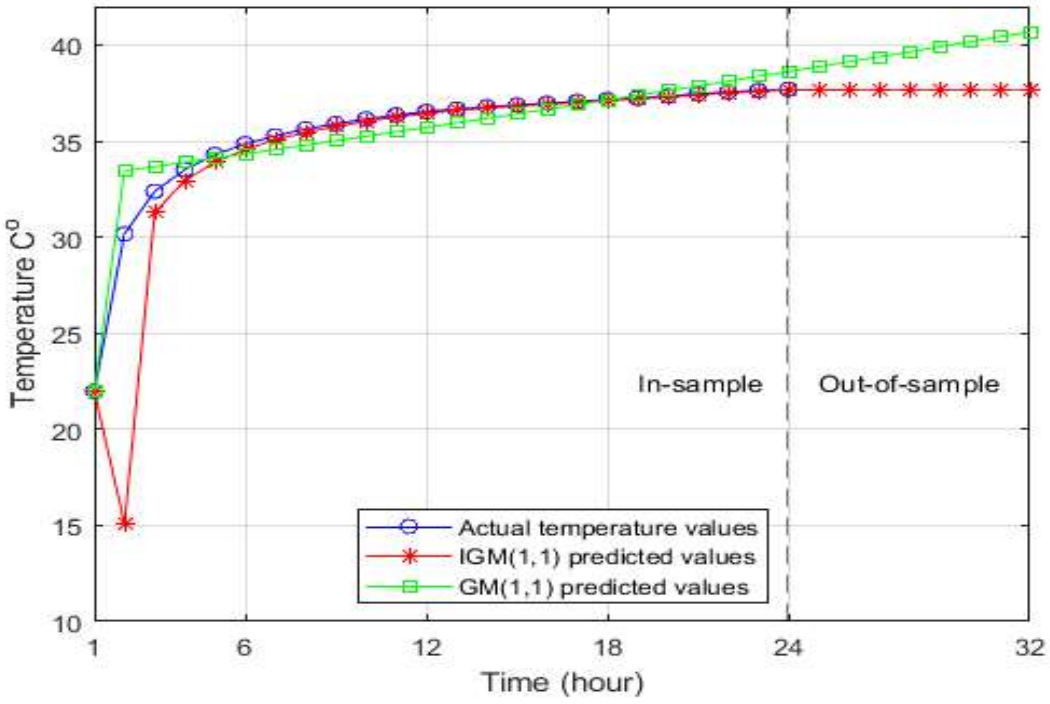

Figure 7.15. Actual (in-sample) and predicted (out-of-sample) GHPS's output temperature for Oklahoma State University.

To further demonstrate the IGM (1,1) model's significant improvement in accuracy prediction, it was used to predict the GHPS output temperature for the following eight hours at both the University of Politècnica de València and Oakland University, respectively. Therefore, the IGM (1,1) and GM (1,1) models were implemented in MATLAB, and predicted values for the two GHPSs output temperatures were observed (shown in Table 7.8, Table 7.9, Figure 7.16, and Figure 7.17).

7.5.2 Case Study II: The Politècnica de València University's GHPS Output Temperature Prediction

According to the prediction results (Figure 7.16), the IGM (1,1) model accurately predicted Politècnica de València University's GHPS output temperature in Celsius (℃) for the next eight hours from 1:00 a.m. on 9 May 2002 to 8:00 a.m. on 9 May 2002, as follows: 19.389, 19.3879, 19.3869, 19.3858, 19.3848, 19.3837, 19.3827, and 19.3817 (see Table 7.8).

Table 7.8. The Hourly Politècnica de València University's GHPS Output Temperature Predictions from 1:00 a.m. to 8:00 a.m. on May 9, 2022.

Time (Hour)	**Actual Temperature Values** ℃	**IGM (1,1) Values** ℃	**GM (1,1) Values** ℃
25	19.31	19.3890	20.1565
26	19.29	19.3879	20.2630
27	19.31	19.3869	20.3701
28	19.25	19.3858	20.4777
29	19.18	19.3848	20.5859
30	19.25	19.3837	20.6947
31	19.18	19.3827	20.8040
32	18.74	19.3817	20.9139

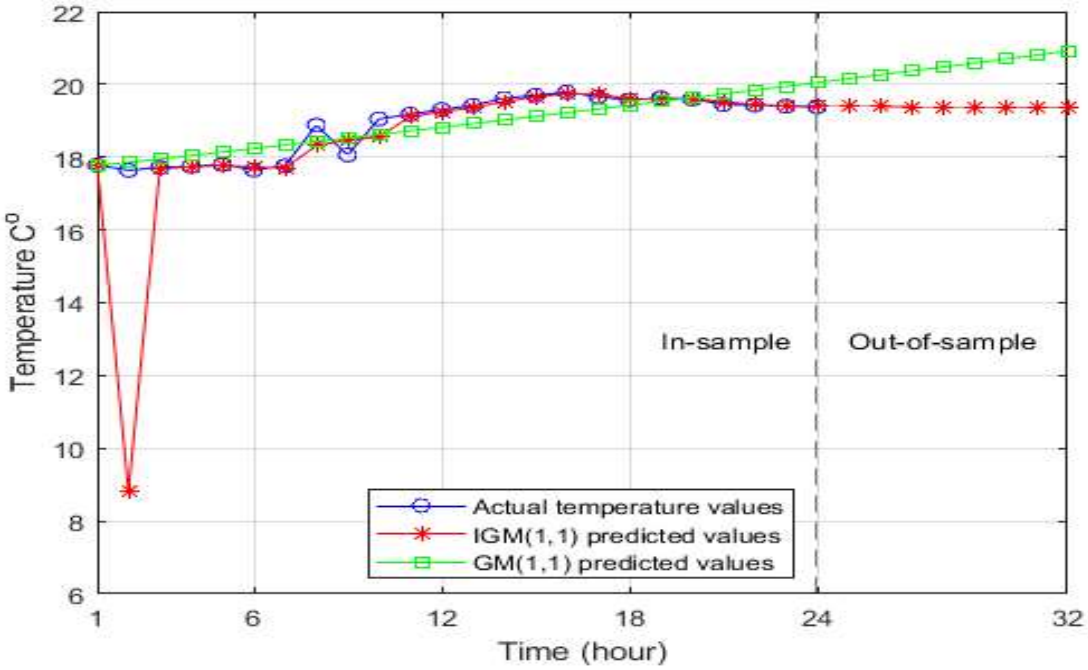

Figure 7.16. Actual (in-sample) and predicted (out-of-sample) GHPS's output temperature for Politècnica de València University.

7.5.3 Case Study III: Oakland University's GHPS Output Temperature Prediction

According to Figure 7.17, the IGM (1,1) model accurately predicted Oakland University's GHPS output temperature in Celsius (℃) for the following eight hours from 1:00 a.m. to 8:00 a.m. on July 2, 2019, as follows: 20.8253, 20.8121, 20.8006, 20.7892, 20.7777, 20.7662, 20.7548, and 20.7433 (see Table 7.9).

Table 7.9. The Hourly Oakland University's GHPS Output Temperature Predictions from 1:00 a.m. to 8:00 a.m. on July 2, 2019.

Time (Hour)	**Actual Temperature Values ℃**	**IGM (1,1) Values ℃**	**GM (1,1) Values ℃**
25	21.11	20.8235	24.6442
26	20	20.8121	24.5149
27	20.56	20.8006	24.5658
28	20	20.7892	24.6167
29	20.56	20.7777	24.6678
30	20.11	20.7662	24.7189
31	23.33	20.7548	24.7702
32	22.78	20.7433	24.8216

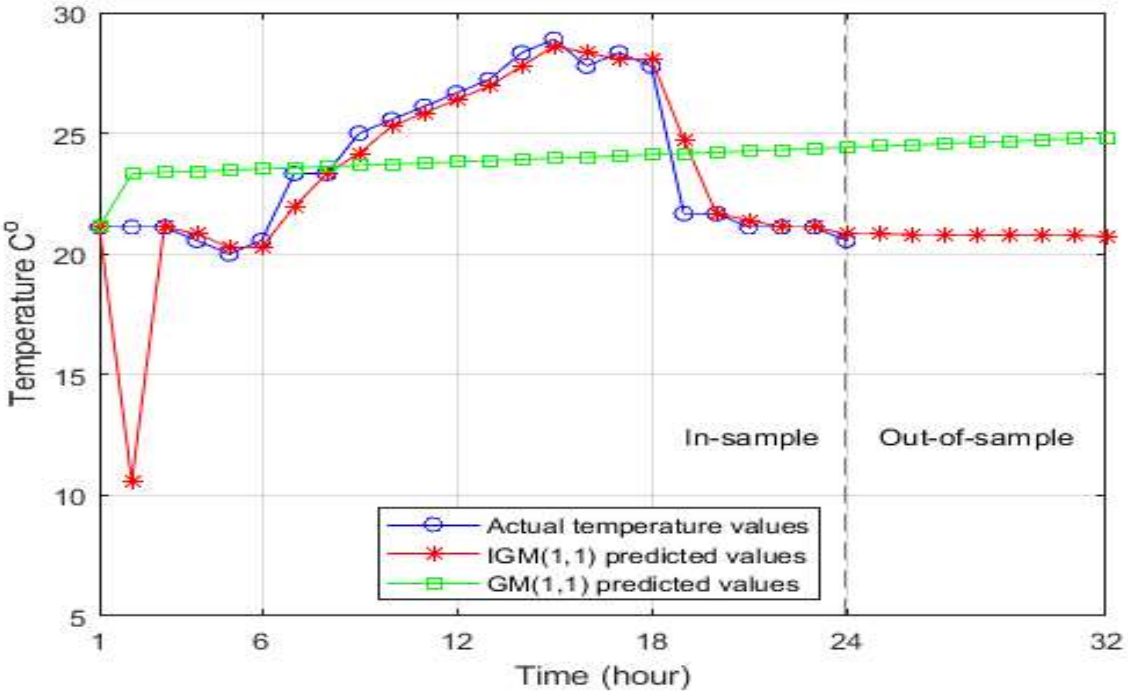

Figure 7.16. Actual (in-sample) and predicted (out-of-sample) GHPS's output temperature for Oakland University.

Table 7.10. The accuracy assessment metrics to compare the GM (1,1), and IGM (1,1) models for three GHPSs' output temperature predictions.

Geothermal Heat Pump System Output Temperature Predictions	**GM (1,1) model**			**IGM (1,1) model**		
	MAE	RMSE	MAPE (%)	MAE	RMSE	MAPE (%)
Oklahoma State University	0.24	1.96	4.98	0.027	0.23	0.56
València University	0.17	1.402	7.02	0.025	0.263	1.033
Oakland University	0.144	3.625	16.66	0.038	1.243	4.15

The prediction accuracies of the IGM (1,1) and GM (1,1) models were assessed using the equations (6.12) – (6.14), and the results are depicted in Table 7.10. According to the prediction results, the IGM (1,1) model dramatically improved the prediction accuracy of the GM (1,1) model by minimizing the error prediction during both in-sample and out-of-sample periods. Better yet, the IGM (1,1) model outperformed the traditional GM (1,1) model for all datasets used, with reduced MAE, RMSE, and MAPE (%) values. Even better, the IGM (1,1) model perdition accuracy was validated using 10 geothermal energy capacity installation datasets and the model outperformed the traditional GM (1,1) model for all 10 datasets [8]. This indicated that the IGM (1,1) model ensured error reduction, meaning that it was a suitable method for producing accurate predictions; however, its precision varies from one dataset to another which depends on the self-behaviors of each dataset. For example, the IGM (1,1) model had the highest prediction accuracy for the GHPS output temperature at Oklahoma State University, with MAE, RMSE, and MAPE (%) values of 0.027, 0.23, and 0.56, respectively, followed by the Politècnica de València University, with MAE, RMSE, and MAPE (%) values of 0.025, 0.263, and 1.033, respectively. Then, Oakland University had MAE, RMSE, and MAPE (%) values of 0.038, 1.243, and 4.15, respectively. Simply, Oklahoma State University's GHPS output temperature was the most consistently applied dataset, making it easier for the model to accurately predict the next eight hours. On the other hand, the other two universities' GHPS output temperature datasets were more varied, making it more challenging for the model to predict the next eight hours.

CHAPTER EIGHT

CONCLUSION AND FUTURE WORK

8.1 Conclusions

In this dissertation, a novel mathematical dynamic model of heat transfer behavior between liquid inside the vertical underground pipes and surrounding ground was proposed for heating and cooling modes in a GHE. The proposed dynamic model was applied to three case studies of GHPS at Oakland University, the University Politècnica de València, and Oklahoma State University in both heating and cooling modes to assess its validity and identify the optimal water velocity ranges to maximize the efficiency of their GHE. The proposed dynamic model was implemented in MATLAB using an ODE solver. The simulation results (Figures 7.2 -7.7) demonstrated that the water temperature only reached the ground temperature for both heating and cooling modes when the water velocity was moderate enough to allow sufficient time for heat exchange and reach equilibrium. This indicated that the heat exchange between the water inside the pipe and the surrounding ground required sufficient time to balance. The acceptable range of water velocity in a vertical single U-tube GHE pipe of GHPS at Oakland University, the University Politècnica de València, and Oklahoma State University was between 0.35 and 0.45 m/s, 0.28 and 0.38 m/s, and 0.17 and 0.22 m/s, respectively (see Table 7.5). The Coefficient of Performance (COP) of geothermal heat pump systems at Oakland University, the University Politècnica de València, and Oklahoma State University was 4.1, 4.5, and 4.9, respectively. The results showed that the GHPS at Oklahoma State University was more beneficial than the GHPSs at the University Politècnic de Valitècnic

and Oakland University as it obtained the highest heat from the earth while using the least power for the water circulation pump and heat pump than the GHPSs at the other universities.

Model Predictive Control (MPC) was designed to control the water velocity, which can optimize the water temperature. The MPC predicted the future GHE water temperature, resulting in a high-tracking performance with a reference temperature trajectory, as demonstrated by the simulation result (see Figure 7.12). This resulted in lower power consumption for the circulation water pump and ensured that the heat pump delivered the appropriate temperature.

The Improved Grey Prediction Model (IGM (1,1)) was proposed to increase the traditional GM (1,1) model prediction accuracy. The proposed IGM (1,1) model was based on optimizing the current predicted value by subtracting the error prediction between the previous accumulated time response of the GM (1,1) model and its previous background value. The IGM (1,1) model accurately predicted the GHPS output temperatures for the next eight hours at Oklahoma State University, the University of Politècnic de Valencia, and Oakland University. Three GHPS output temperature datasets were utilized to validate the IGM (1,1) model prediction accuracy. For all utilized datasets, the IGM (1,1) model was more accurate than the traditional GM (1,1) model, demonstrating that it was an efficient and promising approach for accurate short-term forecasting. As a result, the IGM (1,1) model improved the GM (1,1) model's prediction accuracy by minimizing error prediction with varying percentages based on the self-behavior of each dataset.

8.2 Contributions

The following are the main contributions of this dissertation:

- Developed a novel mathematical dynamic model of heat transfer behavior between the liquid inside the pipe and the surrounding ground in a GHE for heating and cooling modes.
- Analyzed the effect of water velocity on GHE performance and loop exit temperature, as well as the energy consumed by the water circulation pump.
- Identified the optimal water velocity for different vertical single U-tube GHE pipes of the GHPS at Oakland University, the University Politècnica de València, and Oklahoma State University.
- Designed and implemented an MPC controller in a real-world case study using a 400-ton GHPS at Oakland University to control water velocity inside the pipe, optimizing the GHE's exit temperature and conserving energy for the water circulation pump.
- Improved a new prediction model that can accurately predict the GHPS's output temperature up to eight hours in advance.

8.3 Future Work

- Designing Gain-Scheduled MPC (GS-MPC) Control for this nonlinear system model.
- Developing a method for detecting anomalies in the water circulation pump readings (i.e., liquid flow rate).

- Improving the IGM (1,1) model for long-term GHPS's output temperature prediction.
- Developing a comparison using GHPS technology for heating and cooling as well as power generation.

References

1. A.K. Raturi, Renewables 2019 global status report. 2019.

2. Office of Energy Efficiency & Renewable Energy. Why Energy Efficiency Upgrades. [cited Jun 02, 2022]; Available from: https://www.energy.gov/eere/why-energy-efficiency-upgrades#:~:text=Typically%2C%2043%25%20of%20a%20home%20utility%20bill%20goes,for%20heating%20and%20cooling%20from%2020%25%20to%2050%25.

3. Environmental Protection Agency. Global Climate Change. 2017 [cited Dec 03, 2022]; Available from: https://archive.epa.gov/climatechange/kids/solutions/technologies/geothermal.html#:~:text=Geothermal%20Power%20Plants%201%20Hot%20water%20is%20pumped,tower%20and%20condenses%20back%20to%20water.%20More%20items.

4. Office of Energy Efficiency & Renewable Energy. Geothermal Technologies Office. [cited Dec 03, 2022]; Available from: https://www.energy.gov/eere/geothermal/geothermal-technologies-office.

5. National Geographic. Geothermal Energy [cited Dec 03, 2022]; Available from: https://education.nationalgeographic.org/resource/geothermal-energy.

6. LAZARD. Lazard's Levelized Cost of Energy Analysis. 2018 [cited Dec 04, 2022]; Available from: https://www.lazard.com/media/450784/lazards-levelized-cost-of-energy-version-120-vfinal.pdf.

7. Statista. Geothermal Energy Capacity Worldwide from 2009 to 2021. 2022 [cited Aug 02, 2022]; Available from: https://www.statista.com/statistics/476281/global-capacity-of-geothermal-energy/.

8. K. Salhein, C.J. Kobus, and M. Zohdy, "Forecasting Installation Capacity for the Top 10 Countries Utilizing Geothermal Energy by 2030", Thermo. Vol. **2**, no. 4, pp. 334-351, 2022.

9. M. Zogg, "History of heat pumps-swiss contributions and international milestones". 2008.

10. R.G. Bloomquist, "Geothermal heat pumps four plus decades of experience", GHC Bulletin. 1999.

11. Office of Energy Efficiency & Renewable Energy, IEA 2020 U.S. Geothermal Report. 2021.

12. Energy Saver. Choosing and Installing Geothermal Heat Pumps. [cited Aug 25, 2022]; Available from: https://www.energy.gov/energysaver/choosing-and-installing-geothermal-heat-pumps.

13. United States General Accounting Office, Geothermal Energy: Outlook Limited for Some Uses But Promising for Geothermal Heat Pumps. 1994.

14. A.J. Philippacopoulos and M.L. Berndt, "Influence of Debonding in Ground Heat Exchangers Used With Geothermal Heat Pumps", Geothermics. Vol. **30**, no. 5, pp. 527-545, 2001.

15. A.M. Omer, "Ground-source heat pumps systems and applications", Renewable and sustainable energy reviews. Vol. **12**, no. 2, pp. 344-371, 2008.

16. J. Parsons. What is Geothermal Energy And How Can I Heat/Cool My House With It? 2020 [cited Jun 05, 2022]; Available from: https://www.climatemaster.com/homeowner/news/geothermal-energy/geothermal-energy/2020-12-11-what-is-geothermal-energy-and-how-can-i-heat-cool-my-house-with-it.

17. G. Heat, Geothermal Energy Outlook Limited for Some Uses but Promising for Geothermal Heat Pumps. 1994.

18. H. Miles. Heat Pump vs. Geothermal Systems: Which is Best? 2021 [cited Jun 03, 2022]; Available from: https://homeinspectioninsider.com/heat-pump-vs-geothermal-systems-which-is-best/.

19. Greensleeves Technologies Corp. CO2 Emissions And Geothermal. 2018 [cited Jun 10, 2022]; Available from: https://www.greensleevestech.com/co2-emissions-and-geothermal/.

20. Manitoba Geothermal Energy Alliance. The Forks. [cited Jun 05, 2022]; Available from: https://www.mgea.ca/lead-project/the-forks/.

21. B. Miller. 17 Geothermal Heat Pump Pros and Cons. 2019 [cited Aug 26, 2022]; Available from: https://greengarageblog.org/17-geothermal-heat-pump-pros-and-cons#:~:text=The%20installation%20of%20a%20geothermal%20heat%20pump%20is,any%20gardens%20that%20may%20be%20on%20your%20property.

22. Energy Saver. Geothermal Heat Pumps. [cited Aug 30, 2022]; Available from: https://www.energy.gov/energysaver/geothermal-heat-pumps.

23. K. Salhein, C. Kobus, and M. Zohdy, "Control of Heat Transfer in a Vertical Ground Heat Exchanger for a Geothermal Heat Pump System", Energies. Vol. **15**, no. 14, pp. 5300, 2022.

24. E.K. Akpinar and A. Hepbasli, "A comparative study on exergetic assessment of two ground-source (geothermal) heat pump systems for residential applications", Building and Environment. Vol. **42**, no. 5, pp. 2004-2013, 2007.

25. Energy Smart Alternatives. How Long Does It Take To Install A Geothermal System? [cited Aug 28, 2022]; Available from: https://energysmartalternatives.com/2016/03/how-long-does-it-take-to-install-a-geothermal-system/#:~:text=Installations%20in%20new%20construction%20typically%20take%20longer%20due,Permitting%20and%20Design%20%E2%80%93%202%20to%203%20Weeks.

26. F. Ruiz-Calvo and C. Montagud, "Reference data sets for validating GSHP system models and analyzing performance parameters based on a five-year operation period", Geothermics. Vol. **51**, pp. 417-428, 2014.

27. J. Leidel, Human Health Science Building Geothermal Heat Pump Systems. 2014, Office of Scientific and Technical Information (OSTI).

28. R.A. Beier, M.D. Smith, and J.D. Spitler, "Reference data sets for vertical borehole ground heat exchanger models and thermal response test analysis", Geothermics. Vol. **40**, no. 1, pp. 79-85, 2011.

29. R.M. Singh, A.K. Sani, and T. Amis, "An overview of ground-source heat pump technology", Managing Global Warming. pp. 455-485, 2019.

30. M. Planck, Treatise on Thermodynamics. 1945: Dover Publications.

31. A. Gultekin, M. Aydin, and A. Sisman, "Thermal performance analysis of multiple borehole heat exchangers", Energy Conversion and Management. Vol. **122**, pp. 544-551, 2016.

32. L. Fang, et al., "Study on the efficiency of single and double U-tube heat exchangers", Procedia Engineering. Vol. **205**, pp. 4045-4051, 2017.

33. G.A. Florides, P. Christodoulides, and P. Pouloupatis, "Single and double U-tube ground heat exchangers in multiple-layer substrates", Applied energy. Vol. **102**, pp. 364-373, 2013.

34. G. Florides and S. Kalogirou, "Ground heat exchangers—A review of systems, models and applications", Renewable energy. Vol. **32**, no. 15, pp. 2461-2478, 2007.

35. M.-J. Kim, et al., "Thermal performance evaluation and parametric study of a horizontal ground heat exchanger", Geothermics. Vol. **60**, pp. 134-143, 2016.

36. Geothermal Solutions. Pond Loop. [cited Jun 20, 2022]; Available from: http://www.geothermalsolutions.net/pond-loop-geothermal-pond-loop-loops.html.

37. P. Cui, H. Yang, and Z. Fang, "Numerical analysis and experimental validation of heat transfer in ground heat exchangers in alternative operation modes", Energy and buildings. Vol. **40**, no. 6, pp. 1060-1066, 2008.

38. C. Sáez Blázquez, et al., "Efficiency analysis of the main components of a vertical closed-loop system in a borehole heat exchanger", Energies. Vol. **10**, no. 2, pp. 201, 2017.

39. A. Zarrella, A. Capozza, and M. De Carli, "Analysis of short helical and double U-tube borehole heat exchangers: A simulation-based comparison", Applied Energy. Vol. **112**, pp. 358-370, 2013.

40. J. Gao, et al., "Thermal performance and ground temperature of vertical pile-foundation heat exchangers: A case study", Applied Thermal Engineering. Vol. **28**, no. 17-18, pp. 2295-2304, 2008.

41. C. Xia, et al., "Experimental study on geothermal heat exchangers buried in diaphragm walls", Energy and Buildings. Vol. **52**, pp. 50-55, 2012.

42. B. Bezyan, S. Porkhial, and A.A. Mehrizi, "3-D simulation of heat transfer rate in geothermal pile-foundation heat exchangers with spiral pipe configuration", Applied Thermal Engineering. Vol. **87**, pp. 655-668, 2015.

43. A.A. Mehrizi, et al., "Energy pile foundation simulation for different configurations of ground source heat exchanger", International Communications in Heat and Mass Transfer. Vol. **70**, pp. 105-114, 2016.

44. S. Yoon, et al., "Evaluation of the thermal efficiency and a cost analysis of different types of ground heat exchangers in energy piles", Energy Conversion and Management. Vol. **105**, pp. 393-402, 2015.

45. J. Luo, et al., "Thermo-economic analysis of four different types of ground heat exchangers in energy piles", Applied Thermal Engineering. Vol. **108**, pp. 11-19, 2016.

46. Y.L.E. Law and S.B. Dworkin, "Characterization of the effects of borehole configuration and interference with long term ground temperature modelling of ground source heat pumps", Applied Energy. Vol. **179**, pp. 1032-1047, 2016.

47. L. Pu, et al., "Structure optimization for horizontal ground heat exchanger", Applied Thermal Engineering. Vol. **136**, pp. 131-140, 2018.

48. A.A. Serageldin, et al., "Parametric analysis, response surface, sensitivity analysis, and optimization of a novel spiral-double ground heat exchanger", Energy Conversion and Management. Vol. **240**, pp. 114251, 2021.

49. X. Song, et al., "Heat extraction performance simulation for various configurations of a downhole heat exchanger geothermal system", Energy. Vol. **141**, pp. 1489-1503, 2017.

50. P. Kushwaha, "PHYSICAL MODEL TO INCREASE THE DISCHARGE TIME OF TES SYSTEM USING U AND W TUBE".

51. S. Yoon, S.-R. Lee, and G.-H. Go, "A numerical and experimental approach to the estimation of borehole thermal resistance in ground heat exchangers", Energy. Vol. **71**, pp. 547-555, 2014.

52. J. Acuña, Distributed thermal response tests: New insights on U-pipe and Coaxial heat exchangers in groundwater-filled boreholes. 2013, KTH Royal Institute of Technology.

53. J. Raymond, S. Mercier, and L. Nguyen, "Designing coaxial ground heat exchangers with a thermally enhanced outer pipe", Geothermal Energy. Vol. **3**, no. 1, pp. 1-14, 2015.

54. A. Zarrella, M. De Carli, and A. Galgaro, "Thermal performance of two types of energy foundation pile: Helical pipe and triple U-tube", Applied Thermal Engineering. Vol. **61**, no. 2, pp. 301-310, 2013.

55. A. Zarrella, A. Capozza, and M. De Carli, "Performance analysis of short helical borehole heat exchangers via integrated modelling of a borefield and a heat pump: A case study", Applied Thermal Engineering. Vol. **61**, no. 2, pp. 36-47, 2013.

56. M. Suzuki, et al., "Development of a spiral type heat exchanger for ground source heat pump system", Energy Procedia. Vol. **96**, pp. 503-510, 2016.

57. M. Habibi and A. Hakkaki-Fard, "Evaluation and improvement of the thermal performance of different types of horizontal ground heat exchangers based on techno-economic analysis", Energy Conversion and Management. Vol. **171**, pp. 1177-1192, 2018.

58. E.D. Kerme and A.S. Fung, "Heat transfer analysis of single and double U-tube borehole heat exchanger with two independent circuits", Journal of Energy Storage. Vol. **43**, pp. 103141, 2021.

59. K. Chen, et al., "Numerical study on the heat performance of enhanced coaxial borehole heat exchanger and double U borehole heat exchanger", Applied Thermal Engineering. Vol. **203**, pp. 117916, 2022.

60. V. Tarnawski, T. Momose, and W. Leong, "Assessing the impact of quartz content on the prediction of soil thermal conductivity", Géotechnique. Vol. **59**, no. 4, pp. 331-338, 2009.

61. K.K. Agrawal, R. Misra, and G.D. Agrawal, "Improving the thermal performance of ground air heat exchanger system using sand-bentonite (in dry and wet condition) as backfilling material", Renewable Energy. Vol. **146**, pp. 2008-2023, 2020.

62. Z. Wang, et al., "Research of heat and moisture transfer influence on the characteristics of the ground heat pump exchangers in unsaturated soil", Energy and Buildings. Vol. **130**, pp. 140-149, 2016.

63. F. Tang and H. Nowamooz, "Factors influencing the performance of shallow Borehole Heat Exchanger", Energy conversion and management. Vol. **181**, pp. 571-583, 2019.

64. J.C. Choi, S.R. Lee, and D.S. Lee, "Numerical simulation of vertical ground heat exchangers: Intermittent operation in unsaturated soil conditions", Computers and Geotechnics. Vol. **38**, no. 8, pp. 949-958, 2011.

65. A. Aizzuddin, T. Yusof, and W. Azmi. Investigation of pipe materials and thermal conductivity of soil on the performance of ground heat exchanger operating under Malaysia climate. in IOP Conference Series: Materials Science and Engineering. 2021. IOP Publishing.

66. C. Lee, et al., "Characteristics of thermally-enhanced bentonite grouts for geothermal heat exchanger in South Korea", Science in China Series E: Technological Sciences. Vol. **53**, no. 1, pp. 123-128, 2010.

67. M. Allan and A. Philippacopoulos. Performance characteristics and modelling of cementitious grouts for geothermal heat pumps. in Proceedings world geothermal congress. 2000.

68. K.S. Chang and M.J. Kim, "Thermal performance evaluation of vertical U-loop ground heat exchanger using in-situ thermal response test", Renewable Energy. Vol. **87**, pp. 585-591, 2016.

69. M.D. Smith and R.L. Perry, "Borehole grouting: field studies and thermal performance testing", ASHRAE Transactions. Vol. **105**, pp. 451, 1999.

70. W. Zhang, et al., "Investigation on influential factors of engineering design of geothermal heat exchangers", Applied Thermal Engineering. Vol. **84**, pp. 310-319, 2015.

71. H. Gao and M. Shao, "Effects of temperature changes on soil hydraulic properties", Soil and Tillage Research. Vol. **153**, pp. 145-154, 2015.

72. B. Liang, M. Chen, and J. Guan, "Assessment on the thermal and moisture migration of sand-based materials coupled with kaolin additive", Journal of Thermal Analysis and Calorimetry. pp. 1-14, 2022.

73. C. Lee, et al., "Viscosity and salinity effect on thermal performance of bentonite-based grouts for ground heat exchanger", Applied clay science. Vol. **101**, pp. 455-460, 2014.

74. M.L. Allan and S.P. Kavanaugh, "Thermal conductivity of cementitious grouts and impact on heat exchanger length design for ground source heat pumps", Hvac&R Research. Vol. **5**, no. 2, pp. 85-96, 1999.

75. Y.A. Kara, "Experimental performance evaluation of a closed-loop vertical ground source heat pump in the heating mode using energy analysis method", International Journal of Energy Research. Vol. **31**, no. 15, pp. 1504-1516, 2007.

76. S. Erol and B. François, "Efficiency of various grouting materials for borehole heat exchangers", Applied thermal engineering. Vol. **70**, no. 1, pp. 788-799, 2014.

77. L. Ahonen, et al., Quality assurance of the bentonite material. 2008, Posiva Oy.

78. Z. Gökalp, M. Başaran, and O. Uzun, "Compaction and swelling characteristics of sand-bentonite and pumice-bentonite mixtures", Clay Minerals. Vol. **46**, no. 3, pp. 449-459, 2011.

79. S. Suzuki, et al., "In situ observations of the swelling of bentonite aggregates in NaCl solution", Applied clay science. Vol. **29**, no. 2, pp. 89-98, 2005.

80. F. Eckhart, Grouting procedures for ground-source heat pump systems. 1991: Ground Source Heat Pump Publications, Oklahoma State University.

81. H. Li, et al., "Evaluation on the thermal and moisture diffusion behavior of sand/bentonite", Applied Thermal Engineering. Vol. **151**, pp. 55-65, 2019.

82. C.P. Remund and J.T. Lund, "Thermal enhancement of bentonite grouts for vertical GSHP systems", ASME, heat pump and refrigeration system-design, analysis, and applications. Vol. **29**, pp. 95-106, 1993.

83. Y. Yang, et al., "Investigation on the preparation, properties, and microstructure of high thermal conductive cementing material in 3500m-deep geothermal well", Geothermics. Vol. **100**, pp. 102322, 2022.

84. C. Lee, et al., "Performance evaluation of closed-loop vertical ground heat exchangers by conducting in-situ thermal response tests", Renewable Energy. Vol. **42**, pp. 77-83, 2012.

85. F. Delaleux, et al., "Enhancement of geothermal borehole heat exchangers performances by improvement of bentonite grouts conductivity", Applied Thermal Engineering. Vol. **33**, pp. 92-99, 2012.

86. S.E. Dehkordi and R.A. Schincariol, "Effect of thermal-hydrogeological and borehole heat exchanger properties on performance and impact of vertical closed-loop geothermal heat pump systems", Hydrogeology Journal. Vol. **22**, no. 1, pp. 189-203, 2014.

87. R. Saeidi, Y. Noorollahi, and V. Esfahanian, "Numerical simulation of a novel spiral type ground heat exchanger for enhancing heat transfer performance of geothermal heat pump", Energy conversion and management. Vol. **168**, pp. 296-307, 2018.

88. L. Alberti, et al., "A numerical study on the impact of grouting material on borehole heat exchangers performance in aquifers", Energies. Vol. **10**, no. 5, pp. 703, 2017.

89. D. Pahud and B. Matthey, "Comparison of the thermal performance of double U-pipe borehole heat exchangers measured in situ", Energy and buildings. Vol. **33**, no. 5, pp. 503-507, 2001.

90. S.W. Carlson, "GSHP bore field performance comparisons of standard and thermally enhanced grout", ASHRAE transactions. Vol. **106**, pp. 442, 2000.

91. H. Wang, Y. Cui, and C. Qi, "Effects of sand–bentonite backfill materials on the thermal performance of borehole heat exchangers", Heat transfer engineering. Vol. **34**, no. 1, pp. 37-44, 2013.

92. S. Xiaofei, W. Zhi, and S. Junlong, "CFD numerical simulation of a U-tube ground heat exchanger used in ground source heat pumps", 工程科学学报. Vol. **29**, no. 3, pp. 329-333, 2007.

93. H. Zhou, J. Lv, and T. Li, "Applicability of the pipe structure and flow velocity of vertical ground heat exchanger for ground source heat pump", Energy and Buildings. Vol. **117**, pp. 109-119, 2016.

94. Y. Li, et al., "Thermal performance investigation of borehole heat exchanger with different U-tube diameter and borehole parameters", Energy Procedia. Vol. **61**, pp. 2690-2694, 2014.

95. H. Zeng, N. Diao, and Z. Fang, "Heat transfer analysis of boreholes in vertical ground heat exchangers", International journal of heat and mass transfer. Vol. **46**, no. 23, pp. 4467-4481, 2003.

96. D. Qi, et al., "Effects of ground heat exchangers with different connection configurations on the heating performance of GSHP systems", Geothermics. Vol. **80**, pp. 20-30, 2019.

97. A. Zarrella, G. Emmi, and M. De Carli, "A simulation-based analysis of variable flow pumping in ground source heat pump systems with different types of borehole heat exchangers: A case study", Energy Conversion and Management. Vol. **131**, pp. 135-150, 2017.

98. H. Zhang, et al., "Study on the influence of borehole spacing considering groundwater flow and freezing factors on the annual performance of the ground source heat pump", Applied Thermal Engineering. Vol. **182**, pp. 116042, 2021.

99. Z. Zheng, W. Wang, and C. Ji, "A study on the thermal performance of vertical U-tube ground heat exchangers", Energy Procedia. Vol. **12**, pp. 906-914, 2011.

100. Pip's Island Home. What Is High Density Polyethylene Pipe? (Usage, Pros & Cons). [cited Sep 05, 2022]; Available from: https://www.pipsisland.com/what-is-high-density-polyethylene-pipe/.

101. J. Araújo, W. Waldman, and M. De Paoli, "Thermal properties of high density polyethylene composites with natural fibres: Coupling agent effect", Polymer degradation and stability. Vol. **93**, no. 10, pp. 1770-1775, 2008.

102. R. Bassiouny, M.R. Ali, and M.K. Hassan, "An idea to enhance the thermal performance of HDPE pipes used for ground-source applications", Applied Thermal Engineering. Vol. **109**, pp. 15-21, 2016.

103. B. Bouhacina, R. Saim, and H.F. Oztop, "Numerical investigation of a novel tube design for the geothermal borehole heat exchanger", Applied Thermal Engineering. Vol. **79**, pp. 153-162, 2015.

104. H. Narei, et al., "In pursuit of a replacement for conventional high-density polyethylene tubes in ground source heat pumps from their composites–A comparative study", Geothermics. Vol. **87**, pp. 101819, 2020.

105. J. Raymond, et al., "Numerical Modeling of Thermally Enhanced Pipe Performances in Vertical Ground Heat Exchangers", ASHRAE Transactions. Vol. **117**, no. 1, 2011.

106. Y. Cui and J. Zhu, "3D transient heat transfer numerical analysis of multiple energy piles", Energy and Buildings. Vol. **134**, pp. 129-142, 2017.

107. D. Qi, et al., "Numerical investigation on thermal performance of ground heat exchangers using phase change materials as grout for ground source heat pump system", Applied Thermal Engineering. Vol. **106**, pp. 1023-1032, 2016.

108. F. Ruiz-Calvo, et al., "Reference data sets for validating and analyzing GSHP systems based on an eleven-year operation period", Geothermics. Vol. **64**, pp. 538-550, 2016.

109. M. Dada and A. Benchatti, "Assessment of heat recovery and recovery efficiency of a seasonal thermal energy storage system in a moist porous medium", Int. J. Heat Technol. Vol. **34**, pp. 701-708, 2016.

110. Z. Mohamad, F. Fardoun, and F. Meftah, "A review on energy piles design, evaluation, and optimization", Journal of Cleaner Production. Vol. **292**, pp. 125802, 2021.

111. A. Casasso and R. Sethi, "Efficiency of closed loop geothermal heat pumps: A sensitivity analysis", Renewable Energy. Vol. **62**, pp. 737-746, 2014.

112. G. Emmi, et al., "Energy performance and cost analysis of some borehole heat exchanger configurations with different heat-carrier fluids in mild climates", Geothermics. Vol. **65**, pp. 158-169, 2017.

113. D. Sui, V.H. Langåker, and Z. Yu, "Investigation of thermophysical properties of Nanofluids for application in geothermal energy", Energy Procedia. Vol. **105**, pp. 5055-5060, 2017.

114. I. Mahbubul, R. Saidur, and M. Amalina, "Influence of particle concentration and temperature on thermal conductivity and viscosity of Al2O3/R141b nanorefrigerant", International Communications in Heat and Mass Transfer. Vol. **43**, pp. 100-104, 2013.

115. V. Kumaresan and R. Velraj, "Experimental investigation of the thermo-physical properties of water–ethylene glycol mixture based CNT nanofluids", Thermochimica Acta. Vol. **545**, pp. 180-186, 2012.

116. H. Narei, R. Ghasempour, and Y. Noorollahi, "The effect of employing nanofluid on reducing the bore length of a vertical ground-source heat pump", Energy Conversion and Management. Vol. **123**, pp. 581-591, 2016.

117. H. Javadi, et al., "Impact of employing hybrid nanofluids as heat carrier fluid on the thermal performance of a borehole heat exchanger", Energies. Vol. **14**, no. 10, pp. 2892, 2021.

118. A. Asadi, "A guideline towards easing the decision-making process in selecting an effective nanofluid as a heat transfer fluid", Energy Conversion and Management. Vol. **175**, pp. 1-10, 2018.

119. Y. Li, et al., "Evaluation of thermal short-circuiting and influence on thermal response test for borehole heat exchanger", Geothermics. Vol. **50**, pp. 136-147, 2014.

120. B. Bouhacina, et al., "Analysis of thermal and dynamic comportment of a geothermal vertical U-tube heat exchanger", Energy and Buildings. Vol. **58**, pp. 37-43, 2013.

121. S. You, et al., "In-situ experimental study of heat exchange capacity of CFG pile geothermal exchangers", Energy and buildings. Vol. **79**, pp. 23-31, 2014.

122. A. Casasso and R. Sethi, "Sensitivity analysis on the performance of a ground source heat pump equipped with a double U-pipe borehole heat exchanger", Energy Procedia. Vol. **59**, pp. 301-308, 2014.

123. Z. Li, et al., "Heat transfer performance of a vertical buried internally helically groove tube in soil/polyacrylamide under hot climate", Applied Thermal Engineering. Vol. **124**, pp. 403-412, 2017.

124. Z. Wang, et al., "Field test and numerical investigation on the heat transfer characteristics and optimal design of the heat exchangers of a deep borehole ground source heat pump system", Energy conversion and management. Vol. **153**, pp. 603-615, 2017.

125. L. Zhu, et al., "Transient heat transfer performance of a vertical double U-tube borehole heat exchanger under different operation conditions", Renewable Energy. Vol. **131**, pp. 494-505, 2019.

126. J. Zhao, et al., "Experimental investigation and theoretical model of heat transfer of saturated soil around coaxial ground coupled heat exchanger", Applied Thermal Engineering. Vol. **28**, no. 2-3, pp. 116-125, 2008.

127. S.P. Kavanaugh, Field tests for ground thermal properties--methods and impact on ground-source heat pump design. 2000, University of Alabama.

128. L.G. F, "Newton's law of cooling", American Journal of Physics. Vol. **25**, no. 648, pp. 9, 1957.

129. F.W. Dittus, "Heat transfer in automobile radiators of the tubler type", Univ. Calif. Pubs. Eng. Vol. **2**, pp. 443, 1930.

130. M. Morari and J.H. Lee, "Model predictive control: past, present and future", Computers & Chemical Engineering. Vol. **23**, no. 4-5, pp. 667-682, 1999.

131. L. Wang, Model predictive control system design and implementation using MATLAB®. 2009: Springer Science & Business Media.

132. F. Salem and M.I. Mosaad, "A comparison between MPC and optimal PID controllers: Case studies". 2015.

133. M.H. Marzaki, et al. Comparative study of Model Predictive Controller (MPC) and PID Controller on regulation temperature for SSISD plant. in 2014 IEEE 5th Control and System Graduate Research Colloquium. 2014. IEEE.

134. A. Nikoofard, et al., "Design and comparison of constrained mpc with pid controller for heave disturbance attenuation in offshore managed pressure drilling systems". 2014.

135. A. Li, Comparison between model predictive control and PID control for water-level maintenance in a two-tank system. 2010, University of Pittsburgh.

136. K. Vivek, M.A. Sheta, and V. Gumtapure. A comparative study of Stanley, LQR and MPC controllers for path tracking application (ADAS/AD). in 2019 IEEE International Conference on Intelligent Systems and Green Technology (ICISGT). 2019. IEEE.

137. S. Franko, et al. Mpc and lqr type controller design and comparison for an unmanned helicopter. in Proceedings of the 2011 Summer Computer Simulation Conference. 2011.

138. S. Dani, et al. Performance evaluation of PID, LQR and MPC for DC motor speed control. in 2017 2nd international conference for convergence in technology (I2CT). 2017. IEEE.

139. A. Michopoulos and N. Kyriakis, "Predicting the fluid temperature at the exit of the vertical ground heat exchangers", Applied Energy. Vol. **86**, no. 10, pp. 2065-2070, 2009.

140. W. Gang and J. Wang, "Predictive ANN models of ground heat exchanger for the control of hybrid ground source heat pump systems", Applied energy. Vol. **112**, pp. 1146-1153, 2013.

141. H. Esen, et al., "Predicting performance of a ground-source heat pump system using fuzzy weighted pre-processing-based ANFIS", Building and Environment. Vol. **43**, no. 12, pp. 2178-2187, 2008.

142. S.K. Park, et al., "Application of a multiple linear regression and an artificial neural network model for the heating performance analysis and hourly prediction of a large-scale ground source heat pump system", Energy and Buildings. Vol. **165**, pp. 206-215, 2018.

143. Y. Zhang, et al., "Prediction of Layered Thermal Conductivity Using Artificial Neural Network in Order to Have Better Design of Ground Source Heat Pump System", Energies. Vol. **11**, no. 7, pp. 1896, 2018.

144. X. Zhang, et al., "Machine learning-based performance prediction for ground source heat pump systems", Geothermics. Vol. **105**, pp. 102509, 2022.

145. K. Salhein, J. Ashraf, and M. Zohdy, "Output temperature predictions of the geothermal heat pump system using an improved grey prediction model", Energies. Vol. **14**, no. 16, pp. 5075, 2021.

146. J. Deng, "Essential topics on grey system: theory and application", A report on the project of National Science Foundation of China. 1988.

147. D. Ju-Long, "Control problems of grey systems", Systems & control letters. Vol. **1**, no. 5, pp. 288-294, 1982.

148. T.P. Talafuse and E.A. Pohl, "Small sample reliability growth modeling using a grey systems model", Quality Engineering. Vol. **29**, no. 3, pp. 455-467, 2017.

149. F.-M. Tseng, H.-C. Yu, and G.-H. Tzeng, "Applied hybrid grey model to forecast seasonal time series", Technological Forecasting and Social Change. Vol. **67**, no. 2-3, pp. 291-302, 2001.

150. L. Wu, et al., "The effect of sample size on the grey system model", Applied Mathematical Modelling. Vol. **37**, no. 9, pp. 6577-6583, 2013.

151. Y. Wang, et al., "The research of improved grey GM (1, 1) model to predict the postprandial glucose in type 2 diabetes", BioMed research international. Vol. **2016**, 2016.

152. W. Zhou and J.-M. He, "Generalized GM (1, 1) model and its application in forecasting of fuel production", Applied Mathematical Modelling. Vol. **37**, no. 9, pp. 6234-6243, 2013.

153. L.-C. Hsu, "Applying the grey prediction model to the global integrated circuit industry", Technological forecasting and Social change. Vol. **70**, no. 6, pp. 563-574, 2003.

154. Y. Wang, et al., "An approach to increase prediction precision of GM (1, 1) model based on optimization of the initial condition", Expert Systems with Applications. Vol. **37**, no. 8, pp. 5640-5644, 2010.

155. X. Ma, W. Wu, and Y. Zhang, "Improved GM (1, 1) model based on Simpson formula and its applications", arXiv preprint arXiv:1908.03493. 2019.

156. M. Yao and X. Wang, Electricity consumption forecasting based on a class of new GM (1, 1) model, in Mechatronics and Automatic Control Systems. 2014, Springer. p. 947-953.

157. Y.-S. Lee and L.-I. Tong, "Forecasting energy consumption using a grey model improved by incorporating genetic programming", Energy conversion and Management. Vol. **52**, no. 1, pp. 147-152, 2011.

158. M. Madhi and N. Mohamed, "An initial condition optimization approach for improving the prediction precision of a GM (1, 1) model", Mathematical and Computational Applications. Vol. **22**, no. 1, pp. 21, 2017.

159. E. Twumasi, et al., "Improvement of gray system model using particle swarm optimization", Journal of Electrical Systems and Information Technology. Vol. **8**, no. 1, pp. 1-15, 2021.

160. C.-H. Wang and L.-C. Hsu, "Using genetic algorithms grey theory to forecast high technology industrial output", Applied mathematics and computation. Vol. **195**, no. 1, pp. 256-263, 2008.

161. C.-C. Hsu and C.-Y. Chen, "Applications of improved grey prediction model for power demand forecasting", Energy Conversion and management. Vol. **44**, no. 14, pp. 2241-2249, 2003.

162. K. Li and T. Zhang, "A novel grey forecasting model and its application in forecasting the energy consumption in Shanghai", Energy Systems. Vol. **12**, no. 2, pp. 357-372, 2021.

163. M. Madhi and N. Mohamed, "Improving GM (1, 1) Model Performance Accuracy Based on the Combination of Optimized Initial and Background Values in Time Series Forecasting", Open Access Library Journal. Vol. **9**, no. 4, pp. 1-17, 2022.

164. M. Madhi and N. Mohamed, "An improved GM (1, 1) model based on modified background value", Information Technology Journal. Vol. **16**, no. 1, pp. 11-16, 2017.

165. J. Corberan, et al., "A quasi-steady state mathematical model of an integrated ground source heat pump for building space control", Energy and Buildings. Vol. **43**, no. 1, pp. 82-92, 2011.

166. C. Montagud, et al., "Analysis of the energy performance of a ground source heat pump system after five years of operation", Energy and Buildings. Vol. **43**, no. 12, pp. 3618-3626, 2011.

LIST OF PUBLICATIONS

Journal paper:

1- K. Salhein, C. Kobus, and M. Zohdy, "Control of Heat Transfer in a Vertical Ground Heat Exchanger for a Geothermal Heat Pump System", Energies. Vol. **15**, no. 14, pp. 5300, 2022.

2- K. Salhein, C.J. Kobus, and M. Zohdy, "Forecasting Installation Capacity for the Top 10 Countries Utilizing Geothermal Energy by 2030", Thermo. Vol. **2**, no. 4, pp. 334-351, 2022.

3- K. Salhein, J. Ashraf, and M. Zohdy, "Output Temperature Predictions of the Geothermal Heat Pump System using an Improved Grey Prediction Model", Energies. Vol. **14**, no. 16, pp. 5075, 2021.